SATELLITE REMOTE SENSING OF MIXING DYNAMICS AT A LARGE RIVER CONFLUENCE

BY

MUHAMMAD UMAR

DISSERTATION

Submitted in partial fulfillment of the requirements
for the degree of Doctor of Philosophy in Geography
in the Graduate College of the
University of Illinois at Urbana-Champaign, 2017

Urbana, Illinois

Doctoral Committee:

Professor Bruce Rhoads, Chair and Director of Research
Assistant Professor Jonathan Greenberg
Professor James Best
Professor Marcelo Garcia

ABSTRACT

Although past work has noted that contrasts in turbidity often are detectable on remotely sensed images of rivers downstream from confluences, no systematic methodology has been developed for assessing mixing over distance of confluent flows with differing suspended sediment concentrations. In contrast to field measurements of mixing below confluences, remote-sensing data can provide detailed information on spatial patterns of surficial mixing over long distances along river systems, which can be utilized for mixing studies downstream of large river confluences.

This dissertation consists of three main themes. The first study presents a methodology that uses remote sensing and USGS gaging station data to estimate spatial patterns of surficial suspended sediment concentrations (SSC) downstream of confluences along large rivers and to determine changes in the amount of mixing over distance from confluences. The method develops a calibrated Random Forest (RF) model by relating SSC data from river gaging stations to individual bands and derived spectral indices for the pixels corresponding to the locations of USGS gaging stations. The calibrated model is then used to predict SSC values for every river pixel in remotely sensed images, which provides basis for mapping of spatial variability in SSCs along the river. A new methodology is introduced to average surficial SSC data at cross sections spaced uniformly along the river. The method works as proxy to existing time averaging techniques in the fields. Mixing value at each cross-section is computed using the spatially averaged cross-section data and a new mixing metric that can work with low initial concentrations differences between tributaries and takes into account upstream SSC variance.

The section provides three examples of model application where spatial pattern of changes in this metric over distance is used to define rates and length scales of surficial mixing of suspended sediment downstream of a confluence.

The second study comprised of investigation of influence of different potential controlling factors on mixing downstream of confluences. Based on dimensional analysis and extant literature, the factors that could be calculated with remote sensing and available gaging station data were identified and regressed against observed mixing lengths to determine influence of each one of them on lateral mixing. Longitudinal variations in mixing with changes in channel geometry was also determined. Contrary to the current understanding, none of the factors identified in the literature showed any relation with the mixing lengths. The lack on observed relation between all of the factors indicates that mixing processes at large rivers are more complex then at small confluences. The study ascertains the need for additional applications of the methodology on other large rivers to identify uniqueness or commonalities between this confluence and other large confluences around the world. Furthermore, the methodology can also be used to evaluate how variations in mixing over time and space influence water quality and ecological conditions along the river.

The third part presents a methodology to implement streamtube method to compute lateral mixing lengths downstream of the confluence. The method uses planform data from satellite imageries, hydrologic data from USGS, and bathymetric data from USACE to compute streamtube parameters. Mixing lengths determined by streamtube method are compared with the mixing lengths observed in the second study. Streamtube method relies heavily on flow discharges and mixing lengths decrease linearly with increasing discharge. However, the second study did not find any such relation between the discharge and mixing lengths. It is therefore

concluded that the simple theoretical assumptions embodied in the streamtube model do not hold well for the mixing downstream of the confluence.

ACKNOWLEDGEMENTS

The journey of completing my dissertation has been the most exciting endeavor of my life and I would like to thank the people who contributed to such a great experience.

First of all, I would like to express my sincere gratitude to my advisor, Prof. Bruce Rhoads, for his immeasurable support and guidance at all stages of my research, and the amount of time and efforts he has put into design and execution of this research project. His insights into the complex dynamics in the geomorphic systems and excellent research writing skills have been a true blessing. Thank you, Bruce, for all of your patience and constructive criticism, and most of all believing in me and pushing me in the right direction whenever I felt lost. I would also like to thank Dr. Jonathan Greenberg for his constant source of expertise and good advice in the field of remote sensing and process automation that were essential to this work. I am also grateful to Dr. James Best and Dr. Marcelo Garcia for serving on my doctoral committee and providing thoughtful comments during the development of my proposal and thesis.

I would also like to acknowledge the many that helped me in various ways. I owe gratitude to my fellow colleagues Frank Engel, Kory Konsoer, Jessica Zinger, Quinn Lewis, and Mingjing Yu for their moral support and friendship. I am especially grateful to Jessica Zinger and Quinn Lewis for providing much assistance and encouragement throughout my time as graduate student. Finally, special thanks to Dr. Jonathan Reno from Southern Illinois University, Carbondale, for providing me bathymetric data of my study reach that formed the basis for this research.

I am especially thankful to my parents for their unending love, support, and prayers throughout my life. The feeling of you being there for me, even when it meant just a phone call, was a source of much needed encouragement and inspiration. This work is dedicated to the memory of my mother who passed away during my time as a graduate student. It is gratifying that I have been able to honor her with this work.

I owe endless gratitude to my wife, Tooba Rehman, without whom none of this would have been possible. Tooba has been a source of encouragement and support throughout my graduate program. Thank you, Tooba, for your sleepless nights with kids so I could meet the deadlines, for delicious foods to ease my tension during stressful times, and simply for being there for me through this arduous path toward the completion of my Ph.D.

To my family with love:

Tooba, Hafsa and Sobaan

and my parents

TABLE OF CONTENTS

LIST OF FIGURES xii

LIST OF TABLES xvi

CHAPTER 1: INTRODUCTION 1

1.1 MOTIVATION 1

1.2 RESEARCH QUESTIONS 4

1.3 RESEARCH ORGANIZATION 5

CHAPTER 2: SUSPENDED SEDIMENT MIXING DOWNSTREAM OF A LARGE RIVER CONFLUENCE: A CONCEPTUAL FRAMEWORK 7

2.1 INTRODUCTION 7

2.2 REMOTE SENSING OF INLAND WATERS 7

2.3 LATERAL MIXING IN RIVERS 11

2.3.1 Constant coefficient model 12

2.3.2 Streamtube method 14

2.3.3 Uniform flow method 16

2.4 FLOW STRUCTURE AT CONFLUENCE 17

2.5 LATERAL MIXING AT CONFLUENCES 20

2.6 SUMMARY AND RELATION TO CONDUCTED RESEARCH 23

CHAPTER 3: USE OF BROAD-BAND SATELLITE REMOTE SENSING TO ASSESS MIXING OF SUSPENDED SEDIMENT DOWNSTREAM OF LARGE RIVER CONFLUENCES 24

3.1 INTRODUCTION 24

3.2 STUDY AREA 27

3.3 METHODOLOGY 28

3.3.1 Development of an empirical model of surficial SSC 29

3.3.1.1 Image data 29

3.3.1.2 Discharge and suspended sediment data 30

3.3.1.3 Channel edge and centerline 31

3.3.1.4 Modelling SSSC 32

3.3.2 Spatial averaging of SSSCs and quantification of mixing 33

3.3.2.1 Spatial representation of river cross-sections 33

3.3.2.2 Spatial averaging of SSSC 35

3.3.2.3 Calculation of mixing metric 36

3.4 RESULTS 38

3.4.1 Accuracy of the SSSC predictions 38

3.4.2 Patterns of SSSC for three test cases 41

3.4.2.1 Case 1: Rapid mixing 41

3.4.2.2 Case 2: Slow mixing 45

3.4.2.3 Case 3: Minor mixing 48

3.5 DISCUSSION AND CONCLUSION 50

CHAPTER 4: ASSESSMENT OF SUSPENDED SEDIMENT MIXING DOWNSTREAM OF A LARGE RIVER CONFLUENCE 54

4.1 INTRODUCTION 54

4.2 STUDY AREA 57

4.3 DIMENSIONAL ANALYSIS OF MIXING IN RIVERS 58

4.4 DATA AND METHODOLOGY 59

4.5 RESULTS 62

4.5.1 Mixing lengths and controlling factors 63

4.5.1.1 Momentum ratio 64

4.5.1.2 Total discharge and mean flow depth at confluence 66

4.5.1.3 Upstream water temperature and SSSC contrast 69

4.5.2 Apparent mixing due to SSSC variation along the channel 71

4.5.2.1 Reduction in suspended sediment concentrations 72

4.5.2.2 Apparent mixing and increases in sediment concentration 75

4.6 DISCUSSION 78

4.7 CONCLUSION 86

CHAPTER 5: COMPARISON OF OBSERVED MIXING LENGTHS VERSUS MIXING LENGTHS USING THE STREAMTUBE METHOD 89

5.1 INTRODUCTION 89

5.2 METHODOLOGY 89

5.2.1 Flow characteristics 89

5.2.2 Channel width 91

5.2.3 Local depth-averaged velocities 94

5.2.4 Defining streamtubes *94*

5.2.5 Dimensionless shape factor *98*

5.2.6 Transverse dispersion coefficient *100*

5.3 RESULTS AND DISCUSSION 101

5.3.1 Transverse dispersion coefficient *102*

5.3.2 Factor of diffusion *105*

5.4 CONCLUSION 108

CHAPTER 6: CONCLUSION 111

6.1 SUMMARY OF FINDINGS 111

6.2 FUTURE WORK 118

REFERENCES 120

LIST OF FIGURES

Figure 2.1: Major zones within the CHZ, (A) Symmetrical confluence, (B) Asymmetrical confluence 18

Figure 3.1: Confluence of the Mississippi and Missouri rivers at Illinois-Missouri border. Locations of USGS stations upstream and downstream of the confluence are shown along with station numbers 28

Figure 3.2: Flowchart of the methodology. 29

Figure 3.3: Example of s-n coordinate system for spatial averaging and mixing calculations. The shaded pixels represent the pixels with different s coordinates but standardized n coordinates that fall within the 30m interval on the representative cross section (R CS) denoted by the black rectangle. Values of SSC for these pixels are averaged to produce a mean SSC for the corresponding interval on the RCS (black rectangle). 34

Figure 3.4: Plot of predicted versus observed SSC at gaging stations upstream (at Grafton) and downstream (at St. Louis) of the confluence of the Mississippi River and Missouri River confluence. Dashed line represents 1:1 relationship. Solid line is linear regression relation between predicted and observed values. 41

Figure 3.5: Maps of predicted surficial SSCs (mg l-1) over an initial 21 km section of the 110km study reach downstream of the confluence of Mississippi and Missouri Rivers (note difference in SSC scales in each frame). Images were acquired on (a) March 30, 1988, (b) April 24, 1991, and (c) September 26, 2001. Mississippi River is on the right side while Missouri River joins in from the left (west). 42

Figure 3.6: Cross-stream variations in SSC at different locations along the Mississippi River downstream from the confluence with the Missouri River for case 1. Normalized distance is equal to each pixel's N-value/half channel width. Numbers at the top of each panel indicate the distance downstream from the confluence in kilometers. Distance from the confluence is shown on the top left corner while the computed Pmx values are shown in the bottom right corner of each plot. 43

Figure 3.7: Changes in values of Pmx with distance from the confluence for case 1. Channel width variations are shown as histogram. Initial spike in the Pmx corresponds to the maximum channel width. 45

Figure 3.8: Cross-stream variations in SSC at different locations along the Mississippi River downstream from the confluence with the Missouri River for case 2. Numbers at the top left of each panel indicate the distance downstream from the confluence in kilometers. 47

Figure 3.9: Changes in the values of Pmx with distance from the confluence for case 2. 48

Figure 3.10: Cross-stream variations in SSC at different locations along the Mississippi River downstream from the confluence with the Missouri River for case 3. Numbers at the top of each panel indicate the distance downstream from the confluence in kilometers. 49

Figure 3.11: Changes in the values of Pmx with distance from the confluence for case 3. 50

Figure 4.1: Velocity-discharge relationship for Mississippi (blue) and Missouri River (red) confluences. 65

Figure 4.2: Plot of observed temperature at USGS station versus Landsat derived temperature… 66

Figure 4.3: Relationship between different potential controlling factors and observed mixing lengths; momentum ratio (top left), discharge ratio (top right), width-depth ratio measured the confluences about 250m downstream of the upstream junction corner (bottom left), and total flow depth. 68

Figure 4.4: Relationship between SSC ratio (SSCMO/SSCMS) and the mixing length..... 70

Figure 4.5: Cross section profiles at 0.5 km, 1.5 km, 6.5 km, and 29 km from left to right, top to bottom respectively, downstream of the upstream junction corner. X-axis is normalized distance and is equal to each pixel's N-value/half channel width. Numbers at the bottom of each panel indicate the mixing metric value corresponding to the plot. Blue line is the expected SSC value calculated using equation 4.7. 73

Figure 4.6: Longitudinal SSC profile from the confluence to the location of complete mixing – 28 km downstream of the confluence. Each data point represents SSC value in individual cell within the path drawn on each side of the river. The left figure represents longitudinal profile downstream of the confluence on the Missouri Side while the right one is for the Mississippi side. 75

Figure 4.7: Cross section profile at 250m, 30 km, 60 km, and 100 km downstream of the upstream junction corner. Horizontal blue line indicates expected mixed value. 76

Figure 4.8: Longitudinal SSC profile from the confluence to the location of complete mixing – 100 km downstream of the confluence. Each data point represents SSC value in individual cell within the path drawn on each side of the river. The left figure represents longitudinal profile downstream of the confluence on the Missouri Side while the right one is for the Mississippi side 77

Figure 4.9: Cross sectional bathymetric profile at the Mississippi River just upstream of the confluence in 2001 (top) and 2010 (bottom). 79

Figure 4.10: Cross sectional bathymetric profile at the Missouri River just upstream of the confluence in 2001 (top) and 2010 (bottom). 79

Figure 4.11: Variations in the mixing rates within initial six channel widths as functions of different PCFs. Higher slopes mean faster mixing. 81

Figure 4.12: Variations in the mixing rates within initial 30 channel widths as functions of different PCFs. 82

Figure 4.13: Variations in the mixing with longitudinal variations in width-depth ratio; for sediment reduction case (left), and for sediment addition case (right). 84

Figure 4.14: Densimetric Froude number distribution among all the observed cases. 86

Figure 5.1: Water Surface slopes between St. Louis, MO and Chester, IL corresponding to Landsat image acquisition dates between 1984 and 2011. 91

Figure 5.2: A hypothetical cross-sectional profile with complete bathymetric data (a) and with missing data (b). b is the surface width of the channel from the digitized river boundaries using Landsat Images, vertical lines in the channel represent local flow depths h measured at every pixel location from flow depth raster that intersected with the cross-section line, and H is the mean depth at the cross section. Red dotted line shows the areas where bathymetric data are not available. 92

Figure 5.3: Shallower (left) side pixel from figure (2b) has been extended to the edge of the channel width resulting in an area of constant flow depth. Δz is the distance between two consecutive pixels. Notice a larger interval on the left side due to pixel's relocation to the channel boundary. 93

Figure 5.4: Flowchart of the procedure for defining 20 streamtubes. The procedure is performed at each cross section one by one along the entire study reach. 95

Figure 5.5: Transformation of original cross-section profile (a) into a more detailed profile (b) by linear interpolation between consecutive points. Each new point has a value for location, local depth and cumulative discharge. Red dots are the locations where flow depths and velocities and discharge values were initially available. 97

Figure 5.6: A hypothetical 500 m sub reach (shaded region) with 15 streamtubes. The dashed line is the channel centerline where longitudinal distance is measured to define sub reaches (AB). The central cross section is where width of the channel is determined and pixel values from flow depth raster are extracted. Streamtube intervals are shown in blue colors where discharge values are equal. Right bank (CD) is shorter than the left bank (EF). Linear interpolation between CD and EF will result in side lengths with values between 450 m and 550 m as shown in dotted lines for streamtube 1 and streamtube i. 99

Figure 5.7: Relationship between dimensionless dispersion coefficient and b/Rc for the eleven cases. 103

Figure 5.8: Relationship between transverse dispersion coefficient and the factor of diffusion for all the cases. 104

Figure 5.9: Relationship between flow discharge and reach-averaged factor of diffusion. The value of D increases as power function with discharge/..... 106

Figure 5.10: Relationship between flow discharge and mixing lengths computed through streamtube method. 107

Figure 5.11: Comparison of mixing lengths obtained from the method reported in chapter 4 (Lx) and mixing lengths computed using the streamtube method (Lz). 108

LIST OF TABLES

Table 3.1: Physical and hydrological characteristics of Mississippi and Missouri Rivers upstream of the confluence (Carlston, 1969)..... 27

Table 3.2: Summary of available SSC data and basic statistics at the three USGS stations within the study reach 31

Table 3.3: Spectral indices for water constituent concentrations retrieval from medium resolution multispectral sensors..... 33

Table 3.4: Summary of important parameters for the three cases 38

Table 3.5: Statistical relationship between model predicted and observed SSC values at the USGS stations..... 39

Table 3.6: Predictor variables ranked by their importance in the prediction..... 40

Table 4.1: Summary of available flow discharge and SSC data and basic statistics at the three USGS stations within the study reach. The stations on Mississippi River at Grafton, IL and Mississippi River below Grafton, IL are only 5.5 mile apart so the discharge data from both stations has been combined into one record. 60

Table 4.2: Ranges for different PCFs for the observed cases. 62

Table 4.3:Distribution of mixing lengths among various cases..... 63

Table 4.4:Statistics of the observed completely mixed cased..... 63

Table 4.5: Statistics of the observed Pmx values at the downstream end for unmixed cases 63

Table 4.6: Results of linear regressions of different factors against observed mixing lengths shown in Figure 4.3..... 69

Table 4.7: Results of linear regressions of SSC and temperature ratios against observed mixing length (Figure 4.4). 71

Table 4.8: Summary of important parameters for the two cases 72

Table 5.1: Table of important variables. Range of values are provided for the variables that vary in the downstream direction..... 102

Table 5.2: Mixing lengths observed at similar discharges. NAs represent the cases where streamtube method has not been applied. 107

CHAPTER 1: INTRODUCTION

1.1 Motivation

River confluences are the sites where two rivers join together and are ubiquitous features of all fluvial networks. Confluences play an important role in routing flows from different watersheds through the fluvial networks, which has consequences for flooding, bed and bank stability, and water quality downstream of the confluences. It is not surprising that confluences have received attention from a wide range of scientific disciplines. To geomorphologists, confluences represent sites of significant changes in hydraulic conditions, channel geometry, and bed material characteristics. To sedimentologists, confluences are sites of unique facies produced by characteristic erosional/depositional features. For ecologists, mixing processes at confluences are of interest because of the consequences of such mixing for water quality and nutrient dynamics at and downstream of the confluence. To engineers, confluence hydrodynamics are important for flood routing and management within drainage networks.

Mixing at confluences is initiated when incoming flows with different physical and chemical properties join together and start to mix laterally. The dynamics of transverse-mixing processes at confluences essentially determine water quality downstream of these locations. Local rates of mixing depend on flow structure within the confluence, which are largely controlled by planform symmetry, junction angle, relative strengths of the incoming flows, and density and bed elevation differences between the two channels (Bradbrook et al., 2000, 1998, Constantinescu et al., 2016, 2011; De Serres et al., 1999; Laraque et al., 2009; Ramón et al., 2014; Ramõn et al., 2013; Rhoads and Kenworthy, 1998, 1995). Extensive research on flow structure has been conducted in the immediate vicinity of a confluence, where

hydrodynamic conditions are strongly affected by flow convergence – a region referred to as the confluence hydrodynamic zone (CHZ) (Kenworthy and Rhoads, 1995). Studies of mixing at and downstream of confluences are less common. Mixing at small confluences show that considerable mixing can happen within the CHZ (Biron et al., 2004; Gaudet and Roy, 1995; Rhoads and Kenworthy, 1995; Rhoads and Sukhodolov, 2001), whilst studies on large river confluences indicate that mixing lengths often extend hundreds of channel widths downstream of the confluence (Bouchez et al., 2010; Kabeya et al., 2008; Lane et al., 2008; Laraque et al., 2009; Mackay, 1970; Rathbun and Rostad, 2004). Past studies are limited mostly to a restricted range of hydrodynamic conditions of the incoming flows or to measurements at particular locations downstream of confluences and thus may not adequately capture spatial and temporal variations in mixing lengths in response to varying flow conditions. Because rates of transverse mixing downstream of confluences are largely unknown, the influence of tributary contributions on spatial patterns of water quality in large river systems is poorly understood. Therefore, there is a clear need for additional research that examines characteristics of mixing downstream of large-river confluences over large temporal and spatial scales and the factors that might influence rates of mixing and mixing lengths.

As flows from major tributaries, often with different biogeochemical characteristics, converge at confluences, the mixing interface between both flows can usually be identified visually based on contrasts in visible properties of the flow (e.g. turbidity, color) (Roy et al., 1999). Semi-theoretical analysis suggests that mixing lengths scale with width of the channel. Hence, for big rivers, in the absence of strong near-field effects, large absolute length scales are required for the cross-channel contrast to completely disappear. Many empirical studies in large river systems have reported slow mixing rates and very large length scales where flows remain

unmixed downstream of confluences for hundreds of kilometers (Bouchez et al., 2010; Kabeya et al., 2008; Krouse and Mackay, 1971; Laraque et al., 2009; Mackay, 1970; Matsui et al., 1976; Rathbun and Rostad, 2004; Stallard, 1987). However, mixing lengths of a few channel widths downstream of confluences have also been reported for large rivers (Lane et al., 2008; Maurice-Bourgoin et al., 2003). Current knowledge of lateral mixing downstream of confluences is limited to particular hydrological relations between the tributaries that cannot necessarily be translated to other hydrological conditions even for the same confluence. To date, no such studies have considered in details wide range of hydrological conditions and how these conditions influence the rates and length scales of mixing at large river confluences.

The lack of detailed studies of mixing downstream of confluences represents a major gap in the understanding of fluvial processes in large river systems. Although small confluences and large confluences exhibit some similarities (e.g. bed scour), the hydrodynamics of small confluences may not be identical to those of large confluences. Because shear layer vortices scale with channel depth and width changes far rapidly than depth in the large confluences than those of small confluences, the expected width of the shear layer and the rate at which it expands downstream relative to the channel width is much smaller in larger rivers than in smaller rivers (Rhoads, 2006). Additionally, bed discordance may be minimal or completely absent at the large confluences, resulting in the lack of shear layer distortion that can promote rapid mixing (Gaudet and Roy, 1995). The effects of tributary mouth bars may also be not as prominent as in small confluences because slopes of these bars are often much gentler than the slopes of tributary mouth bars found in smaller confluences (Parsons et al., 2008). Furthermore, channel-scale secondary flows may not be similar to those observed at small confluences. For example, Parsons et al., (2007) found no evidence of secondary flows while Szupiany et al., (2007) found

small localized flow cells that were limited to <25% of the channel width. Thus, further research is needed to determine whether results on mixing obtained for small river confluences apply to large river confluences, where hydrodynamic conditions may differ from those for small confluence. The purpose of this research is to examine surficial mixing using satellite remote sensing data to elucidate the influence of tributary contributions on spatial patterns of water quality in large river systems.

1.2 Research questions

The main objective of this research is to increase our knowledge of mixing dynamics at and downstream of confluences by examining patterns of lateral surface mixing of suspended sediment downstream of a large-river confluence and by evaluating relations between dominant flow conditions and mixing rates and lengths using satellite remote sensing and ground data from USGS stations. The specific objectives of this research are to;

1) Develop a satellite remote-sensing-based methodology to determine spatial patterns of suspended sediment downstream of a large river confluence.

2) Apply the methodology to a large river confluence to evaluate rates and length scales of transverse surficial mixing of suspended sediment for a wide range of hydrological conditions

3) Evaluate the effects of potential controlling factors (PCFs), such as momentum ratio, total flow discharge, width-depth ratio, sediment-concentration ratios, and density differences on rates and length scales of mixing downstream of a large river confluence.

4) Determine whether changes in the “apparent” amount of mixing, as determined from a mixing metric, might reflect factors other than mixing, such as additions or losses of sediment from the water column over distance.

5) Develop a stream-tube model of mixing lengths and compare predicted lengths scales of mixing with observed length scales of surface mixing derived from remote sensing analysis.

The outcome of this research enhances the capacity to assess water quality parameters like suspended sediment concentration (SSC) and temperatures in rivers, offering a means to evaluate SSC and thermal mixing at any large river with contrasting initial values. Using the proposed mixing metric, the research provides substantial insights into transverse mixing in large rivers. In particular, it provides insight into the dynamics of mixing downstream of large river confluences. Results from this research will also benefit the society because large rivers are equally important for humans and aquatic habitats and improved understanding of mixing is critical for water quality applications.

1.3 Research organization

The process of mixing in river confluences mainly occur though three main mechanisms: (i) the development of shear between the conjoining flows, (ii) secondary flows due to the flow curvature, and (iii) bed discordance between the two tributaries. A substantial amount of previous research has examined near-field processes in confluences. Chapter 2 provides an overview of existing literature concerning the use of remote sensing to examine the optical properties of water bodies and relate optical properties to constituent concentrations of water bodies. It also reviews literature on flow and mixing dynamics at confluences. The chapter starts by reviewing literature on remote sensing of suspended sediment concentrations in rivers and other water bodies. It then describes current understanding of lateral mixing in rivers in the context of flow dynamics at different scales, including flow at confluences. Finally, gaps in lateral mixing at and downstream of large confluences are presented.

Chapter 3 describes methodology for using remote sensing for detection of surficial SSC (SSSC) quantitatively. The chapter provides details of the SSSC modeling techniques with remote sensing and ground data from USGS stations and proposes a new way to quantify mixing at cross section spaced at regular intervals. By investigating spatial pattern of mixing, mixing is evaluated for the three case studies.

Chapter 4 builds on the methodology developed in Chapter 3 by using the technique to evaluate relationships between momentum ratio, total flow discharge, width-depth ratio, density differences, and channel curvature and mixing rates and length scales at the confluences of two of the largest rivers of USA - Mississippi and Missouri Rivers. By evaluating the relationships, the study reports influences of the factors on controlling mixing lengths.

Chapter 5 describes implementation of streamtube method for the determination of transverse mixing lengths downstream of a confluence. Streamtube model parameters have been calculated and mixing lengths have been determined for eleven cases where complete mixing occurred within the study reach. The study evaluates the streamtube model's predictive capability by comparing mixing lengths computed by the streamtube model to observed mixing lengths from Chapter 4.

Chapter 6 summarizes the main findings of the research and provides specific findings related to the research questions. In addition, the chapter discusses limitations of the methodology used for studying mixing processes and provides directions for future work.

CHAPTER 2: SUSPENDED SEDIMENT MIXING DOWNSTREAM OF A LARGE RIVER CONFLUENCE: A CONCEPTUAL FRAMEWORK

2.1 Introduction

River confluences are nodes in fluvial network where complex hydrodynamic and morphodynamic processes take place. Despite considerable research on flow structures and sediment transport at confluences, mixing of often contrasting biogeochemical properties, such as suspended sediment concentrations, temperature differences, salinities and organic matters, of the incoming flows are not yet fully understood. The dynamics of the mixing processes determine water quality downstream of the confluence, therefore understanding of these dynamics is important not only for humans, but also for aquatic ecosystems. Understanding of the mixing processes that influence the spatial distribution of water quality downstream of confluences is important for effective water resource management. The purpose of this chapter is to provide extant literature review on topics that are relevant to the objectives of research provided in chapter 1. These topics include applications of remote sensing in inland waters, semi theoretical analysis of lateral mixing in rivers, flow dynamics at river confluences, and lateral mixing at and downstream of confluences.

2.2 Remote sensing of inland waters

Inland waters not only provide resources for human uses, but they also support high biodiversity by providing diverse habitat and ecosystem services (Brönmark and Hansson, 2002; Duker and Borre, 2001). Pollutions like nutrients and organic and inorganic matter pose a threat to these ecosystems (Palmer et al., 2015). Over the past few years, the effects of land use and climate change on water resources have been widely recognized and attentions have been paid to the monitoring and management of these resources. Traditionally, inland water quality has been assessed using in situ data collection procedures which have very limited spatial and temporal

coverage. Additionally, field data collection requires considerable funding that may not be available for some of the water bodies, especially in developing countries. Therefore, only few of these water bodies are being monitored regularly around the world.

Satellite remote sensing, with synoptic coverage and consistency of temporal data, offers significant advantages over traditional methods by providing adequate information on water quality that can be utilized for the regions where conventional monitoring is limited or non-existent (Navalgund et al., 2007). Although, inland waters are optically complex (Morel and Prieur, 1977) and present a challenge due to the changing concentrations of water constituents like phytoplankton, colored dissolved organic matter (CDOM), and triptons over short distances, recent advances in computer technologies and satellite instruments have greatly increased number of successful applications of remote sensing for water bodies, allowing near real-time monitoring of water quality at inland waters (Matthews, 2011; Odermatt et al., 2012).

Water quality parameters like SSSC can be derived quantitatively from remotely sensed imagery through an empirical approach that relates water quality parameters directly to spectral properties using various statistical techniques. Many studies have demonstrated the ability to link water quality parameters to their spectral responses observed at space-borne sensors (e.g. Dekker et al., 2002; Matthews, 2011; Odermatt et al., 2012). Multispectral sensors including Landsat 5, are mainly intended for terrestrial applications and have fewer broad bands with limited spectral and radiometric resolution that impedes the detection of certain water quality parameters. Yet, many studies have successfully exploited higher spatial resolution of these sensors, relative to the resolution of sensors specifically designed for water applications, for estimation of different inland water quality parameters (Chang et al., 2004; Dekker et al., 2001; Doxaran et al., 2006; Hellweger et al., 2007; Kutser et al., 2005; Thiemann and Kaufmann, 2000; Vincent et al., 2004).

Empirical algorithms are relatively simple in terms of derivation and applications compared to the analytical approach. Generally, steps for empirical approaches include; 1) acquisition of atmospheric and water quality data simultaneously with the satellite image acquisitions, 2) geometric and atmospheric corrections of images to produce surface reflectance, 3) determination of a statistical relation between the satellite data and water quality parameter of interest that leads to development of the empirical algorithm, and lastly, 4) application of the algorithm to satellite images to derive estimates of the parameter within the image scene. The main advantages of empirical algorithms are their computational simplicity and ease of use. Among other water quality parameters such as phytoplankton, colored dissolved organic matter CDOM, the focus of this study is only on suspended sediment concentrations, so only remote sensing of SSSC is discussed here.

Suspended sediment concentrations in water can be related to turbidity, secchi disk (SD) depth – a special type of round disk which is used to detect depths at which it is no longer visible by naked eye and is a measure of water clarity, or total suspended solids (TSS). Turbidity is a measure of light beam attenuation through water column or alternatively, a measure of scattering of light by particulate matter in the water. Landsat based empirical algorithms have been used quite extensively for measuring turbidity in inland water (Brezonik et al., 2005; Kallio et al., 2008; Lathrop and Lillesand, 1986; Vincent et al., 2004; Wang et al., 2006). Algorithms using single band or band ratios, most commonly involving red wavelength (band 3 of Landsat 5 TM, or simply TM3), have been successful in determining TSS concentrations in the water (Kallio et al., 2008). Secchi disk can also be used as proxy for gross particulate matter because remote sensing algorithms used for SD depth measurements essentially provide total particulate load information (Matthews, 2011). Similar to turbidity, red wavelength is commonly used for SD

depth measurements, either as single band or in a band ratio (Cox et al., 1998; Duan et al., 2009; Härmä et al., 2001; Hellweger et al., 2007; Kallio et al., 2008; Lathrop, 1992; Lavery et al., 1993; Wu et al., 2008). For the most part, relation between the red band or red band based indices provides a nonlinear relationship between SD to brightness, therefore SD depth is usually log transformed for use in regressions. In addition to the red band only, the ratio of red to blue is also commonly used, given that blue is largely uncorrelated to SD and serves as a brightness normalization factor for the red band. Another variant of red and blue bands is multiple regression of the form TM3/TM1 + TM1 which has become a standard because of its consistency in successful detection of SD depths (Brezonik et al., 2005; Kloiber et al., 2002; Lavery et al., 1993; Olmanson et al., 2008). TSS is a measure of total sediment mass per unit volume of water and includes organic and inorganic matters and is related to sediment transport and water quality (Dekker et al., 2002). Doxaran et al., (2002) has shown that increasing scatter with increasing sediment load in near infrared (NIR) wavelength can be used for high turbid waters. Many studies have used regressions of single bands or band ratios to achieve high correlations (R^2>0.82) (Doxaran et al., 2009, 2006, 2002a; Miller and McKee, 2004; Onderka and Pekárová, 2008; Östlund et al., 2001; Sváb et al., 2005; Tyler et al., 2006), however, Matthews, (2011) noted that there is still a lack of consensus on the choice of bands or band ratios for TSS estimation. For example, Lathrop and Lillesand, (1989) used red and NIR bands for high sediment concentrations, Dekker et al., (2002) found that average of green (TM2) and red bands (TM3) had exponential relationship with TSS, and Doxaran et al., (2009, 2006, 2002b) showed robust relation between NIR-to-red and NIR-to-green ratios with the TSS.

2.3 Lateral mixing in rivers

Mixing in rivers is a natural physical process which is responsible for the transportation and dispersion of tracers/pollutants laterally and longitudinally. Significant research conducted during 1960s and 1970s has provided basis for development of semitheoretical models capable of predicting mixing lengths (L_z) downstream of the tracer injection point and has contributed to well understanding of lateral mixing processes (Elhadi et al., 1984; Fischer et al., 1979; Rutherford, 1994). Recently, many studies have focused on lateral mixing in natural rivers at different scales (Boxall and Guymer, 2003; Lane et al., 2008; Seo et al., 2006; Zhang and Zhu, 2011). Accuracy of mixing calculations depends on the accuracy of measurements of flow characteristics, channel bathymetry, banks and planform geometry, and the slope of the channel. Dispersion rates are most commonly calculated by injecting nontoxic tracers such as Rhodamine WT into the channel and measuring tracer concentrations downstream of the source. For water quality problems, tracers in effluents can also be used for the same purpose. Tracers are usually sampled from a boat by surveying strategically selected transects such that enough data are collected for the calculations of average concentrations at each location. The average in mixing problems is usually an ensemble mean where data from identical tests are averaged. Therefore, the calculation of the transverse dispersion coefficient requires traversing the same transect many times so that the results can be averaged. On the other hand, longitudinal dispersion coefficient calculations require sampling long reaches to measure concentration changes.

When a tracer is added to a flowing water body, it is subjected to two fundamental processes; advection and diffusion. Advection of fluid is the mass transport due to the motion of the fluid while the diffusion occurs due to the random movements of molecules and turbulent eddies. Diffusion in natural rivers occurs in two ways; molecular diffusion and turbulent diffusion. Molecular diffusion occurs due to the random movements of molecules and is

independent of the flow conditions. It only depends on the properties of solvent and solute and has a typical constant value of $10^{-9}m^2s^{-1}$. Molecular diffusion can be described by Fick's law. Fick, (1855) hypothesized that mass of a solute passing through a unit area per unit time in a given direction is proportional to the solute concentration gradient in that direction. One dimensional form of Fick's law can be written in mathematical form as;

$$q_m = -e_t \frac{\partial C}{\partial x} \tag{2.1}$$

where q_m is the fluid mass flux, *C* is the mass concentration of solute and e_t is the constant of proportionality with units (length)^2/time and is called diffusion coefficient. The negative sign indicates that flow is from high to low concentration. In natural rivers, turbulence significantly enhances the diffusion process and hence mixing. Turbulent eddies deform the tracer cloud resulting in increased local concentration gradients, which according to Fick's law are a main factor promoting molecular diffusion. Tracer particles from a same point source may follow totally different and highly irregular paths in turbulent flows. Turbulent diffusion (k) is a function of flow and varies with varying velocities due to the turbulence in the flow. Molecular diffusion and diffusion due to the turbulent eddies are collectively called turbulent diffusion. Turbulent diffusion coefficients (typically $10^{-3}m^2s^{-1}$) are much larger than molecular diffusion coefficients (typically $10^{-9}m^2s^{-1}$).

2.3.1 Constant coefficient model

For a conservative tracer with a steady source in a straight channel, longitudinal dispersion term can be neglected from three-dimensional advection/diffusion equation, and assuming the tracer is vertically well mixed, the analysis of the equation becomes two dimensional (Rutherford, 1994). In this case, depth averaged transverse (z) velocity is zero, and the mean flow depth and flow velocities in the downstream (x) directions as well as transverse

dispersion coefficient (k_z) are constant. Therefore, complete advection/diffusion equation can be rewritten as follows:

$$u_x \frac{\partial c}{\partial z} = k_z \frac{\partial^2 c}{\partial z^2} \tag{2.2}$$

Equation (2.2) is called constant coefficient model of transverse mixing. As the transverse tracer flux at both banks is zero and k_z is constant, $\frac{\partial c}{\partial z} = 0$ for z= 0 and z = b. The solution of the equation (2.2) is given by Fischer et al., (1979) for this case as:

$$k_z = \beta \frac{u_x b^2}{L_z} \tag{2.3}$$

Where u_x is longitudinal velocity (assumed constant for constant coefficient model), b is the channel width and L_z is the distance at which a tracer is completely mixed across the channel (the ratio of minimum and maximum tracer concentrations is close to 1, i.e. $P_m = \frac{S_{min}}{S_{max}} > 0.9$). The constant β depends on P_m and the source location. For $P_m = 0.98$, β=0.536 for a bankside outfall and 0. 134 for a mid-channel source (Rutherford, 1994). Equation (2.3) can be re arranged as;

$$L_z = \beta \frac{u_x b^2}{k_z} \tag{2.4}$$

Equation (2.4) indicates that concentration gradients in transverse direction decrease monotonically before vanishing asymptotically, in the absence of strong near-field effects. For a source in mid-channel, a distance of 100-300 channel widths are required to achieve complete lateral mixing. The confluence of two similar size rivers can be considered a mid-channel source and hence it can be expected that complete lateral mixing downstream of confluences will happen over 10s to 100s of kilometers of large rivers. This inference is consistent with most empirical research on mixing downstream of confluences in large rivers where the two flows

remain unmixed for hundreds of channel widths downstream of the confluence (Bouchez et al., 2010; Kabeya et al., 2008; Krouse and Mackay, 1971; Laraque et al., 2009; Mackay, 1970; Matsui et al., 1976; Rathbun and Rostad, 2004; Stallard, 1987). However, recent work has shown that rapid mixing can occur at large river confluences if local conditions within the confluence promote strong near-field mixing (Lane et al., 2008), but that these conditions may be specific to particular hydrological relations between the tributaries and that slow mixing also occurs at the same confluence.

The constant coefficient model has been used mostly only to get a rudimentary estimate of mixing because it is too simplified to be useful for most real-world cases. It assumes that the flow is completely uniform, and velocity and the transverse dispersion coefficients do not change laterally and longitudinally. Besides the shortcomings, equation (2.4) allows us to determine k_z for the visually observed mixing length albeit with some uncertainty.

2.3.2 Streamtube method

Natural rivers are irregular features where bathymetric irregularities cause non-zero depth averaged transverse velocity resulting in transverse dispersion of tracer cloud. The most famous of all models is the streamtube model developed by Yotsukura and Sayre, (1976) for non-uniform channels. This method requires measurements of cumulative flow distribution at each transect which can be obtained by using ADCP. For a steady tracer source in steady river flow, the rate of change of tracer and longitudinal terms from conservation of mass equation in curvilinear coordinates can be dropped and the equation is reduced to

$$\frac{\partial c}{\partial \alpha} = \frac{\partial}{\partial q}\left(m_\alpha h^2 u_\alpha k_\beta \frac{\partial c}{\partial q}\right) \tag{2.5}$$

where α and β are coordinates in curvilinear system and are parallel and orthogonal to the mean depth average longitudinal velocity respectively, q is the cumulative discharge, h is the

local flow depth, m_α is a metric coefficient included in equation to account for channel curvature (1.0 for straight channel, while 0.8-1.2 for meandering channels), u_α is the local depth averaged longitudinal velocity, and k_β is local transverse dispersion coefficient. The product of different terms in equation (2.5)

$$D(\alpha, q) = m_\alpha h^2 u_\alpha k_\beta \tag{2.6}$$

is called factor of diffusion and has units m^5s^{-2}. Lau and Krishnappan, (1981) found that the variation in *D* across the channel was smaller than the variations in *D* along the channel. Based on this finding, the streamtube model can be simplified by assuming that D is constant across the channel. At a location within a channel, curvilinear coordinates α and β can be aligned with Cartesian coordinate x and z, with x pointing along the channel and z across the channel. Equation (2.6) can be rewritten as

$$D = \psi H^2 V_x k_z \tag{2.7}$$

where *H* is the mean flow depth and V_x is the mean flow velocity and ψ is a dimensionless shape factor whose value ranges between 1.0 and 3.6 (Beltaos, 1980; Sayre, 1979). Several studies have concluded that *D* can also be treated as constant along the channel (Holly, 1985; Sayre, 1979; Yotsukura and Cobb, 1972), which yields the simplified streamtube model

$$\frac{\partial c}{\partial z} = D \frac{\partial^2 c}{\partial q^2} \tag{2.8}$$

As the transverse tracer flux at both banks is zero and *D* is constant, $\frac{\partial c}{\partial q} = 0$ for q = 0 and q = Q. Sinuosity and irregularities in the bathymetry of natural rivers means that the value of shape factor ψ changes over distance and therefore it is recommended that *D* be estimated at multiple locations within a river to calculate a reach averaged value of *D*:

$$D = \frac{1}{L}\sum_{i=1}^{N} D_i \, \Delta x_i \tag{2.9}$$

where L is the total reach length, N is the total number of reach segments, and D_i and Δx_i are factor of diffusion and length of the subsection respectively. Similar to equation (2.4), the streamtube method can also be used to estimate mixing length. For center discharge to achieve 98% mixing

$$L_z = 0.536\frac{Q^2}{D} \tag{2.10}$$

The biggest advantage of streamtube model is that it does not require measurements of transverse velocity v_β and yet accounts for the transverse movement of water. The simplified form of streamtube model, which assumes that the factor of diffusion remains constant across the channel, provides a useful tool for preliminary estimations of tracer concentrations in irregular rivers. However, application of the model based on the assumption of constant diffusion overestimates transverse mixing rates for tracers released close to the bank.

2.3.3 Uniform flow method

Another field method to calculate transverse diffusion coefficient is determining the rate of change of spatial variance of tracer concentrations with time.

$$k_z = \frac{1}{2}\frac{d}{dt}(\sigma_z^2) \tag{2.11}$$

Equation (2.11) requires that the channel must be uniform, the tracer source should be steady, and the tracer should not impinge on the banks. Another important requirement is that the tracer dispersion must obey Fick's law. With these conditions, plume velocity does not change and the variance in the transverse direction increases linearly with time. Equation 2.11 can therefore be written in the finite difference form

$$k_z = \frac{1}{2} u_x \left(\frac{\sigma_z^2(x_2) - \sigma_z^2(x_1)}{x_2 - x_1} \right) \quad (2.12)$$

Where u_x is the longitudinal velocity and is constant and variance σ_z^2 can be estimated by the relation;

$$\sigma_z^2 = \frac{1}{4}(z_{0.84} - z_{0.16})^2 \quad (2.13)$$

where $z_{0.84}$ and $z_{0.16}$ are the transverse distances where tracer concentrations are 0.84 and 0.16 respectively. A major limitation of the uniform flow method, other than the strict requirements discussed above, is the requirement of measuring tracer concentrations over entire transect. Concentration measurements near the edges of the plume are very difficult to obtain as the tracer concentrations are small and may not be detected with field instruments.

2.4 Flow structure at confluence

Confluences are important features of all drainage basins not only due to their role in shaping river morphology but also in computation of flood routing as well as dispersal of pollutants. Confluences are divided into two broad types; symmetric confluences ('Y' shaped) and asymmetric confluences ('y' shaped) based on their planform geometry. The confluence hydrodynamic zone (CHZ) is a zone within vicinity of confluence where hydrodynamic conditions are affected by interaction of converging flows (Kenworthy and Rhoads, 1995). The CHZ has the following distinct zones (Figure 2.1); (1) a zone of relative flow stagnation at upstream junction corner, (2) flow deflection zone at the entrance of each stream, (3) flow separation zone/s below the downstream junction corner, (4) flow acceleration zone where velocity is maximum, (5) a zone of flow recovery, (6) and a shear layer – a zone of elevated levels of turbulence that develops due to transverse velocity gradient between converging flows (Best, 1988). The mixing interface – defined by lateral gradient in conservative property,

coincides with the shear layer within CHZ, but may not be identical to the shear layer as it can persist for long distances downstream of the confluence, well beyond the downstream limits of increased turbulence associated with fluid shear (Rhoads and Sukhodolov, 2008). The position, spatial extent, and the nature of the flow within these zones are controlled predominantly by planform symmetry (θ_2/θ_1: ratio of angles between each channel's centerline and receiving channel's centerline), junction angles (orientations of incoming flows), momentum ratios ($M_r = \frac{\rho_t Q_t U_t}{\rho_m Q_m U_m}$), where subscripts *t* and *m* are for tributary and main channel respectively), and bed morphology (concordance/ discordance; i.e. whether flows meet at same bed height or different) (Best, 1987; Mosley, 1976; Rhoads and Kenworthy, 1995; Rhoads and Sukhodolov, 2001).

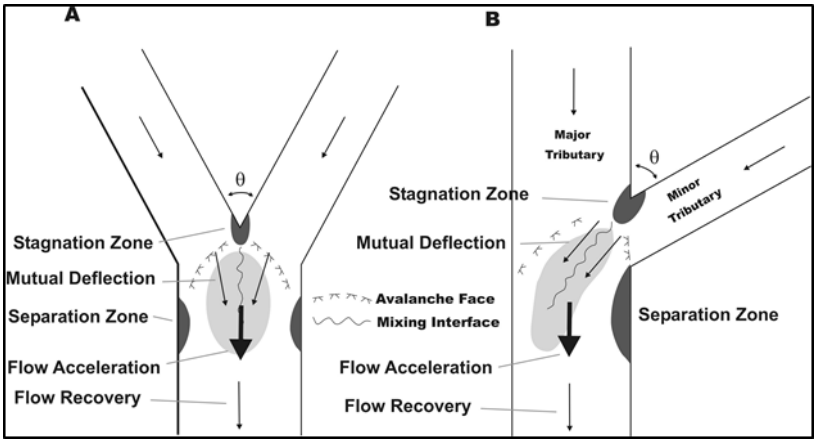

Figure 2.1: Major zones within the CHZ, (A) Symmetrical confluence, (B) Asymmetrical confluence

Flow stagnation zone is a zone at the upstream junction corner. This zone is created as a result of mutual deflection of flows downstream of this zone (Best, 1987). Flow velocities and shear stresses are low in this zone therefore fine sediments can be deposited here which may result in a bar formation. In case of asymmetric confluences, with any increase in discharge ratio or junction angle, the deflection of flows increases, increasing the size of the stagnation zone. Downstream of the stagnation zone, the shear layer, or mixing interfaces forms between the two confluent flows where significant flow turbulence and vortices entrain sediment and scour the

bed. The shear layer is marked by large scale coherent turbulent structures. When two flows meet at confluence, both flows are mutually deflected and curve to align with the orientation of the receiving channel. Turning of flows can produce the same effect as curvature in meandering rivers. Super elevated flow at the mixing interface produces a second force, pressure gradient in the opposite direction. This force is weak compared to centrifugal force where velocities are higher (at surface) and strong where velocities are lower (near the bed). Centrifugal force directs water at the surface towards the outer bank while the pressure gradient force directs flow towards the inner bend creating a spiraling pattern of fluid motion. This pattern of flow in combination with dominant downstream flow generates a helical cell.

Another major feature at a confluence is separation zone which forms at the downstream junction corner if the tributary joins at sufficient angle with fast enough flow to detach from the bank (Best and Reid, 1984; Rhoads and Kenworthy, 1995). Flow separation zone constricts the post confluence channel width. Like the stagnation zone, the size of separation zone is also a function of discharge ratios and junction angles. The width of this zone increases in proportion to the discharge ratio and junction angle. Flow at this zone is recirculating with velocities usually only a fraction of those characterizing the adjacent freestream flow. This flow recirculation promotes deposition of finer particle from suspension. Upstream-directed ripples may also be found in this region when flow recirculation is strong. This zone is a region of low water surface elevation and low fluid pressure. Separation zone bars are most clearly present in small channel confluences, but they may be absent in large river confluences.

Downstream of the separation zone, flow accelerates creating the zone of maximum downstream velocity. Sediment transport accelerates in response to higher velocities and hence scour of the bed often occurs in the flow acceleration zone. Acceleration occurs in response to

narrowing of channel width compared to the combined widths of the individual upstream channels and to the development of flow recirculation. Farther downstream flow recovers as the influence of the confluence on flow structure diminishes.

2.5 Lateral mixing at confluences

Detailed reviews by Fischer et al., (1979) and Rutherford, (1994)on transverse mixing of tracers in open channels demonstrates that the lateral mixing in rivers is well understood. A tracer released into the river is mixed across the width of the channel by molecular diffusion, turbulent diffusion, and advection (Rutherford, 1994). Molecular diffusion, a function of concentration gradient, is generally ignored in rivers because of its minimal effect on mixing as compared to the turbulent mixing. Turbulent diffusion is a function of flow and varies with varying velocities due to the turbulence in the flow. Turbulence in natural rivers deforms the tracer cloud, resulting in increased local concentration gradients which according to Fick's law is a main factor in promoting molecular diffusion. Advection of fluid is the mass transport due to the motion of the fluid in three dimensions, e.g. secondary currents.

Flow structure within the CHZ controls the amount of mixing between converging flows, which has implications for water quality downstream of the confluence as well as for channel change by erosion and deposition. Within the CHZ three factors affect the "near-field" mixing of confluent flows: 1) the development of a shear layer between the flows, 2) secondary flows, including helical motion, associated with flow curvature and 3) bed discordance, or the effects produced by a difference in elevation (i.e. a "step") between the bed of the lateral tributary and the bed of the main channel at the confluence.

The development of a shear layer between the converging flows is coincident with the development of a mixing interface (Best, 1987). The mixing interface and shear layer coincide in

the near field regions (CHZ) and can be used interchangeably (Rhoads and Sukhodolov, 2008). However, turbulent eddies generated by shear usually exist only within a short distance downstream of the confluence. Farther downstream the shear layer disappears, leaving turbulent diffusion with the bulk flow as the only dominant mixing process. In the absence of any secondary current due to channel curvature, the mixing interface can persist over many hundreds of kilometers (Bouchez et al., 2010; Krouse and Mackay, 1971; Laraque et al., 2009; Mackay, 1970; Rathbun and Rostad, 2004). In this case, the spatial extent of the shear layer is not necessarily the same as the spatial extent of the mixing interface (Sukhodolov and Rhoads, 2001).

Large-scale secondary circulation, which enhances advective mixing, can arise from flow curvature within the CHZ as incoming flows mutually deflect one another and become aligned with the orientation of the downstream channel (Ashmore et al., 1992; Rhoads, Bruce, 1996; Rhoads and Kenworthy, 1998, 1995; Rhoads and Sukhodolov, 2001). Bed discordance, or unequal bed elevations of the tributaries, can also have a strong influence on mixing within the CHZ by distorting the shear layer and generating secondary flows (Best and Roy, 1991; Pascale Biron et al., 1996; Boyer et al., 2006; De Serres et al., 1999). Bed discordance can increase mixing rates 5-10 times above those expected without discordance (Best and Rhoads, 2008; Gaudet and Roy, 1995). Both field studies and numerical modeling indicate that these three factors strongly affect rates of mixing at small confluences with the two flows often mixing completely a few channel widths downstream of the confluence (Biron et al., 2004; Gaudet and Roy, 1995; Kenworthy and Rhoads, 1995). However, channel scale secondary flows and significant avalanche faces are often absent or limited in large river confluences (Parsons et al.,

2007; Szupiany et al., 2007) and hence, secondary flows and bed discordance may not be a significant factor in controlling mixing lengths for large confluences.

Mixing at confluences can be further complicated by the density differences between the incoming flows. Density differences due to differences in SSC or temperature of the two flows can lead to flow interpenetration in to one another. With strong density contrast, buoyant, less dense fluid may spread over the denser fluid across the channel resulting in faster mixing (Lewis and Rhoads, 2015a; Rhoads and Kenworthy, 1995; Rutherford, 1994)s. However, strong density differences are not very common in large river confluences.

Most of the current studies of transverse mixing focus on field studies where data are collected at a few (<5) widely spaced cross sections downstream from a small river confluence (Gaudet and Roy, 1995; Kenworthy and Rhoads, 1995; Rhoads and Sukhodolov, 2001; Sukhodolov and Rhoads, 2001). These studies indicate that mixing occurs within a few channel widths downstream of the confluence due either to the effects of bed discordance or to strong advective effects associated with helical motion generated by flow curvature. The results of these studies are not scalable from small confluences to the large confluences because width increases faster than the depth, making width-depth ratio of small confluences much smaller than that of large confluences (Lane et al., 2008; Leopold and Maddock, 1953; Parsons et al., 2007; Rhoads, 2006). Channel geometry differences between small and large confluences may influence large scale helical motions and the turbulent flow structures, affecting mixing (Rhoads, 2006). Studies at large river confluences have received relatively little attention. Even fewer studies have examined mixing over a range of flow conditions, so our knowledge of lateral mixing processes is not complete.

2.6 Summary and relation to conducted research

The influence of complex 3-D processes within CHZ on lateral mixing at large rivers is not fully understood. Although semi-theoretical models and flume and field experiments have advanced our understanding of mixing dynamics, these studies cannot be extrapolated beyond the hydrological conditions in these investigations. Thus, there is a need for development of a method that can yield a wealth of information on length scales and rates of mixing in large river systems, thereby improving our understanding of this important water-quality process. Satellite remote sensing has the potential to fill the necessary water quality information gap because of its capacity to provide wide areal coverage at regular intervals. Many studies have demonstrated the capacity of empirical approach in providing reliable information of water constituents for inland waters. Chapter 3 develops a method on using remote sensing data to provide new ways of studying mixing downstream of large river confluences.

Chapter 4 makes use of the methodology developed in previous chapter to investigate the influence of different potential controlling factors on the mixing lengths. Surficial patterns of mixing have been observed within CHZ, 30 channel widths, and 110 km downstream of the confluence along with in longitudinal variations in channel widths. Chapter 5 describes a methodology to compute mixing lengths using a streamtube model and compares predicted lengths with lengths determined empirically in Chapter 4.

CHAPTER 3: USE OF BROAD-BAND SATELLITE REMOTE SENSING TO ASSESS MIXING OF SUSPENDED SEDIMENT DOWNSTREAM OF LARGE RIVER CONFLUENCES

3.1 Introduction

The transport of suspended sediment and associated nutrients or contaminants within river systems plays an important role in watershed processes. These material fluxes influence water quality, habitat conditions, biogeochemical cycles, and channel morphodynamics (Beschta et al., 1987; Doxaran et al., 2009, 2002a). The transport of suspended sediment within large river systems traditionally has been evaluated by obtaining measurements of sediment concentrations at gaging stations (Edwards and Glysson, 1999). This approach, while useful, does not permit evaluations of spatial variability in SSC within a river system. Such variability is often pronounced, especially at and downstream of river confluences.

Confluences are important sites for mixing within river systems. At these locations, flows with potentially different physical and chemical properties converge and begin to mix. Within and downstream of a confluence, a mixing interface, defined by an abrupt lateral contrast in turbidity, conductivity, or temperature (Gaudet and Roy, 1995; Konsoer and Rhoads, 2013; Rhoads and Kenworthy, 1995; Rhoads and Sukhodolov, 2008) typically exists between the two confluent flows. This interface is visible at the surface if the two flows have a pronounced contrast in turbidity. The mixing interface can either dissipate over a short distance downstream of the confluence if the two flows mix rapidly (Lane et al., 2008) or persist for long distances downstream of the confluence if the two flows mix slowly (Bouchez et al., 2010; Mackay, 1970). The efficacy of transverse-mixing processes largely determines the quality of water downstream of a confluence.

Mixing of suspended sediment downstream of confluences has not been extensively studied. Past work investigating this issue in small streams has relied on manual collection of samples using a depth-integrated sampler (Kenworthy and Rhoads, 1995). Such an approach is time-consuming and only suitable for wadeable streams. In large rivers, suspended sediment concentrations are typically measured using heavy reel-mounted samplers deployed from a bridge, cableway, or boat (Diplas et al., 2008; Edwards and Glysson, 1999). Access to confluences is limited, particularly when measurements are obtained from bridges, as is most often the case. More recently, acoustic methods have been used to estimate suspended sediment concentrations in rivers (Guerrero et al., 2016; Szupiany et al., 2012). All such methods perform well for determining the distribution of suspended sediments within individual cross sections at a particular time. However, the capacity of such methods to characterize spatial and temporal variations of SSCs over long distances is limited. Patterns of mixing downstream of confluences can occur over varying lengths from a few channel widths to lengths as long as several hundred channel widths depending on different controlling factors. To characterize these patterns, new methods are needed that can provide detailed information on the spatial distribution of SSCs at large temporal and spatial scales. Such observations are crucial for understanding the dynamics of mixing downstream of confluences in large river systems.

An alternative method for evaluating water quality conditions at and downstream of confluences is to use remote sensing techniques. Satellite remote sensing, with synoptic coverage and consistency of temporal data, provides an ideal platform with which to study processes at large spatial and temporal scales. The estimation of SSSCs from remotely sensed imagery can be realized through an empirical approach that relates water quality parameters directly to spectral properties using various empirical modeling techniques. Many studies have linked turbidity and

SSSCs in lakes or estuaries to spectral indices (Cox et al., 1998; Dekker et al., 2002; Duan et al., 2009; Hellweger et al., 2004; Kallio et al., 2008; Kloiber et al., 2002; Lathrop, 1992; Lavery et al., 1993; Odermatt et al., 2012; Olmanson et al., 2008; Pattiaratchi et al., 1994; Wu et al., 2008). However, past studies are limited to specific ranges of SSSCs found within a particular water body, which may not work well for rivers where concentrations can vary substantially both spatially and temporally.

Thus far, few studies have used remote sensing to explore SSSCs in inland rivers (Matthews, 2011), mostly because of complexities associated with substantial variability in concentrations; the constrained spectral, spatial, and radiometric resolution of sensors for relatively narrow linear features like rivers; and inherent optical properties (IOPs) of SSSCs (Hestir et al., 2015; Lymburner et al., 2016; Odermatt et al., 2012). Recent work has shown that SSSCs in rivers can be detected at relatively high levels of accuracy based on empirical models that incorporate data from broadband sensors like Landsat (Matthews, 2011), but the challenge is to develop a model that can estimate SSSC equally well over a wide range of concentrations.

The goal of this chapter is to present a method based on multispectral remote sensing imagery for characterizing in detail spatial patterns of SSSCs in large rivers and to illustrate how the method can be used to assess surficial lateral mixing of suspended sediment at and downstream of large river confluences. The method yields a wealth of information on length scales and rates of surficial mixing in large river systems, allowing spatial variation in mixing to be examined at an unprecedented level of detail, thereby improving our understanding of this important water-quality process.

3.2 Study area

To develop the methodology for analyzing mixing at and downstream of large river confluences using remote sensing, a reach beginning at the confluence of the Mississippi and Missouri Rivers and extending 110 km downstream was selected for analysis (Figure 3.1). The watershed of the Mississippi River basin upstream of the confluence of the Mississippi and Missouri rivers drains an area of about 1,800,000 km^2 with the drainage area of the Mississippi River equal to 500,000 km^2 and the drainage area of the Missouri River equal to 1,300,000 km^2. Although the Missouri River has a substantially larger drainage area than the Mississippi River, its mean annual discharge at the confluence is substantially less than that of the upper Mississippi River. However, the mean SSSC of the Missouri River (395mg/l) is over twice as large as the mean SSSC of the Mississippi River (140mg/l) (Table 3.1).

Table 3.1: Physical and hydrological characteristics of Mississippi and Missouri Rivers upstream of the confluence (Carlston, 1969).

	Mean Annual Discharge (m^3/s)	Mean Annual SSC (mg/l)	Slope	Length (km)
Mississippi River	3,600	140	0.000086	1,700
Missouri River	2,265	395	0.00017	3,620

Both the Mississippi and Missouri rivers have been subjected to extensive anthropogenic modifications over the past 150 years for purposes of flood control and commercial navigation. Alterations include, but are not limited to, impoundments, construction of levees, deepening of the channel, and construction of lock and dams. These modifications, along with major changes in conservation practices in the watersheds of these rivers, have generally produced declines in the suspended sediment loads of the Mississippi and Missouri rivers since 1950 (Heimann et al. 2011).

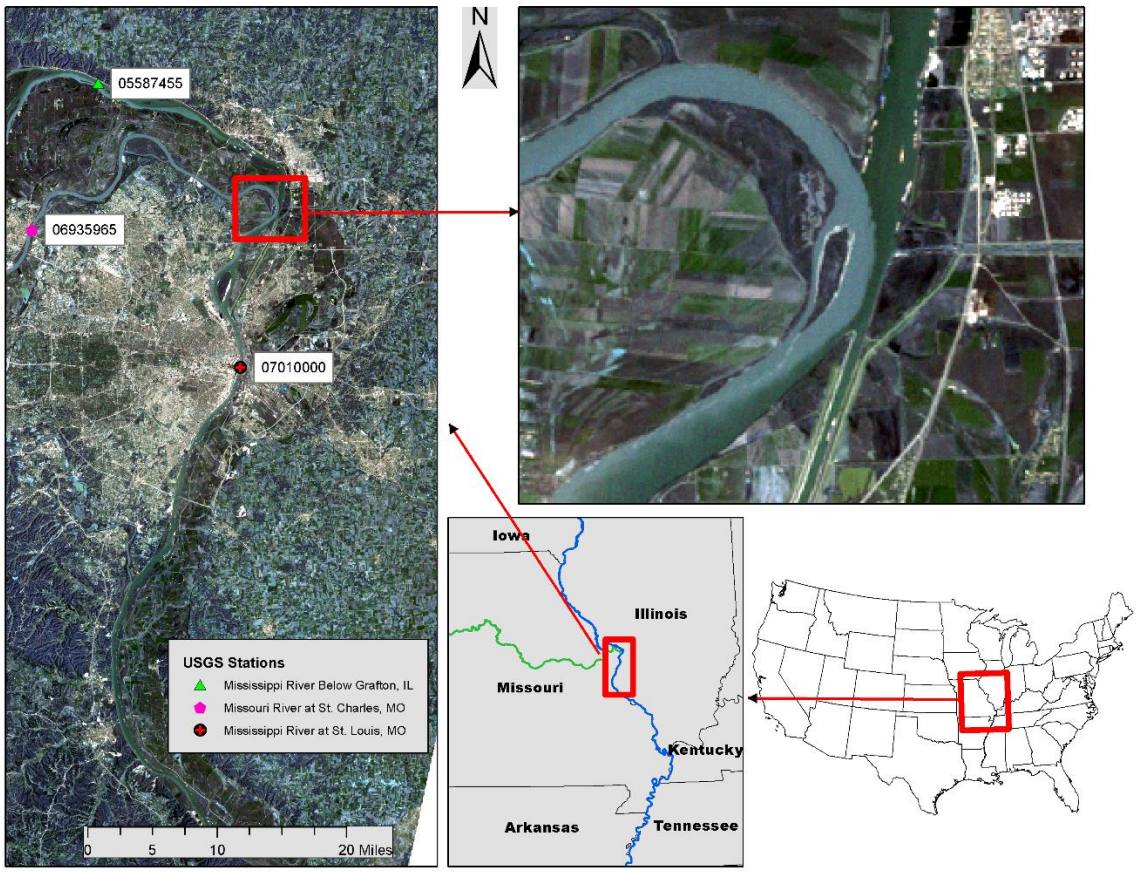

Figure 3.1: Confluence of the Mississippi and Missouri rivers at Illinois-Missouri border. Locations of USGS stations upstream and downstream of the confluence are shown along with station numbers

3.3 Methodology

The methodology for examining mixing downstream of river confluences involves development of an empirical model for predicting SSSC concentrations of each river pixel in a remotely sensed image and development of a model for spatially averaging the SSSC data based on geographical and geometrical characterization of the river channel (Figure 3.2). SSSC modeling focuses on the use of satellite imagery and Random Forest (RF) analysis to develop an empirical model for predicting SSSCs from spectral information. Spatial averaging focuses on spatial representation of the river system along the path of the river for the purpose of determining spatial variation in SSSCs over discrete segments of the river system. The

combination of these two methodological components leads to estimates of an index of mixing, which can be mapped over the entire reach of the river downstream of the confluence.

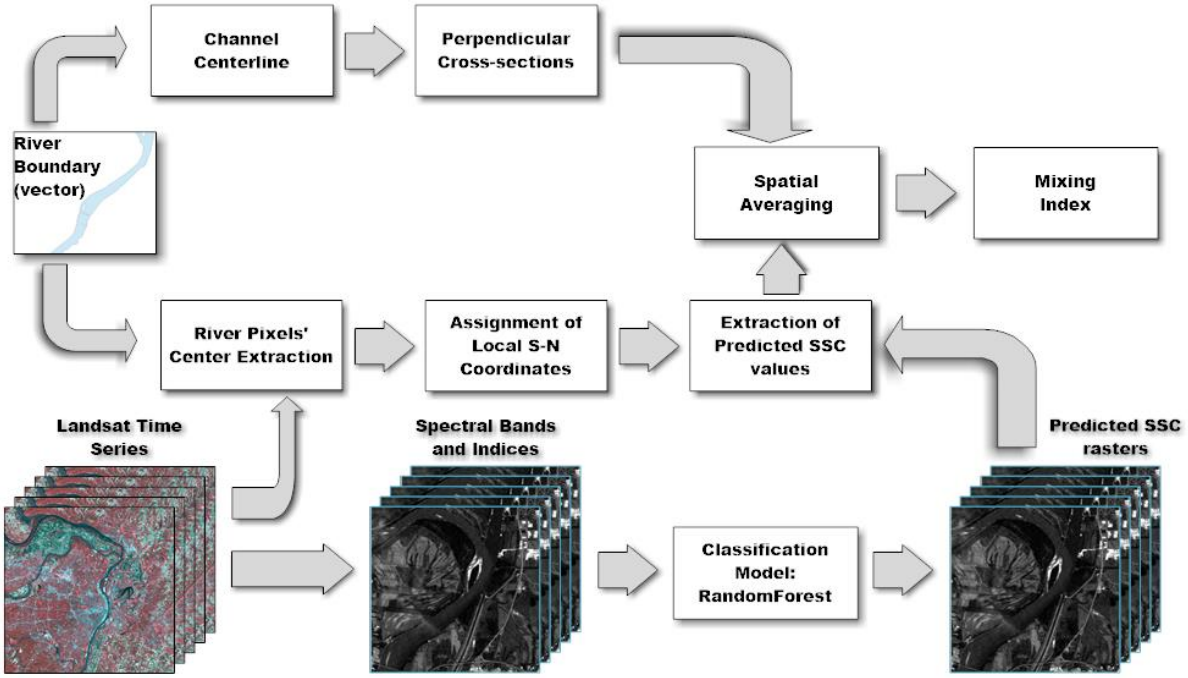

Figure 3.2: Flowchart of the methodology.

3.3.1 Development of an empirical model of surficial SSC

3.3.1.1 Image data

Landsat 5 Thematic Mapper (TM) imagery of the study reach collected between 1985 and 2011 were used as input data for development of a model to estimate values of SSSC. Landsat 5 was selected because of its extensive historical availability, a spatial resolution conducive to mapping large rivers (30m ground sample distance), and sufficient spectral information for performing SSSC mapping (Matthews, 2011). The imagery was calibrated to surface reflectance using the Landsat Ecosystem Disturbance Adaptive Processing System (Masek et al., 2013). Only 100% cloud free imagery was used in model development, resulting in an input dataset of 143 images over 26 years.

3.3.1.2 Discharge and suspended sediment data

Data on discharge and suspended sediment concentrations in the Mississippi River and Missouri River were obtained from U.S. Geological Survey river gaging stations located within the study reach (Figure 3.1). The discharge data provide information on the relative strength of the flows at the confluence and the SSC data are required to calibrate and test the predictive model of SSSC using spectral data from satellite imagery. Daily discharge data are available for Mississippi River at Grafton, IL (upstream of the confluence) and at St. Louis, MO (downstream of the confluence) for the period 1985 to 2011. The St. Charles station (USGS station 06935965, Figure 3.1) on the Missouri River started collecting discharge data in 2000.

USGS stations that provide SSC data are categorized as either daily or periodic stations, defined by the frequency and number of samples collected. USGS SSC data collection procedures follow methods described by Edwards & Glysson (1999). For daily stations, vertical samples are collected once each day at a single location. Single location data are adjusted on the basis of multi-vertical samples collected less frequently at 5 to 10 additional locations across the channel using either equal discharge increment (EDI) or equal width increment (EWI) method (Edwards and Glysson, 1988). Final computations of SSC are performed using the method described by Porterfield (1977).

Stations on Mississippi River upstream (Grafton, IL) and downstream (St. Louis, MO) of the confluence are daily SSC stations where sufficient discharge and SSC data are collected to produce reliable daily SSC values. The daily data at St. Louis station are available for the entire period of analysis, whereas SSC data were collected at the Mississippi River station (05587450) from 1989 to 2011. SSC data are also available for the Missouri River station at St. Charles (06935965) for three years beginning in October 2005 (Table 3.2).

Table 3.2: Summary of available SSC data and basic statistics at the three USGS stations within the study reach

Station No.	Location	Period of record	SSC (mg/l)		
			Min	Max	Std. dev
05587455	Mississippi River below Grafton, IL	1989-10-12 to 2014-09-30	26	6720	497
06935965	Missouri River at St. Charles, MO	2005-10-01 to 2008-09-30	25	882	88
07010000	Mississippi River at St. Louis, MO	1980-10-01 to 2014-09-30	82	3560	421

3.3.1.3 Channel edge and centerline

Edges of water of the river digitized for each image in ArcGIS provided the basis for masking the images so that only pixels consisting entirely of water were included in boundary delineation of the river; pixels that included land or a mixture of water and channel banks were excluded from the analysis. Using the right and left edges of water, a centerline along the river downstream of the Missouri-Mississippi confluence was created with Planform Statistics Tool developed by National Center for Earth-Surface Dynamics (NCED) in University of Minnesota (https://repository.nced.umn.edu/browser.php?current=keyword&keyword=5&dataset_id=15). The tool uses the right and left edges of water to establish evenly spaced river centerline points at user-defined intervals. Centerline vertex locations were saved as text file as well as an ESRI shapefile. A MATLAB program, PCS Curvature, developed by Güneralp & Rhoads (2008) was used to fit piecewise cubic splines (PCS) to the centerline points to provide a continuous representation of the channel centerline. This program can also determine the coordinates of endpoints of cross sections oriented orthogonal to the channel centerline at user-specified intervals. In this study, orthogonal cross sections were established at a spacing of 500 m beginning at the confluence of the Missouri and Mississippi Rivers and extending 110 km to the downstream end of the study reach.

3.3.1.4 Modelling SSSC

In this study, SSSC was modeled as a function of the non-thermal Landsat bands and spectral indices using a Random Forest ("RF") regression model (Liaw and Wiener, 2002). RF, a machine learning algorithm, is relatively insensitive to noise and outliers, and is effective at predicting responses for relationships that may be nonlinear or contain interaction effects (Breiman, 2001; Cutler et al., 2007; Rodriguez-Galiano et al., 2012). A training and testing database was constructed by identifying the pixels for each of the 143 Landsat images that correspond to the locations of the three USGS stations with SSC data. If sediment data were available for all three gaging stations for the complete set of 143 images, a dataset of n = 429 would have existed for model development and calibration. Because sediment data were not available for all three stations for all images, the total number of cases for model development and calibration was n = 271. For each image acquisition date, the USGS gaging station SSC measurement for the same date, if available, was determined, and reflectance values for different spectral bands of the pixel at the position of the gaging station were linked to the SSC measurement. In addition to the reflectance values, the SSC measurement was also related to a set of indices that have been found to be useful in predicting SSSC (Table 3.3).

A RF model was developed by randomly selecting half of the dataset (n = 136) as training data. The resulting model consisted of 8,000 trees and had mtry value of 5. The model was developed in R using the raster package for working with raster datasets, the spatial.tools package for parallel raster processing, and the randomForest package for modeling (Jonathan, 2014; Liaw and Wiener, 2002; Robert, 2016). The model was tested by applying it to the remaining half of the dataset (n = 135), and calculating the root mean square error (RMSE), mean absolute error (MAE), Pearson's R, and percent bias of predicted versus observed values. Both the training and test datasets had similar statistical characteristics. The mean SSSC of the

training dataset was 219 mg/l with a range of 19 mg/l to 1700 mg/l, whereas the mean SSSC of the test dataset was 213 mg/l with a range of 34 mg/l to 1270 mg/l.

Table 3.3: Spectral indices for water constituent concentrations retrieval from medium resolution multispectral sensors

Algorithm	Water quality parameter	r^2	Reference
(Green + Red)/2	TSS	0.99	Dekker et al., 2002
Blue/Red	Secchi depth	0.71-0.92	Kallio et al., 2008; Kloiber et al., 2002
Green/Red	TSS	0.88	Sváb, Tyler, Preston, Présing, & Balogh, 2005
Red/Green	Turbidity, Secchi depth	0.93, 0.91	David Doxaran, Froidefond, & Castaing, 2003; Duan et al., 2009
NIR/Green, NIR/Red	TSS	0.67-0.88	D. Doxaran, Castaing, & Lavender, 2006; David Doxaran et al., 2003
Red/Blue + Blue	Secchi depth		Kloiber et al., 2002
Red/Green + NIR	TSS	0.93	Lathrop & Lillesand, 1989

3.3.2 Spatial averaging of SSSCs and quantification of mixing

3.3.2.1 Spatial representation of river cross-sections

Quantification of mixing from the model predicted SSSC rasters involves several steps aimed at generating spatially distributed data that can be used to compute spatially averaged values of SSSCs downstream of the confluence. The first step involved masking of the image data to limit the extent of the analysis to the water pixels within the river channel on all images and to store extracted raster pixel values for further analysis (Figure 3.2). The river centerline and transects orthogonal to this centerline provide the basis for coordinate transformation from geographic coordinates of each pixel (latitude, longitude) to local *s* (streamwise) and *n* (cross stream) coordinate system, a common frame of reference for meandering rivers (Legleiter and

Kyriakidis, 2007). The centroids of all pixels within the river were assigned *s* coordinates based on arc-length longitudinal distance from the upstream junction corner (*s* = 0) along the channel centerline (*s*-coordinate) and *n* coordinates based on the distance along transects orthogonal to the channel centerline (*n* coordinate) (Figure 3.3). The centerline has an *n* coordinate of zero; values of *n* to the right of the channel centerline (looking downstream) are positive, whereas values of *n* to the left of the centerline are negative. This coordinate transformation was achieved by calculating the Euclidean distance from a pixel to the centerline, which becomes the *n* coordinate of the pixel.

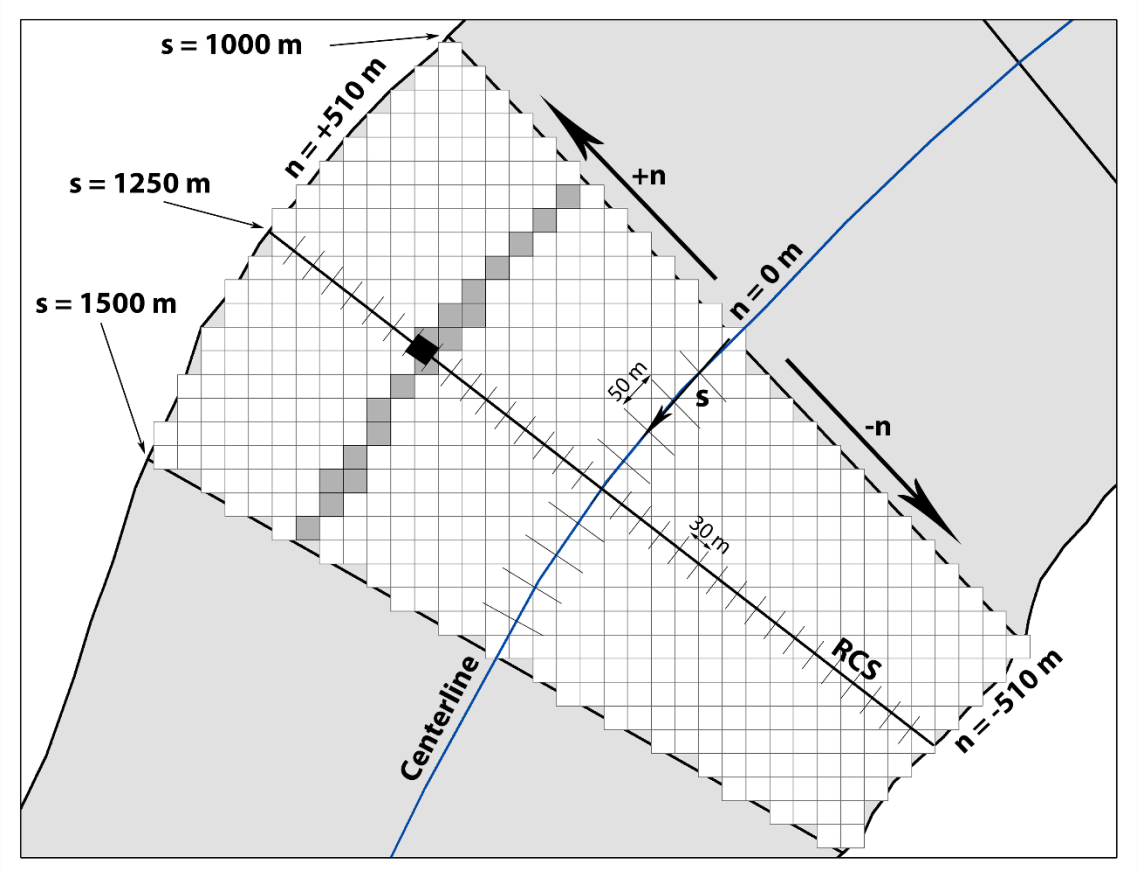

Figure 3.3: Example of s-n coordinate system for spatial averaging and mixing calculations. The shaded pixels represent the pixels with different s coordinates but standardized n coordinates that fall within the 30m interval on the representative cross section (R CS) denoted by the black rectangle. Values of SSSC for these pixels are averaged to produce a mean SSSC for the corresponding interval on the RCS (black rectangle).

3.3.2.2 Spatial averaging of SSSC

Spatial averaging is performed to reduce noise in SSSC values produced by spatial variations in spectral properties on the river surface associated with local variations in the turbidity of turbulent flow at the time the image was acquired. The area of the river within the study reach was divided into 500m long segments based on *s*-coordinate values such that a representative cross section (RCS) lies at the center of each segment (Figure 3.3). For example, if an RCS has an *s* value of 500m, the segment domain includes all locations with *s* values between 250m and 750m. This RCS is established to capture the mean characteristics of SSSCs within the entire 500 m long segment.

Each 500m segment region was divided into 10 subsegments, each with a length of 50m in the *s*-direction. For each image date, all SSSC pixels within this subsegment were extracted. The *n* coordinates of each pixel within the subsegments were normalized to the width of the RCS:

$$n_n = Pixel's\ n\ value \times \frac{Width\ of\ RCS}{Local\ Width\ of\ 50\ m\ \ subsegment} \tag{3.1}$$

Thus, if the width of the RCS and a subsegment are the same, the normalized and absolute *n* values of a pixels are identical. However, where the width of the river is not constant over the 500m block, the normalized and absolute n values differ. This normalization was performed to accommodate changes in width within a segment so that pixels near the bank in a subsegment project onto a position near the banks on the RCS. To determine the appropriate lateral position of each pixel projected onto the RCS, the RCS was divided laterally into evenly spaced 30 m bins. All pixels within the 500m segment with standardized *n* coordinates that lie within a particular 30m bin along the RCS were then determined (Figure 3.3). The mean of the predicted SSSC values for all of these pixels was computed and the average value was assigned to that

particular bin along the RCS. This process was completed for all 500m segments within the 110km study reach. The spatial averaging procedure produced cross sections spaced at 500 m intervals containing mean values of surficial SSSCs at 30m lateral intervals. These mean values represent average concentrations of SSSC along the cross sections as derived from SSSC values for all individual pixels within 500-meter swaths of the river centered on the cross sections.

3.3.2.3 Calculation of mixing metric

Most established indices of river mixing are not useful for determining the magnitude of mixing downstream of confluences because these indices do not adequately distinguish between mixed and unmixed cases when the initial contrast in tracer values of the confluent flows is low. A commonly used index of mixing is (Rutherford, 1994);

$$P_{mr} = \frac{X_{min}}{X_{max}} \tag{3.2}$$

where P_{mr} is mixing ratio and X_{min} and X_{max} are minimum and maximum values, respectively, of a tracer within a river cross section. An alternative metric (Yotsukura & Cobb, 1972) is:

$$P_m = 1 - \frac{1}{2}\int_0^Q \left|\frac{X}{\bar{X}} - 1\right| dq \tag{3.3}$$

where P_m is the percent mixing in a cross section, X is the local value of a local quantity of interest, $\bar{X}$ is the cross-sectionally averaged value of X and Q is the total discharge at the cross section. Both of these metrics are insensitive to initial differences in magnitudes of X, the quantity being mixed, between two confluent rivers. If two confluent rivers have small initial differences in values of X, the values of P_{mr} and P_m will be close to one immediately below the confluence, even if the two rivers have not mixed at all (i.e. values of X on one side of the mixing interface are consistently different than values of X on the other side of the mixing

interface). Ideally, a mixing index for a confluence should be evaluated in relation to the initial contrast in characteristics of X where the flows initially converge.

To accommodate shortcomings in previous mixing metrics, we developed a new model:

$$P_{mx} = 1 - \left[\frac{\frac{\sum_1^n |X_i - \bar{X}|}{n} - \left(\frac{\sum_1^a |X_{k1} - \hat{X}_1| + \sum_1^b |X_{k2} - \hat{X}_2|}{a+b} \right)}{\sum_1^m \frac{|X_{ju} - \bar{X}_u|}{m}} \right] \quad (3.4)$$

where P_{mx} is the percent transverse mixing in a cross section, X_i is the value of SSSC for a pixel in a cross-section downstream of the confluence, $\bar{X}$ is the mean value of X at the downstream cross-section, n is the number of pixels in the downstream cross section, X_{ju} is the value of SSSC for a pixel in the two cross sections upstream of the confluence – one cross section on each confluent river, $\bar{X}_u$is the mean of the pixels for the two cross sections upstream of the confluence, and m is the number of pixels in the two cross sections upstream of the confluence. The term $\frac{\sum_1^a |X_{k1} - \hat{X}_1| + \sum_1^b |X_{k2} - \hat{X}_2|}{a+b}$ is the mean initial variability in the upstream tributaries. This parameter accommodates the effect of inherent variability in the tracer values at cross sections upstream of the confluence. Here $\widehat{X}_1$ and $\widehat{X}_2$ are the mean values of X_k in tributaries 1, and 2 respectively, while a and b are total number of pixels in each tributary. The value of P_{mx} starts from 0 at the confluence and increases to a maximum value of 1 for fully mixed flow. However, due to the low radiometric resolution of Landsat imagery for water bodies, achieving $P_{mx} = 1$ may not be possible. Thus, values of $P_{mx} \geq 0.95$ are considered fully mixed. Plots of P_{mx} values over distance along the downstream channel provide information on spatial variations in the rate of mixing.

Using this index, spatial patterns and rates of transverse mixing of SSSC downstream of the confluence of the Mississippi and Missouri Rivers were calculated using the RF model and

the spatial averaging procedure for three test cases. These cases were selected based on differences in incoming flow conditions and spatial patterns of mixing downstream from the confluence. On March 30, 1998 (Case 1), both rivers had moderate levels of flow, but the discharge (Q), momentum flux ($M = \rho QU$, where ρ is density and U is mean streamwise velocity) and SSSC in the Missouri River exceeded Q, M, and SSSC in the Mississippi River (Table 3.4). On April 24, 1991 (Case 2), Q and M were nearly twice as large in the Mississippi River as in the Missouri River, but as on March 30, 1998 SSSC in the Missouri River was nearly three times the value in the Mississippi River. On September 26th, 2001 (Case 3), flows on both rivers were relatively low. Although the two rivers have nearly identical discharges, the momentum flux (ρQU) on the Missouri River was about four times the value of M on the Mississippi River due to the high velocity on the Missouri River. Again, the Missouri River had a much greater SSSC than that of the Mississippi River.

Table 3.4: Summary of important parameters for the three cases

	Date	Discharge		QR*	Momentum		MR*	SSSC (mg/l)		SR*
		MS	MO		MS	MO		MS	MO	
Case 1	Mar. 30, 1988	3540	4106	1.1	1998240	5850140	3	174	543	3.1
Case 2	Apr. 24, 1991	7957	3681	0.4	8981490	4501370	0.5	300	1010	3.3
Case 3	Sept. 26, 2001	1670	1900	1.1	459340	1954710	4.2	75	599	7.9

*QR is the flow discharge ratio, MR is the momentum flux ratio ($\rho_t Q_t U_t / \rho_m Q_m U_m$, where t and m stand for tributary and main channel respectively), and SR is SSSC ratio between tributary and the main channel.

3.4 Results

3.4.1 Accuracy of the SSSC predictions

Overall, the RF model predicts values of SSSC reasonably well in the Mississippi and Missouri Rivers (Table 3.5, Figure 3.4). The R value of the fitted model was 0.84. Linear

regression analysis between the test SSC data for the gaging stations, which were not used in model development, and the corresponding predicted SSSC values for these gaging stations shows a strong correlation ($R^2 = 0.7$), which is comparable to results ($R^2 = 0.78$) reported in a previous study aimed at predicting SSSCs from remotely sensed imagery in freshwater systems (Olmanson et al., 2008). The predictions have a net bias of -0.7%, underestimating slightly SSCs relative to the observed data. The pattern of bias varies with SSC magnitude. Predicted values of SSSC tend to be overestimated for concentrations < 200 mg/l and underestimated for concentrations > 200 mg/l (Figure 3.4). For high observed SSCs (>600 mg/l), variance of the SSSC data increases noticeably, a tendency observed with data on SSSCs derived from other spaceborne sensors like MODIS (Park and Latrubesse, 2014). Values of RMSE and MAE suggest that SSSC predictions should be interpreted cautiously when contrasts in SSSCs between the two rivers are small (< 100 mg/l).

Table 3.5: Statistical relationship between model predicted and observed SSC values at the USGS stations

Number of pairs	RMSE (mg/l)	MAE (mg/l)	Pearson's R	Percent bias
136	114.67	68.3	0.84	-0.7

The metric %IncMSE, which provides a measure of the importance of each variable included in the model, shows that the red to green ratio along with the near-infrared (NIR) and red bands are the most effective predictors of SSSC concentrations (Table 3.6). These findings are consistent with previous studies where high correlations (> 0.8) between predicted and observed data were reported using similar spectral bands and indices (Table 3.3) (Doxaran et al., 2003; Duan et al., 2009; Onderka and Pekárová, 2008; Wu et al., 2008).

Table 3.6: Predictor variables ranked by their importance in the prediction

	%IncMSE
Red/Green	58.26382
NIR	40.82293
Red/Green+NIR	39.9513
Red	32.27685
Red/Blue	29.71599
NIR/Green	23.78704
(Red+Green)/2	20.93913
NDVI	18.25673
Blue	13.7215
SWIR-1	13.62441
Red/Blue + Blue	13.09081
SWIR-1/Green	12.74095
Blue/Red + Blue	12.29001
Red/Green + Green	11.30311
SWIR-2	10.637
Green	10.05089

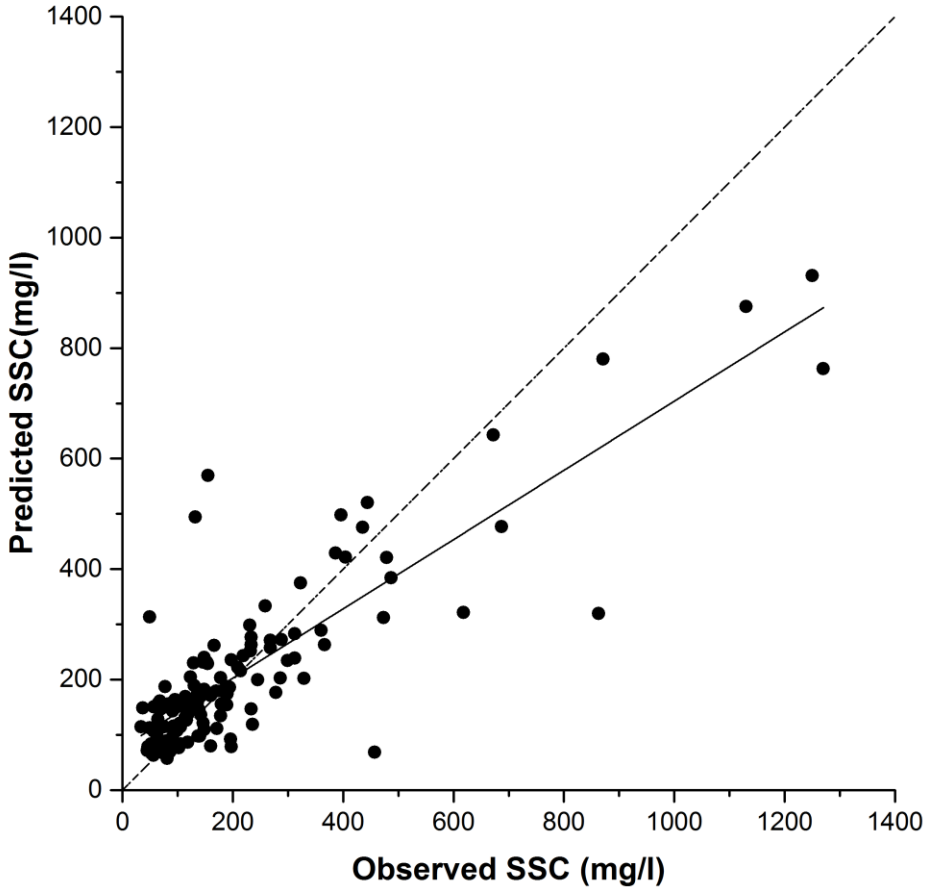

Figure 3.4: Plot of predicted versus observed SSC at gaging stations upstream (at Grafton) and downstream (at St. Louis) of the confluence of the Mississippi River and Missouri River confluence. Dashed line represents 1:1 relationship. Solid line is linear regression relation between predicted and observed values.

3.4.2 Patterns of SSSC for three test cases

Differences in patterns and rates of mixing for the three test cases illustrate the utility of the method for capturing spatial and temporal variations in lateral mixing downstream of confluences in large rivers.

3.4.2.1 Case 1: Rapid mixing

On March 30, 1988, the discharges in both rivers were nearly identical, but the Missouri River, with its higher velocities, had about three times the momentum of the Mississippi River (Table 3.4). The SSSC of the Missouri River was 543 mg/l, which was more than three times the

SSSC of the Mississippi River (174 mg/l). The map of contrast in SSSC indicates that high initial SSSC contrast across the channel at the confluence rapidly diminishes within few channel widths downstream on this date (Figure 3.5a). This case represents relatively rapid mixing.

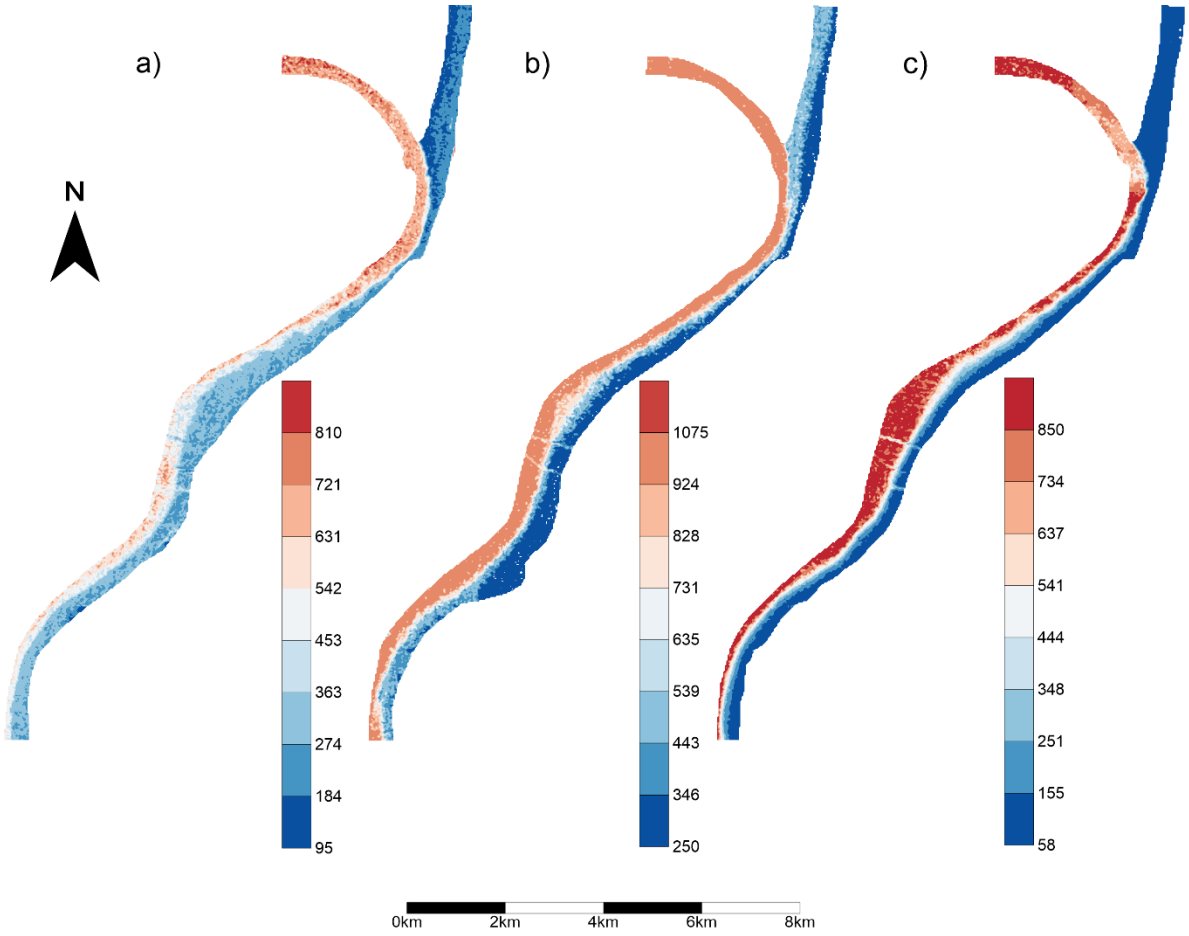

Figure 3.5: Maps of predicted surficial SSCs (mg/ l) over an initial 21 km section of the 110km study reach downstream of the confluence of Mississippi and Missouri Rivers (note difference in SSSC scales in each frame). Images were acquired on (a) March 30, 1988, (b) April 24, 1991, and (c) September 26, 2001. Mississippi River is on the right side while Missouri River joins in from the left (west).

Immediately downstream of the confluence (x = 0.5 km) concentrations on the Missouri River and Mississippi River sides of the confluence differ dramatically, indicating a lack of mixing (Figure 3.6). The pronounced gradient in SSSC between the two sides of the confluence marks the location of the mixing interface separating the confluent flows. The value of P_{mx} at this location (0.08) shows that little to no mixing has occurred relative to conditions upstream of the

confluence, where, by definition, $P_{mx} = 0$. The cross-sectional plots of reach-averaged SSSC reveal that the slope of the maximum contrast gradient delimiting the mixing interface remains near the center of the channel ($n_n = 0$) and rapidly diminishes downstream (Figure 3.6). Mixing is essentially complete ($P_{mx} >= 0.95$) 27.5 km downstream from the confluence. Mixing in this case results in a cross-sectional average value of SSSC that is more similar to that of Mississippi River upstream of the confluence than the average concentrations of two rivers upstream of the confluence.

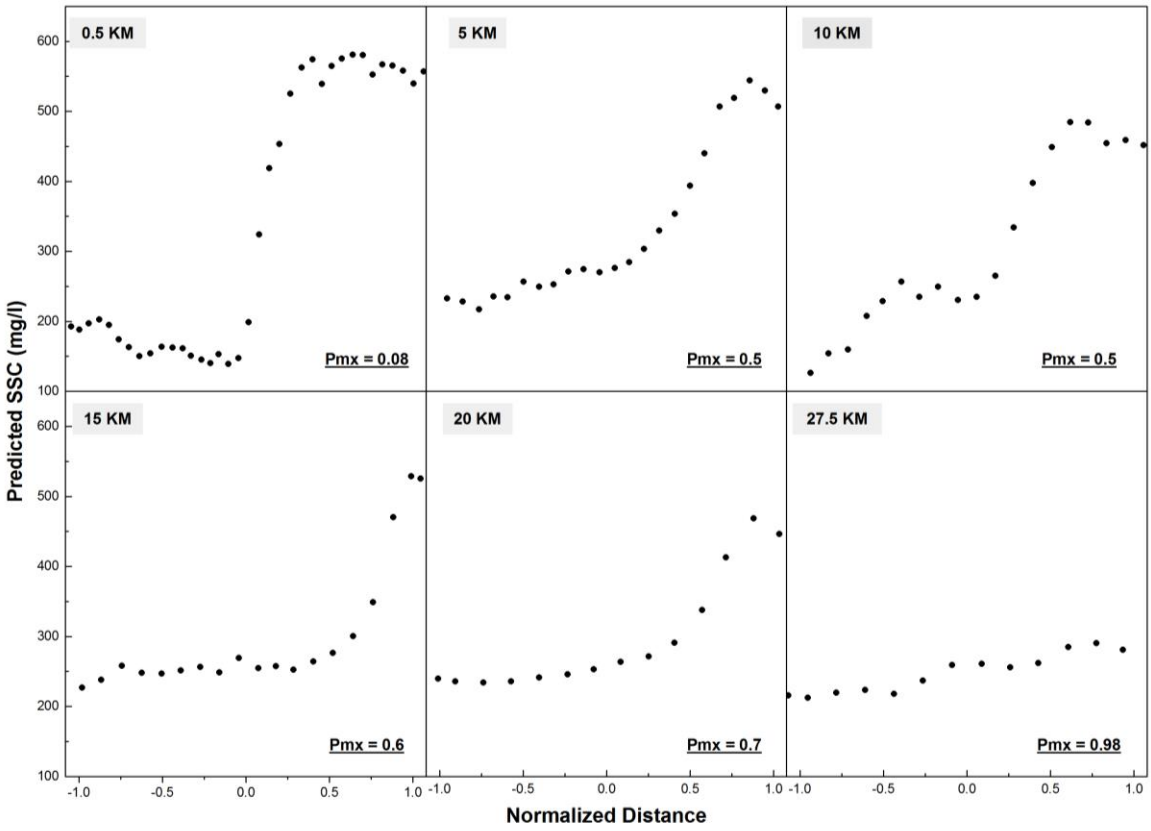

Figure 3.6: Cross-stream variations in SSSC at different locations along the Mississippi River downstream from the confluence with the Missouri River for case 1. Normalized distance is equal to each pixel's N-value/half channel width. Numbers at the top of each panel indicate the distance downstream from the confluence in kilometers. Distance from the confluence is shown on the top left corner while the computed Pmx values are shown in the bottom right corner of each plot.

Values of percent mixing for each RCS depict the evolution of mixing downstream of the confluence (Figure 3.7). Mixing increases rapidly over the first 6 km in a linear fashion until

reaching a peak and then subsequently declines locally. This peak corresponds to a section of the river where the channel is relatively wide compared to other locations downstream of the confluence (Figure 3.7). At this location the mixing interface remains near the same absolute location with respect to the left bank of the river as upstream and downstream, but shifts location in position relative to the channel centerline (n_n) due to local widening of the channel. Thus, the number of pixels on the right (Missouri) side of the mixing interface increases relative to the number of pixels on the left (Mississippi) side, resulting in an apparent increase in mixing, i.e. the contrast in SSSC relative to conditions upstream of the confluence decreases because the percentage of pixels corresponding to flow on the Missouri River side of the MI increases. Although this apparent increase in mixing could be accommodated by weighting the contribution of each pixel to the P_{mx} value by the proportion of the total discharge this pixel represents, such an approach would require information on the distribution of the discharge across each RCS. P_{mx} values decrease over the next 4 km as the channel narrows back to its width upstream of the widened section, leading to an apparent "unmixing" in the plot. Downstream from a distance of 10km mixing again increases linearly but at a lower rate than immediately downstream of the confluence.

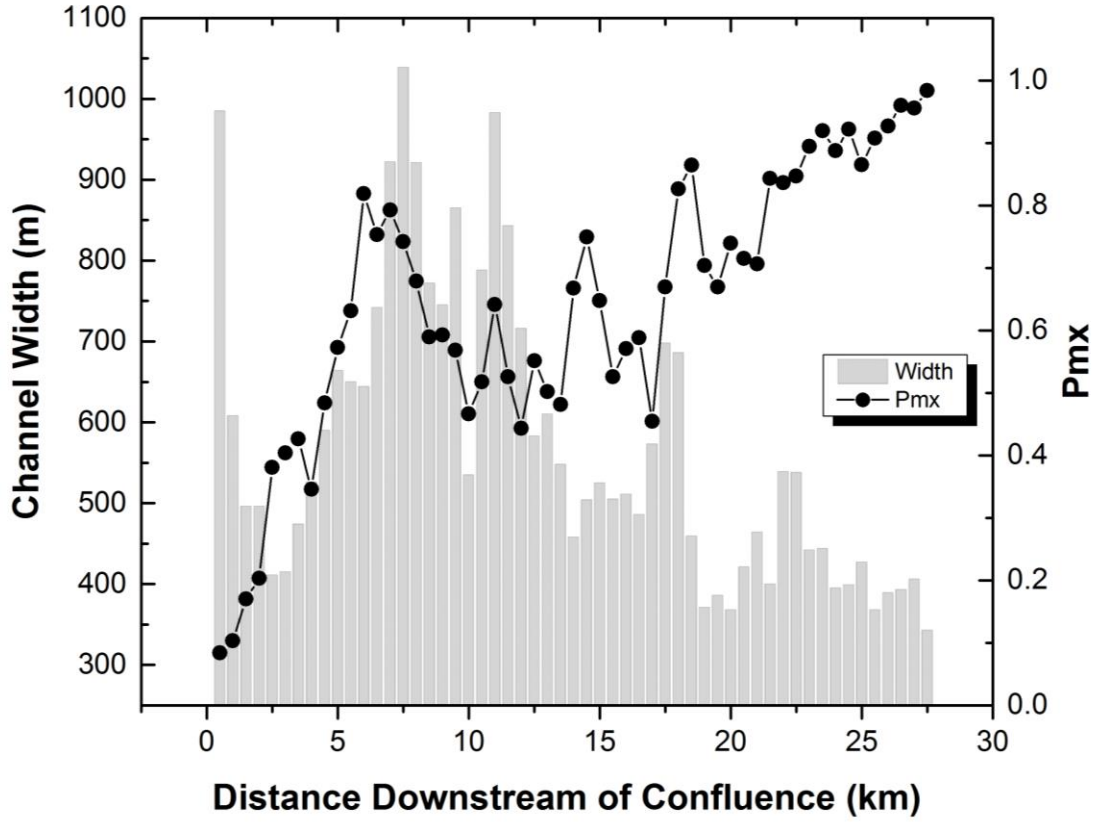

Figure 3.7: Changes in values of Pmx with distance from the confluence for case 1. Channel width variations are shown as histogram. Initial spike in the Pmx corresponds to the maximum channel width.

3.4.2.2 Case 2: Slow mixing

On April 24th, 1991, the total discharge at the confluence was relatively large, but the discharge of the Mississippi River was more than two times the discharge of the Missouri River, resulting in relatively low discharge and momentum ratios (Table 3.4). Despite having a higher discharge than the Missouri River, the Mississippi River was far less turbid with a SSSC value of 300 mg/l, about one-third of the SSSC of the Missouri River (1010 mg/l). As can be seen from the map of SSSCs (Figure 3.5), flows from each river remain clearly separated immediately downstream from the confluence, eventually mixing much farther downstream. This case represents relatively slow mixing. Notable in this case is the cross-channel contrast in SSSC on the Mississippi River upstream of the Mississippi River-Missouri River confluence, which

reflects the contribution of relatively clear water to the Mississippi River from the Illinois River, which joins the Mississippi River about 35km upstream.

In contrast to the case 1, the SSSC contrast between the two confluent flows remains mostly unchanged within initial 30 km downstream of the confluence (Figure 3.8). The gradient in SSSC near the center of the channel defining the mixing interface decreases over distance, indicating expansion of this interface. Between 40 and 80 km, slow mixing continues to reduce the SSSC contrast across the channel to less than half of its initial value. Complete mixing (P_{mx} >= 0.95) is achieved near the end of the study reach at 107 km downstream of the confluence. In this case, the cross sectional average SSSC at the location of complete mixing is about 800 mg/l – a value intermediate between the initial concentrations of the two rivers, but more similar to the SSSC of the Missouri River than to the SSSC of the Mississippi River upstream of the confluence. Thus, in contrast to Case 1, the addition of sediment by the Missouri River resulted in a substantial increase in the SSSC of the Mississippi River. Overall, the spatial pattern of mixing along the reach is characterized by a slow, linear increase in values of P_{mx} in the downstream direction (Figure 3.9).

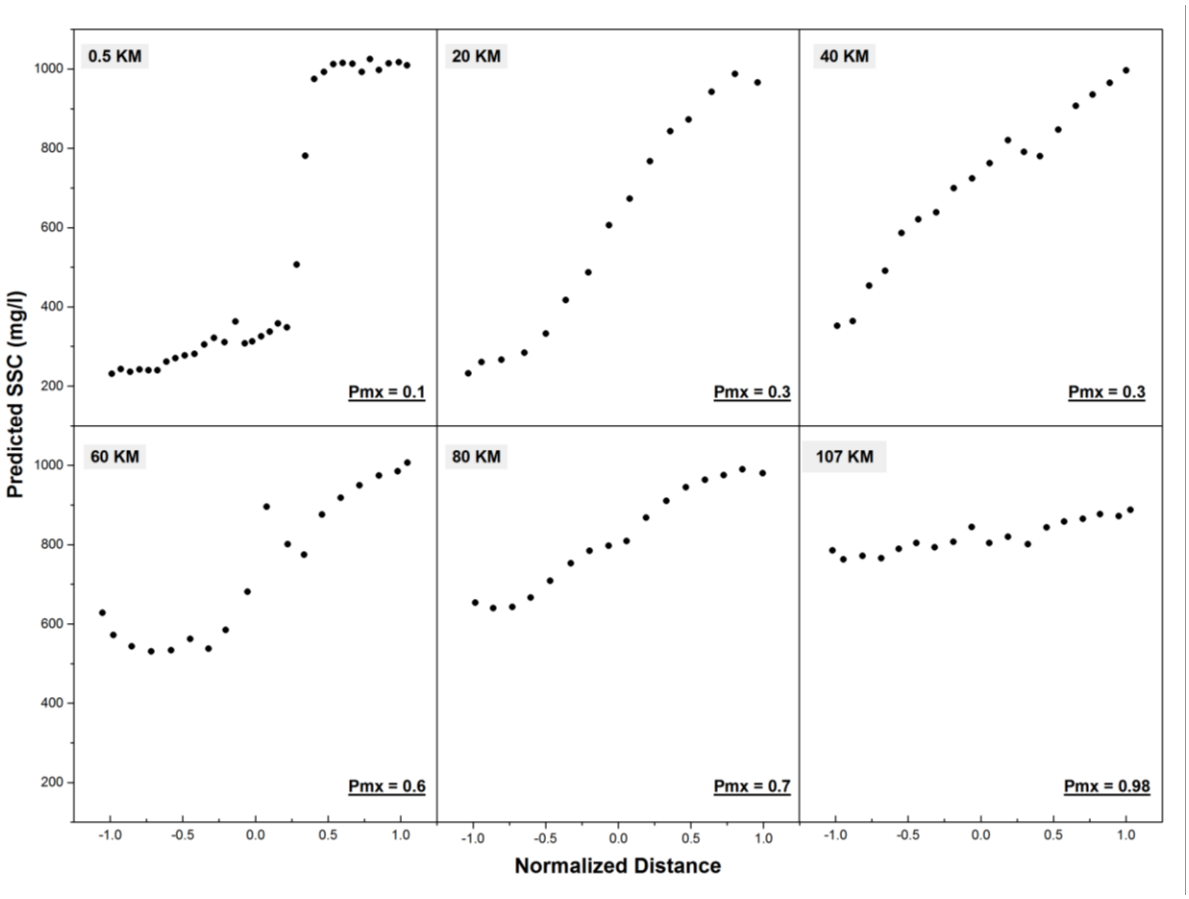

Figure 3.8: Cross-stream variations in SSSC at different locations along the Mississippi River downstream from the confluence with the Missouri River for case 2. Numbers at the top left of each panel indicate the distance downstream from the confluence in kilometers.

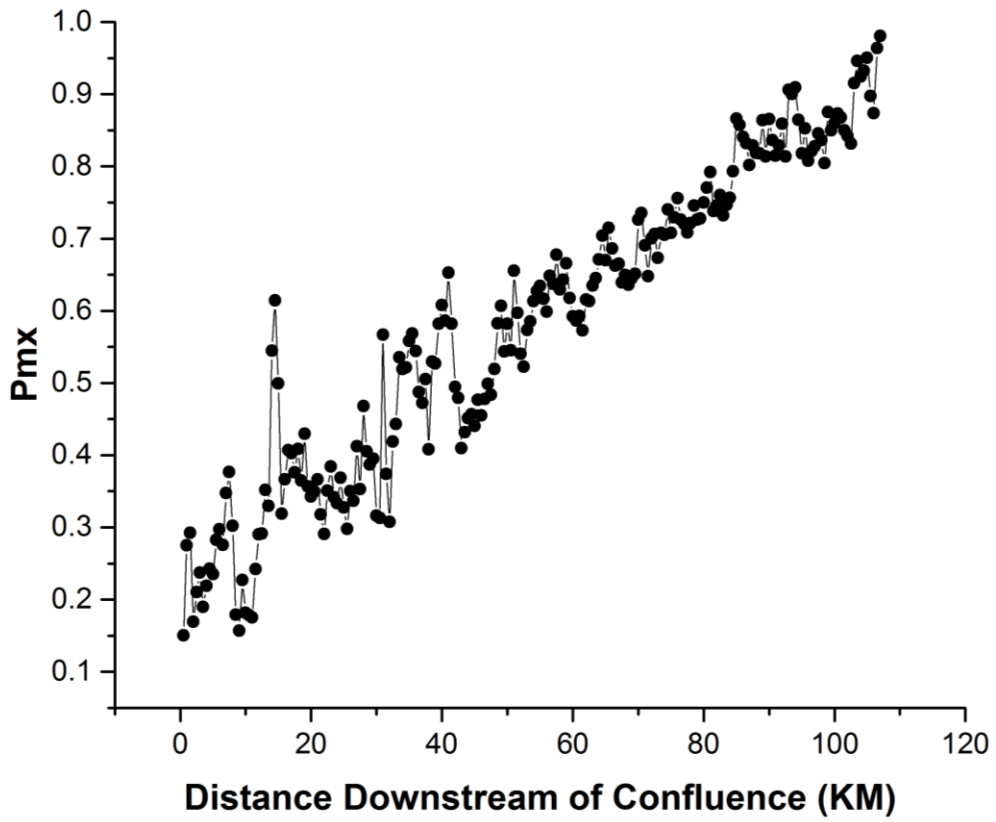

Figure 3.9: Changes in the values of Pmx with distance from the confluence for case 2.

3.4.2.3 Case 3: Minor mixing

On Sept 26, 2001, discharges of both rivers upstream of the confluence were relatively low discharges with the discharge of the Mississippi River being slightly less than the discharge of the Missouri River discharge (Table 3.4). The higher discharge and velocity in the Missouri River compared to the Mississippi River on this date resulted in a high momentum ratio. The SSSC of the Missouri River was nearly eight times greater than the SSSC of the Mississippi River, being 599 mg/l and 75 mg/l respectively. The two flows generally remain separate in the upstream portion of the study reach (Figure 3.5c) and do not mix much downstream over the entire length of the study reach. This case represents minor mixing.

Cross sectional plots of RCS at different locations downstream of the confluence show that complete mixing does not occur over the length of the study reach. The value of P_{mx} at a distance of 110 km is only 0.5 and although the total range in concentrations has diminished slightly, a strong lateral gradient in SSSC is still evident at this location (Figure 3.10).

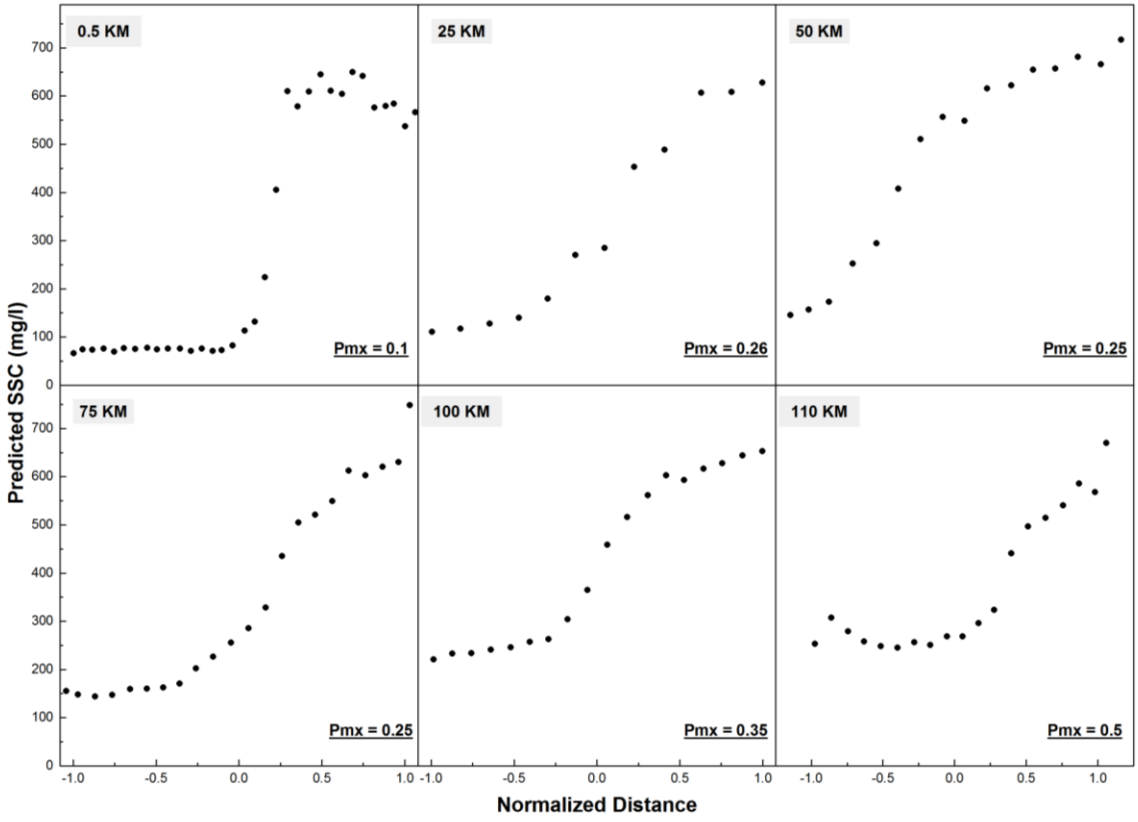

Figure 3.10: Cross-stream variations in SSSC at different locations along the Mississippi River downstream from the confluence with the Missouri River for case 3. Numbers at the top of each panel indicate the distance downstream from the confluence in kilometers.

The lack of mixing is also evident from the P_{mx} plot, which exhibits considerable scatter and no clear trend over the length of the reach (Figure 3.11). Values of P_{mx} lie between 0.125 and 0.30 over the first 15 km from the confluence and then increase very gradually to values between 0.25 and 0.5 between 15 km and 75 km. Over the last 35 km of the reach, values increase

somewhat systematically from about 0.25 to 0.5, but this trend is disrupted by local increases in P_{mx} above 0.5 locally.

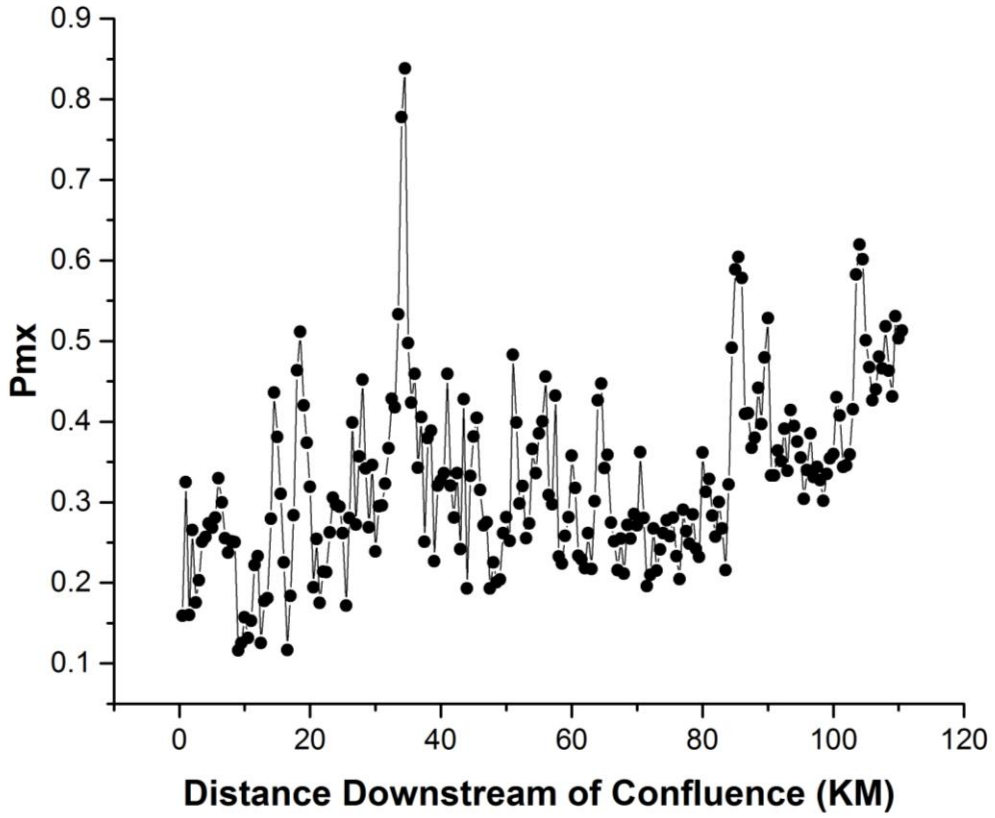

Figure 3.11: Changes in the values of Pmx with distance from the confluence for case 3.

3.5 Discussion and conclusion

The availability of medium spatial resolution multispectral satellite imagery over the past few decades provides a unique opportunity to understand spatial and temporal variations in mixing in river systems. Although past work has indicated that remote sensing is useful for qualitatively depicting lateral mixing downstream of large river confluences (Park and Latrubesse, 2014), the research presented in this chapter has developed a method for quantifying the amount of surficial mixing. An advantage of the method is that it provides an effective alternative to ground-based measurements of mixing in large rivers that are time-consuming and expensive to obtain and can only provide information on mixing over a limited spatial and temporal domain. By contrast,

remote sensing approach yields maps depicting spatio-temporal heterogeneity in surficial suspended sediment concentrations that can be used to characterize lateral mixing at specific cross sections along the river and to quantify changes in the magnitude of lateral mixing over long distances downstream from a confluence. The availability of remote sensing data for many different times also provides a basis for determining how mixing downstream of confluences varies over time and with different flow and suspended-sediment conditions.

The RF model shows that a robust relationship exists between SSSC and ratios of red and green bands, and NIR and green bands. These results confirm the findings reported in literature for remote sensing of turbidity or secchi disk depths using broad band sensors (Doxaran et al., 2006, 2003; Duan et al., 2009) where high correlations were achieved using red/green and NIR/green band ratios. The results of model testing as well as application of the model to three test cases indicate that, although absolute values of SSSC may in some cases be biased, the model can capture spatial patterns that reflect differences in SSSC concentrations between confluent flows. The RF model based on Landsat 5 TM data performed reasonably well in estimating SSSCs, but overestimated values slightly for cases where SSC < 200 mg/l and underestimated suspended sediment concentrations > 200 mg/l. The shift from positive bias in the lower concentrations to negative bias for the higher concentrations contributed to the root mean square error and mean absolute error of predicted versus observed values. Most observed SSCs for the Mississippi River and Missouri River gaging stations are < 400 mg/l (Figure 3.4) and the problem of substantial bias for high values of SSC is not a major concern for this particular confluence. Nevertheless, caution should be applied in evaluating mixing when the initial SSSC contrast between the two confluent flows is low.

Obviously not all of variation in reflectance in the bands used to model SSC is due to variation in sediment alone. Other properties, such as suspended organic solids, undoubtedly contribute to variations in reflectance. Moreover, the RF model is fitted using average spectral characteristics for the set of pixels that extends across the river at the locations of gaging stations where mean sediment concentrations are reported. The mean concentrations for a cross section of the river are based on rating relations between an individual sample collected each day locally within the cross section and cross-sectional concentrations. These relations are not precise and can introduce error. The individual samples from which cross-sectional concentrations are derived are collected beneath the surface, whereas the spectral information from remote sensing represents conditions at the surface. The specific time of day at which the individual sample is collected usually will not coincide with the time of day the sensor obtained the image. Noticeable local spatial variation in reflectance related to turbulence at the river surface was evident in the images, which will introduce variability into surface values of reflectance obtained at specific times. All of these factors complicate the effort to model with a high degree of accuracy the relation between spectral information derived from remotely sensed imagery and reported suspended sediment concentrations in rivers.

Despite these concerns, application of the method to three test cases with different characteristics of flow and sediment concentration at the confluence of the Missouri and Mississippi Rivers demonstrates that satellite remote sensing can provide an effective tool for characterizing lateral mixing of suspended sediment downstream of confluences within large river systems. The test cases reveal substantial differences in amounts and spatial patterns of surficial mixing for different flow events. In the cases of rapid and minor mixing, both have similar discharge ratios and momentum ratios, but mixing was completed within 28 km in one

case while the two rivers remained relatively unmixed for 110 km in other. The only major difference is the initial SSSC difference between the two flows. In the minor mixing case, the initial SSSC difference is much greater than in the rapid mixing case and in the slow mixing case. Thus, for the three contrasting cases examined in this study, no clear relationship is evident between characteristics of flow and sediment at the confluence and downstream patterns and rates of lateral mixing. Relationships between controlling factors (discharge ratio, momentum flux ratio, sediment concentration ratio, total discharge) and mixing may not be apparent in only three cases. Further analysis using a large number of cases is needed to determine whether variations in incoming flow and sediment characteristics at large river confluences are strongly related to patterns and rates of downstream mixing. Moreover, the analysis using remote sensing data is limited to the surficial patterns of mixing only and does not take into account mixing beneath the surface of the flow. Mixing can be strongly influenced by secondary flows in the immediate vicinity of the confluence that can result in subsurface interpenetration of one flow into the other (Lewis and Rhoads, 2015b; Rhoads and Kenworthy, 1995). Density effects, induced by large differences in temperature or sediment concentrations of confluent flows, can also produce horizontal stratification of flows downstream of confluences that may result in misleading interpretations of mixing based on surface information only (Laraque et al., 2009; Ramõn et al., 2013). Nevertheless, the remote-sensing method developed herein provides detailed spatial information that can be used to provide primary assessments of mixing downstream of confluences in large river systems. Additionally, by combining the method with field investigations, the relation between surficial patterns of mixing at and downstream of confluences with patterns detected throughout the entire flow column can be explored.

CHAPTER 4: ASSESSMENT OF SUSPENDED SEDIMENT MIXING DOWNSTREAM OF A LARGE RIVER CONFLUENCE

4.1 Introduction

Confluences are integral part of drainage networks where flows from two rivers converge (Benda et al., 2004; Osawa et al., 2011; Paola, 1997). A mixing interface between the two convergent flows, often with different biogeochemical characteristics, can usually be identified visually based on contrasts in visible properties of the flow (e.g. turbidity, color) (Roy et al., 1999). This contrast between confluent flows can persist far downstream of the confluence (Mackay, 1970) or it can diminish within short distance downstream of the confluence (Lane et al., 2008), depending on the hydrologic conditions and the dominant processes involved. The dynamics of transverse-mixing processes largely determine the quality of water downstream from these locations. Because large rivers serve as important sources of water for humans and habitat for aquatic organisms, an improved understanding of mixing in these rivers will benefit society and the environment.

Although a significant amount of research has been carried out over the past three decades in order to understand flow structures at river confluences including field investigation at small stream confluences (Ashmore et al., 1992; Biron et al., 1993; Boyer et al., 2006; De Serres et al., 1999; McLelland et al., 1996; Rhoads, Bruce, 1996; Rhoads et al., 2009; Rhoads and Kenworthy, 1998, 1995, Rhoads and Sukhodolov, 2008, 2004, 2001), laboratory flume experiments (Ashmore and Parker, 1983; Best, 1988, 1987; Best and Reid, 1984; Best and Roy, 1991; P. Biron et al., 1996; Pascale Biron et al., 1996; Mosley, 1976), and numerical models for confluence dynamics (Biron et al., 2004; Bradbrook et al., 2001, 2000, Constantinescu et al., 2016, 2012, 2011), only few studies (Bouchez et al., 2011; Lane et al., 2008; Laraque et al., 2009; Mackay, 1970; Park and Latrubesse, 2014; Parsons et al., 2008, 2007, Szupiany et al.,

2007, 2009) have examined the dynamics of mixing downstream of confluences in large river systems. Detailed investigations of mixing at large river confluences are more limited than those for small confluences and the influence of tributary contributions on spatial patterns of water quality in large river systems is largely poorly understood.

Most empirical research on mixing downstream of confluences in large rivers has highlighted the long length scales and slow rates of mixing in these systems (Bouchez et al., 2010; Kabeya et al., 2008; Krouse and Mackay, 1971; Laraque et al., 2009; Mackay, 1970; Matsui et al., 1976; Rathbun and Rostad, 2004; Stallard, 1987). In many of these cases, the two flows do not mix for hundreds of kilometers downstream of the confluence. For the most part these findings are consistent with semi-theoretical considerations, which indicate that the length scale of complete mixing of two rivers (L_x), in the absence of strong near-field effects, should scale with width of the channel:

$$\frac{L_x}{b} = \frac{\alpha U b}{k_z} \tag{4.1}$$

where U is the reach-averaged mean velocity, b is the width of the river, α is a proportionality constant (typically ranging from 0.1 for source at the bank to 0.5 to a source at mid channel), and k_z is the transverse dispersion coefficient (Fischer et al., 1979; Rutherford, 1994). The mean value of $\frac{k_z}{Ub}$ calculated from data for meandering rivers (Rutherford, 1994, Table 3.2) is 0.00057, which yields a mean mixing length of 235 channel widths for tributary mixing treated as a centerline discharge (reasonable if both confluent rivers are roughly the same width) and 935 channel widths for tributary mixing treated as a side discharge (reasonable if a small tributary enters a large main river). Recent work has shown that rapid mixing can occur at large river confluences if local conditions within the confluence promote strong near-field mixing (Lane et al., 2008), but that these conditions may be specific to particular hydrological

relations between the tributaries and that slow mixing also occurs at the same confluence. The same study emphasizes in a qualitative manner the value of remotely-sensed imagery for documenting patterns of surficial transverse mixing downstream of large river confluences, but does not attempt to develop an analytic method for evaluating mixing from such imagery. Therefore, development of such a method is required that will yield a wealth of information on length scales and rates of mixing in large river systems, thereby improving our understanding of this important water-quality process.

Satellite remote sensing, with synoptic coverage and consistency of temporal data, provides an ideal platform with which to study processes at large scales. The estimation of water quality parameters from remote sensing imagery, including SSC, can be realized through two basic approaches: 1) empirical estimation of the water quality parameter using in situ data combined with spectral data from the imagery, and 2) inverse modeling using a radiative transfer model. Inverse modeling using radiative transfer models, while successful in some applications, requires significant calibration through the measurement of a water body's inherent optical properties (IOP), and precise atmospheric correction (IOCCG, 2006). The empirical approach, by contrast, relates water quality parameters directly to spectral properties (typically band values or band ratios) using various empirical modeling techniques. SSCs have been found to be detectable at relatively high levels of accuracy using broadband sensors and empirical models (Matthews, 2011). Utilizing the new advanced atmospheric correction algorithm, LEDAPS (USGS) for Landsat images, it is now possible to develop accurate models of SSC in natural rivers that provide the basis for evaluating patterns of surficial transverse mixing downstream of large river confluences.

This chapter uses a remote sensing technique to examine rates and length scales of mixing at a large river confluence. Surficial SSCs are estimated for 110 km river reach downstream of the confluence of the Mississippi and Missouri Rivers with a calibrated model using the Landsat temporal images from 1985 – 2011. The goal is to use the calibrated method to evaluate rates and length scales of transverse surface mixing downstream of the confluence and to relate these rates and length scales to factors that might influence mixing, such as momentum ratio, discharge ratio, SSSC ratio, and width-depth ratio. Rates and lengths scales are also related to values reported previously in the literature for large rivers. This research provides substantial insight into transverse mixing downstream of large river confluences– an important water-quality process that is not well understood.

4.2 Study area

The confluence of the Mississippi and Missouri Rivers is chosen for the site for this study because of the availability both of medium resolution satellite remote sensing data and historic data on discharge and SSC from US Geological Survey gaging stations upstream and downstream of the confluence. The confluence planform is asymmetric with Missouri River joining the Mississippi River from the west at an angle of about 75° (Figure 3.1).

SSC characteristics of the Mississippi River have been changed significantly over the past 150 years because of extensive anthropogenic modifications throughout the watershed, including the construction of lock and dams, which has resulted in declines in suspended sediment loads (Heimann et al., 2011). The Missouri River on the other hand is relatively less managed and usually contributes more sediment to the confluence than the Mississippi River most of the time (Table 3.1).

4.3 Dimensional analysis of mixing in rivers

Lateral mixing in rivers can be measured in terms of the longitudinal distance (L_x) downstream of the location where mixing is initiated to the location where complete mixing occurs. This distance can be expressed by the functional relationship:

$$L_x = f(U, D, b, Q, \rho, \mu, R_c, u_*, Z_o) \tag{4.2}$$

where U = depth averaged flow velocity, D = flow depth, b = channel width, Q = water discharge, ρ = density, μ = viscosity, R_c = radius of curvature, u_* = shear velocity, and Z_o = combined grain and form roughness height. There are total of 10 dependent and independent variables in equation 4.2. Using 3 fundamental reference dimensions [M, L, T], these variables can be expressed in 10-3 = 7 dimensionless parameters by using Buckingham Pi Theorem (Buckingham, 1914) as;

$$\frac{L_x}{b} = f\left(\frac{\rho U b}{\mu}, \frac{\rho Q}{\mu b}, \frac{\rho u_* b}{\mu}, \frac{b}{D}, \frac{R_c}{b}, \frac{Z_o}{b}\right) \tag{4.3}$$

A complete functional relationship can be written by including dimensionless factors that are known to effect mixing.

$$\frac{L_x}{b} = f\left(\frac{\theta_t}{\theta_m}, \frac{\rho_t Q_t U_t}{\rho_m Q_m U_m}, \frac{bed_t}{bed_m}, \frac{\rho U b}{\mu}, \frac{\rho Q}{\mu b}, \frac{\rho u_* b}{\mu}, \frac{b}{D}, \frac{R_c}{b}, \frac{Z_o}{b}\right) \tag{4.4}$$

Satellite remote sensing along with USGS ground data and USACE bathymetric data is used to derive variables including L_x, D, b, Q, ρ, and R_c. Because the study uses only one confluence, the junction angle is constant so the first term in equation 4.4 was ignored from analysis but it will be important if the results are to be compared with observations at a different confluence. Bed concordance/discordance between the two tributaries was estimated using USACE bathymetric data from 2001 and 2010. No differences in bed elevations of the two tributaries were found so mixing is not expected to be affected by this term at this confluence. The bathymetric data are also used for calculations of flow depths, and hence width-depth ratio.

Only two major bends occur along the study reach, one at the confluence ($\frac{R_c}{b} = 0.4$) and the second about 10 km downstream of the confluence ($\frac{R_c}{b} = 2.4$). Elsewhere, the channel is relatively straight or gently curving. No major changes in mixing were observed at the two major bends; thus, curvature effects were deemed unimportant.

Calculation of momentum flux ratio requires information on water temperature and SSC which were derived from the combined approach using USGS gaging station and remote sensing data, the details of which is presented later in the chapter. Because, viscosity, shear velocity, and grain and form roughness are not available for this study due to lack of necessary data, these variables could not be used directly to test against mixing lengths. To compensate for the lack of data for these terms, other variables that could be estimated from available data were used to explore possible controls of mixing lengths. For example, viscosity is strongly dependent of the temperature, so temperature ratios upstream of the confluence were used as proxy for viscosity in the statistical analysis.

4.4 Data and methodology

Analysis of spatial and temporal variations in surficial SSC mixing downstream of the confluence involves combining flow and sediment data from USGS stations with the spectral properties of the Landsat 5 (TM) images in Random Forest (RF) regression model (Liaw and Wiener, 2002) to achieve continuous quantitative distribution of SSSC within the study reach, determining lateral variations in SSSC by spatially averaging surficial SSSC at regularly spaced intervals to delineate representative cross sections within each subsection of the river, and calculating mixing at each cross section using a mixing metric. The methodology was applied to entire study reach of the river and mixing lengths were determined for the cases where complete mixing ($P_{mx} > 0.97$) was achieved within the study reach.

A total of 143 cloud free Landsat 5 TM images from 1985 to 2011 were obtained to be used for model building and calibration. Landsat 5 TM has long historic data record with sufficient spectral resolution for remote sensing of SSSC (Matthews, 2011). The data were corrected for atmospheric distortions using Landsat Ecosystem Disturbance Adaptive Processing System (LEDAPS) (Masek et al., 2013) and used in RF model along with USGS ground station data for SSSC modeling. Additionally, thermal band of Landsat data is used to determine thermal characteristics of the incoming flows.

Three USGS stations within Landsat image footprint provide sufficient data on flow discharge, and SSC to determine relative strengths of the incoming flows and to calibrate and test RF model in combination with the satellite data. Two of the three USGS stations are located upstream of the confluence – one on each tributary, while one station is downstream of the confluence (Figure 3.1). Table 4.1 provides information on periods of data record available from each USGS station.

Table 4.1: Summary of available flow discharge and SSC data and basic statistics at the three USGS stations within the study reach. The stations on Mississippi River at Grafton, IL and Mississippi River below Grafton, IL are only 5.5 mile apart so the discharge data from both stations has been combined into one record.

Station No.	Location	Period of record	
		Flow Discharge	SSC
05587455/ 05587450	Mississippi River at & below Grafton, IL	1933-04-01 to 2016-12-03	1989-10-12 to 2015-09-30
06935965	Missouri River at St. Charles, MO	2000-04-01 to 2016-12-03	2005-10-01 to 2008-09-30
07010000	Mississippi River at St. Louis, MO	1861-01-01 to 2016-12-03	1980-10-01 to 2014-09-30

This chapter follows methodology for modeling and extracting SSSC values for upstream sediment ratio and mixing calculations provided in Chapter 3. Landsat spectral bands were used to derive spectral indices that are known to perform well in estimating water SSSC and turbidity

(Dekker et al., 2002; Doxaran et al., 2006, 2003; Duan et al., 2009; Kallio et al., 2008; Kloiber et al., 2002; Lathrop and Lillesand, 1989; Sváb et al., 2005). A database of ground based SSC and the satellite spectral bands and derived spectral indices corresponding to the stations' locations are generated with a total sample size of 271. RF model was developed with randomly selected half of this dataset (n = 136) while the other half was used for model calibration. The model produced an R^2 of 0.7 when tested on the second half of the dataset. Calibrated model is applied to all of the images to estimate SSSC continuously over entire study reach. Finally, a set of 57 images are selected based on visible contrast in SSSC at the confluence for further analysis.

To determine SSSC mixing downstream of the confluence, predicted surficial SSC values from model derived rasters within river boundaries are extracted and the data is spatially averaged at every 500m subsection of the study reach downstream of the confluence such that the averaged SSSC represents the entire 500 m subsection of the river. Detail methodology of the spatial averaging procedure was discussed in Chapter 3. Mixing is calculated for each representative cross section using the mixing metric defined by

$$P_{mx} = 1 - \left[\frac{\frac{\sum_1^n |X_i - \bar{X}|}{n} - \left(\frac{\sum_1^a |X_{k1} - \hat{X}_1| + \sum_1^b |X_{k2} - \hat{X}_2|}{a+b} \right)}{\sum_1^m \frac{|X_{ju} - \bar{X}_u|}{m}} \right] \quad (4.5)$$

where P_{mx} is the percent transverse mixing, X_i is the individual pixel's SSSC in a cross-section downstream of the confluence, $\bar{X}$ is the mean value of SSSC at the downstream cross section, *m* and *n* are the total numbers of pixels in the upstream and downstream cross sections respectively, X_u is the value of SSSC in the upstream tributaries with *j* representing *jth* pixel, $\bar{X}_u$ is the mean for the two upstream cross sections. The term $\frac{\sum_1^a |X_{k1} - \hat{X}_1| + \sum_1^b |X_{k2} - \hat{X}_2|}{a+b}$ accounts for the mean upstream variability in SSSC where *a* and *b* are total number of pixels in tributary and

main channel while X_{ki} represents *kth* pixel value in tributary i = 1 or 2, and $\hat{X}$ is the mean of each of the two tributaries. The values of P_{mx} varies between 0 (no mixing) to 1 (completely mixed). However, for the purpose of this study, any value of $P_{mx} > 0.97$ is treated as fully mixed and mixing lengths were determined for the cases where complete mixing was achieved within the study reach.

4.5 Results

Mixing lengths have been computed for all the cases with wide range of hydrological conditions upstream of the confluence (Table 4.2). Out of the 57 cases, complete lateral mixing within the study reach occurred in 44 cases (herein referred to as mixed cases) while for the rest of the 13 cases (referred to as unmixed cases), mixing did not occur within 110 km reach (Table 4.3).

Table 4.2: Ranges for different PCFs for the observed cases.

PCF	Min	Max	Mean
Total Discharge (m^3/s)	2,770	25,060	9,565
Mean depth at confluence (m)	4.0	12.2	8.7
Mean Temperature (K)	273.3	297.2	286.3
Momentum Ratio	0.4	14.09	3.88
Discharge Ratio	0.3	2.54	1.01
Sediment Ratio	0.62	7.5	2.25
Temperature ratio	0.997	1.01	1
W/D	24.49	77.25	34.31

Table 4.3: Distribution of mixing lengths among various cases

Mixing Length (km)	Number of cases
0-20	6
20-40	7
40-60	5
60-80	4
80-100	15
100-110	7
>110 (No mixing)	13

Among all of the mixed cases, half of the cases were mixed after 80 km with median at 77.5 km (Table 4.4). For the unmixed cases, *Pmx* values ranged between 0.5 and 0.89 at the end of the study reach (Table 4.5).

Table 4.4: Statistics of the observed completely mixed cased

	Min	Max	Mean	Median	Std. dev
Mixing Lengths (km)	3.8	105	63.5	77.5	33

Table 4.5: Statistics of the observed Pmx values at the downstream end for unmixed cases

	Min	Max	Mean	Median	Std. dev
Pmx	0.5	0.89	0.72	0.76	0.11

4.5.1 Mixing lengths and controlling factors

To examine the influence of potential controlling factors on the length scale of mixing, spatially averaged SSSC values at each cross section for individual images within the entire study reach were visualized and values of P_{mx} were computed to illustrate SSC mixing patterns downstream of the confluence with different flow depths, upstream SSC contrast, total discharge, momentum ratios, and temperatures. The observed mixing lengths were regressed against each PCF to determine whether a statistical relation exists between the mixing and the PCFs.

4.5.1.1 Momentum ratio

For a particular confluence, the junction angle and planform symmetry remain unchanged and the flow deflection and hence the position of mixing interface is largely determined by momentum ratio – a ratio of momentum of tributary flow to that of the main river that reveals the relative hydraulic importance of each confluent river.

$$M_r = \frac{\rho_t Q_t U_t}{\rho_m Q_m U_m} \tag{4.6}$$

Where ρ is density of water and depends on temperature and SSC of the river, *Q* is discharge, and *U* is the mean velocity. The subscript *t* and *m* denote tributary and main channel respectively. To determine the effects of momentum ratio on mixing, flow measurements were obtained from USGS gauging stations for each image date ranging between 1989 and 2011 (Table 4.1). Daily discharge data and instantaneous cross sectional averaged velocity measurements in the downstream direction were used to plot velocity-discharge curves for the both conjoining rivers (Figure 4.1). The plot was used to derive velocity estimates for the dates where flow velocity data was not readily available through USGS. Missouri River velocities are nearly double the velocities in Mississippi River for similar discharges.

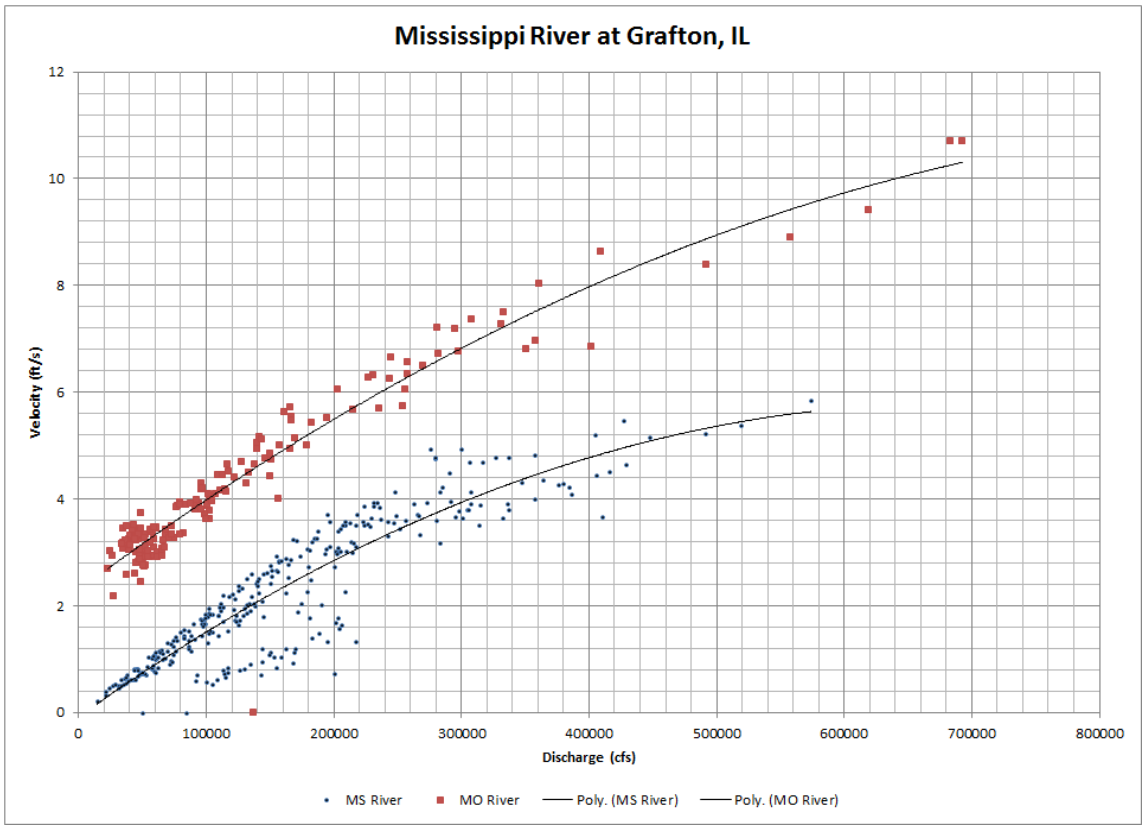

Figure 4.1: Velocity-discharge relationship for Mississippi (blue) and Missouri River (red) confluences.

Density of the water for each date was calculated by using the temperature and SSSC information derived from remotely sensed data. The USGS gaging station on Missouri River does not collect temperature data daily and therefore only limited data on temperature were available that corresponded with the image acquisition dates. The limited available data was plotted against Landsat derived temperatures to establish a relation between these two values (Figure 4.2). For large rivers, diurnal variations in water temperature are small and the Landsat temperature data were highly correlated with the observed data. This relation provided the basis for estimating temperatures in the Missouri River for all Landsat scenes.

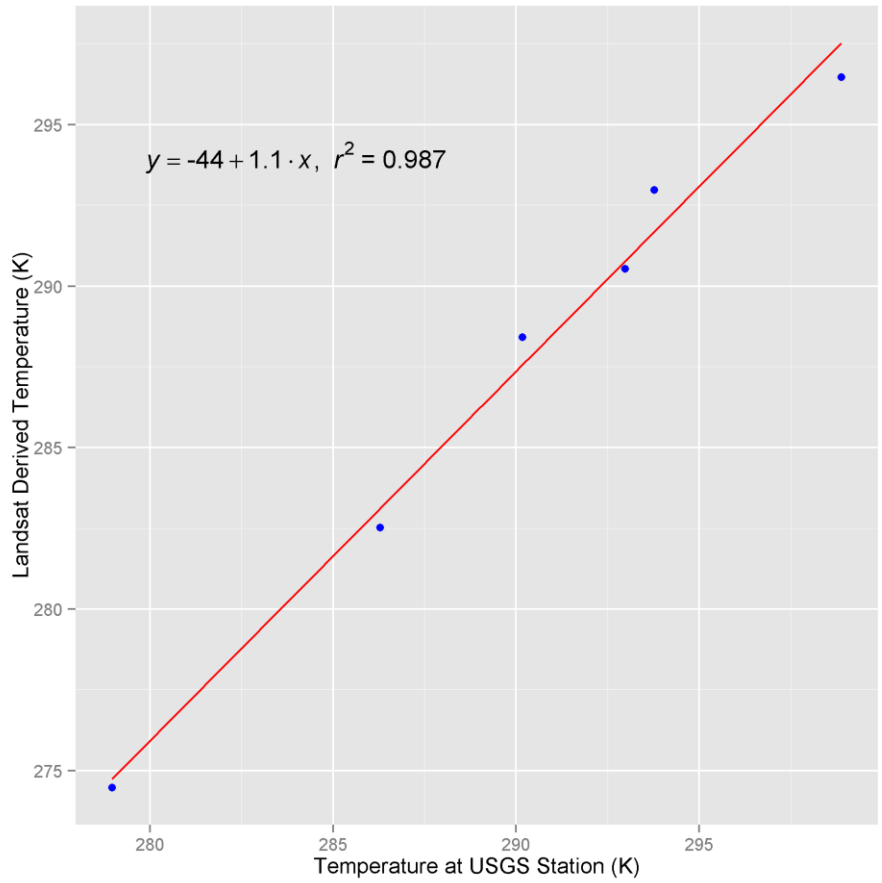

Figure 4.2: Plot of observed temperature at USGS station versus Landsat derived temperature

Equation (4.6) was used to compute momentum flux ratios for all the mixed cases to provide information on the characteristics of the incoming flows. Observed mixing lengths were plotted against momentum ratios to understand the role of momentum ratios on controlling mixing lengths downstream of the confluence (Figure 4.3).

4.5.1.2 Total discharge and mean flow depth at confluence

Flow depths and total discharge are flow condition metrics that can influence mixing at confluences by changing the scale of fluvial processes. Flow discharge data is available through USGS gaging stations. To evaluate the effect of flow depth; bathymetric data, collected in 2001 by USACE, was obtained along with river stages data from upstream USGS gaging station at Grafton, IL and downstream gaging station at St. Louis, MO for each image data to estimate

water surface slope between the two stations. Flow depths were then computed using bathymetric data, water surface slope and longitudinal distance from upstream gaging station (Grafton, IL). Farther downstream from the St. Louis station, a new water surface slope was determined by using river stage values between USGS stations at St. Louis, MO and Chester, IL and flow depths were computed based on these water surface elevations. This approach, although susceptible to errors from backwater effects at the confluence and from the fact that bathymetry is assumed constant over time, provides a good estimate of flow depth distribution along the entire river reach and provides basis for analysis that involves flow depths.

Mean cross sectional flow depths at the confluence and width to depth ratio for each image date were plotted against observed mixing lengths to examine the relationship between flow depth and width-depth ratio on controlling mixing (Figure 4.3). Cross sectional mean depths of about 9 m (Figure 4.3) with standard deviation of 1.5 m indicates the analysis is limited to certain range of variations in flow depth.

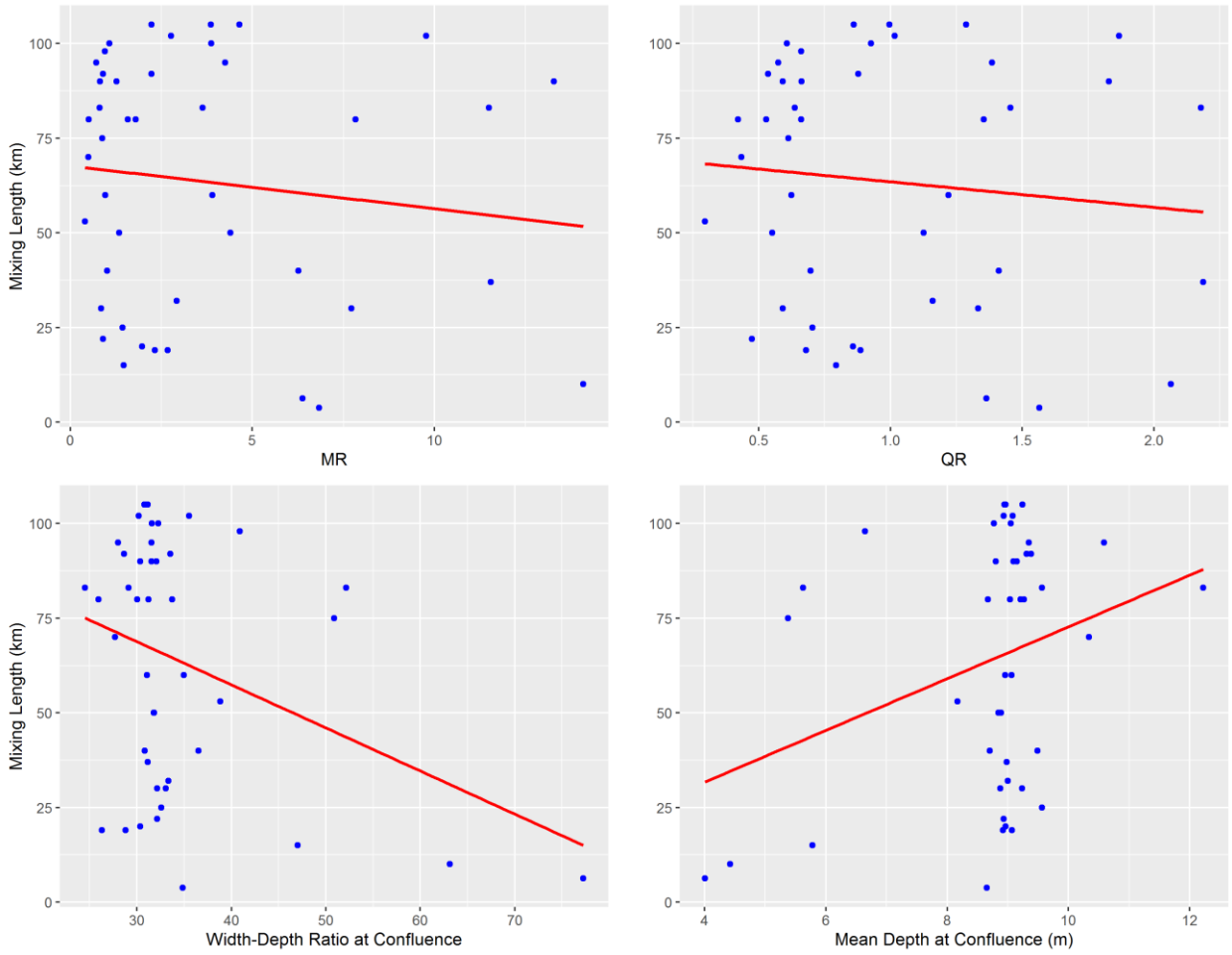

Figure 4.3: Relationship between different potential controlling factors and observed mixing lengths; momentum ratio (top left), discharge ratio (top right), width-depth ratio measured the confluences about 250m downstream of the upstream junction corner (bottom left), and total flow depth.

Figure 4.3 and Table 4.6 show that momentum ratios and discharge ratios have no significant effect on the mixing lengths. Values of R^2 for these relations are less than 0.02. Although, the regression analysis shows a negative correlation, no statistically significant relation exists between momentum flux ratio and discharge ratio with the observed mixing length.

The lack of a strong relationship ($R^2 < 0.12$) between mixing lengths and flow depths and width-depth ratios suggest that rate of change in lateral mixing downstream of the confluence is largely unaffected by the changes in the flow depth, however, p-value < 0.05 indicates that a

statistical significance exists between the two variables (Table 4.6). Again, caution must be practiced because there is not much variation in the flow depth and width-depth ratio for the observed cases (Figure 4.3), therefore the analysis is limited and need more data in order to be able to establish a strong relationship.

Table 4.6: Results of linear regressions of different factors against observed mixing lengths shown in Figure 4.3.

PCF	Equation	R^2	P-value
Momentum Ratio	$y = 68 - 1.1x$	0.015	0.416
Discharge Ratio	$y = 70 - 6.8x$	0.0104	0.51
Width-Depth ratio	$y = 1.3 - 1.1x$	0.114	0.025
Mean Depth at Confluence	$y = 4.4 + 6.8x$	0.098	0.037

4.5.1.3 Upstream water temperature and SSSC contrast

Mixing at confluences can be complicated by the density differences between the incoming flows. Density differences due to differences in SSC or temperature of the two flows can lead to flow interpenetration in to one another. With strong density contrast, buoyant, less dense fluid may ride over the denser fluid across the channel resulting in faster mixing (Kenworthy and Rhoads, 1995; Lewis and Rhoads, 2015a; Ramón et al., 2014; Rutherford, 1994).

Water density is a function of temperature and SSC, and therefore upstream ratio of these variables could be important factors in controlling lateral mixing. Although density differences are inherently included in the momentum flux ratio calculations, it may be desirable to isolate the contributions of SSC and temperature in controlling mixing for better understanding. Water temperature not only defines water density, but also affects the capacity of the flow to transport sediment in suspension by changing viscosity of the water. Sediment discharge decreases with

increasing temperature (Laursen, 1958; Shen and Hung, 1972; Yang, 1979). Therefore, it may be an important factor in affecting mixing at the junctions where changes in water temperature may change stream's capacity to transport suspended sediment.

The ratios between the temperature and SSSC of Missouri River and those of Mississippi River upstream of the confluence were calculated and plotted against observed mixing lengths to test the dependency of mixing lengths downstream of the confluences on the relative temperatures and SSSCs of the two rivers upstream of the confluence (Figure 4.4). The results from linear regression analysis, provided in Table 4.7, again indicate no significant relationships between the SSSC and temperature ratios of the upstream tributaries. It should however be noted that the temperature ratios range between 0.99 and 1.01 (Table 4.2), indicating that the effects of temperature may not be present and further analysis is needed with more pronounced temperature differences between the tributaries.

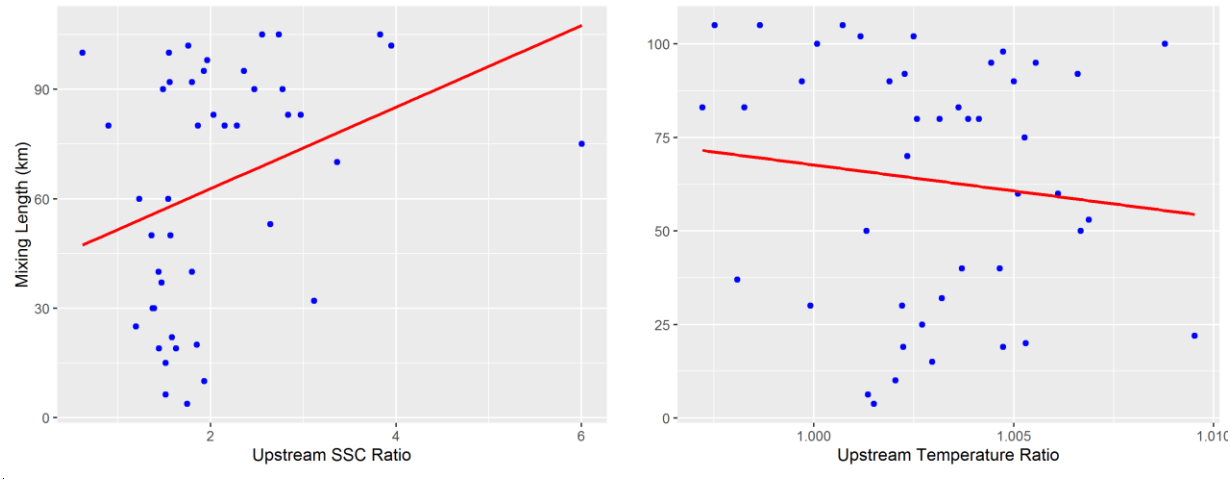

Figure 4.4: Relationship between SSC ratio ($SSSC_{MO}/SSSC_{MS}$) and the mixing length

Table 4.7: Results of linear regressions of SSSC and temperature ratios against observed mixing length (Figure 4.4).

PCF	Equation	R^2	P-value
Suspended Sediment Ratio	$y = 52 - 0.021x$	0.0482	0.152
Temperature Ratio	$y = 1456 - 1388x$	0.014	0.44

4.5.2 Apparent mixing due to SSSC variation along the channel

To understand mixing processes, it is important that the tracer used for the analysis, in this case SSSC, is conservative. While this is generally true for fine suspended sediment (< 0.063 mm), the assumption will not hold if coarse sediment (> 0.063 mm), which is strongly dependent on hydraulic conditions, contributes to the SSSC. Variations in sediment transport capacity related to changes in channel geometry or to water temperature may result in increases or decreases in SSSC if coarse sediment contributes to the surficial sediment load of the river.

To test for conservative behavior of surficial suspended sediment downstream of the confluence, a detailed analysis of changes in cross-sectional profiles of surficial SSSC values is performed. The analysis indicates that increase in *Pmx* values over distance downstream are not always due to mixing of the flows, but rather SSSC converges on values other than the expected value estimated based on mass conservation of sediment in the two incoming flows, where the expected mixed SSSC downstream of the confluence is calculated as:

$$SSC_{expected} = \frac{\mathrm{SSC_{Missouri}} \times \mathrm{Q_{Missouri}}}{\mathrm{Q_{total}}} + \frac{\mathrm{SSC_{Mississippi}} \times \mathrm{Q_{Mississippi}}}{\mathrm{Q_{total}}} \quad (4.7)$$

Further investigation of such cases reveals that the changes in sediment concentration happen often on one side (in unmixed flows) of the post confluence river channel while the other side stays mostly unaffected. Two of such cases are reported here in detail to illustrate this phenomenon; one with “apparent” mixing due to sediment reduction, and the second for “apparent” mixing due to increase in SSSC.

4.5.2.1 Reduction in suspended sediment concentrations

Analysis of the flow on March 30, 1988 is used as a representative case to illustrate apparent mixing downstream of the confluence that appears to be associated with progressive reductions in concentration over distance on one side of the Mississippi River. On this date, the discharge ratio was nearly unity, but the momentum of Missouri River was about three times the momentum of the Mississippi River (Table 4.8). The temperature contrast between the two flows was less than 1^{o}C, with mean temperature 11.94^{o}C of both upstream tributaries (Table 4.8).

Table 4.8: Summary of important parameters for the two cases

	Date	Discharge (m^3/s)		Temperature (^{o}C)		QR*	MR*	SR*
		Mississippi	Missouri	Mississippi	Missouri			
Sediment Reduction	Mar. 30, 1988	3,540	4,106	11.03	11.94	1.1	3	3.1
Sediment Increase	Apr. 24, 1991	7,957	3,681	12.95	13.62	0.4	0.5	3.3

*QR is the flow discharge ratio, MR is the momentum ratio, ansd SR is SSSC ratio between tributary and the main channel.

The SSSC difference between the two flows on this date upstream of the confluence is approximately 400mg/l, with Missouri River SSSC having a cross-sectional average SSSC of 550mg/l compared to an SSSC of 150 mg/l in the Mississippi River. Equation 4.7 is used to calculate expected mixed SSSC value downstream of the confluence and is found to be 357 mg/l. At the first cross section, just 250m downstream of the junction corner, a plot of SSSC reveals a strong gradient just to the left of a standardized width value of zero (Figure 4.5). This narrow zone of strong SSSC gradient defines the mixing interface between turbid water of Missouri River and relatively clearer water from Mississippi River. Outside of this zone, the variations in SSSC are small. These variations may arise from various sources, including turbulence due to

small and large-scale vortices and to noise in the data. At this location, little to no mixing has occurred between the upstream junction corner and this cross section.

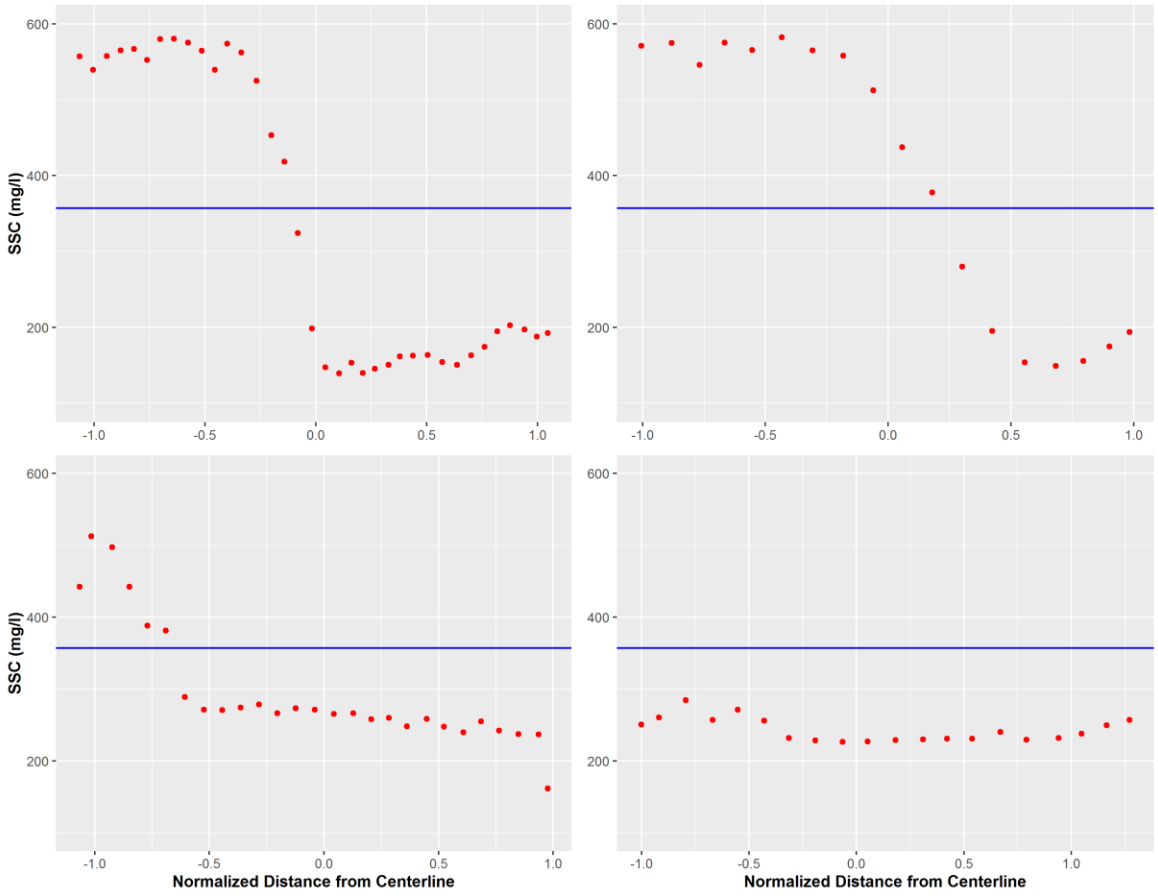

Figure 4.5: Cross section profiles at 0.5 km, 1.5 km, 6.5 km, and 29 km from left to right, top to bottom respectively, downstream of the upstream junction corner. X-axis is normalized distance and is equal to each pixel's N-value/half channel width. Numbers at the bottom of each panel indicate the mixing metric value corresponding to the plot. Blue line is the expected SSSC value calculated using equation 4.7.

Further downstream, at 1.25 km from upstream junction corner, the mixing interface moves to the right side of the channel centerline due to the strong momentum flux and realignment of the Missouri River to enter the downstream channel. A strong gradient in SSSC still exists, although expansion in the width of the zone of mixing indicates that mixing is more pronounced that at the cross section within the confluence. The upper and lower extreme SSSC values are still similar to the first cross section.

Because discharge ratio is close to unity, the mixing interface moves back towards the centerline once the flow recovers from initial effect of strong momentum from Missouri River. This shifting movement of the mixing interface relative to the channel centerline may help in distorting the mixing layer from relative vertical orientation to an angled orientation as the layer moves from deeper zone (Mississippi side) of the channel to a shallower zone (Missouri side) and vice versa. Additionally, the channel starts to expand at about 5 km downstream of the confluence. The position of the mixing interface at 6.5 km suggests that water from Missouri river is flowing through the shallower part of the channel where mid channel bar is often visible during low flows – indicating an area that is more conducive to sediment loss out of the water column, essentially lowering cross sectional mean SSSC. Figure 4.5c shows a mild slope of the mixing interface with peak SSSC below 500 mg/l. The mixing interface has shifted towards the left of the channel centerline and the average SSSC on the Mississippi side has increased from its initial value of 150 mg/l to about 250 mg/l indicating some cross-channel mixing.

Further downstream, the channel's SSSC on the Missouri side decreases even further while Mississippi's SSSC remain mostly unchanged between 6.5 km and 29 km in the downstream direction. At 29 km, enough sediment reduction has taken place from the Missouri-side water column to make it similar to that of the Mississippi River's SSSC (Figure 4.5d). The "mixed" value of SSSC at this location (250 mg/l) is much lower than the expected value of 357 mg/l. Therefore, this apparent mixing can only be attributed to decreases in sediment concentration on the side of the river that initially contained sediment from the Missouri River and not due to the actual mixing process.

Figure 4.6 clearly indicates that the sediments are being reduced over the course of the 29 km downstream of the confluence on the Missouri side of the river. Mississippi side gets some

initial increase in SSSC just downstream of the confluence but remains stable after that. Moreover, the mixed concentration is lower than the average of the two upstream concentrations despite the fact that the two rivers have nearly equal discharges.

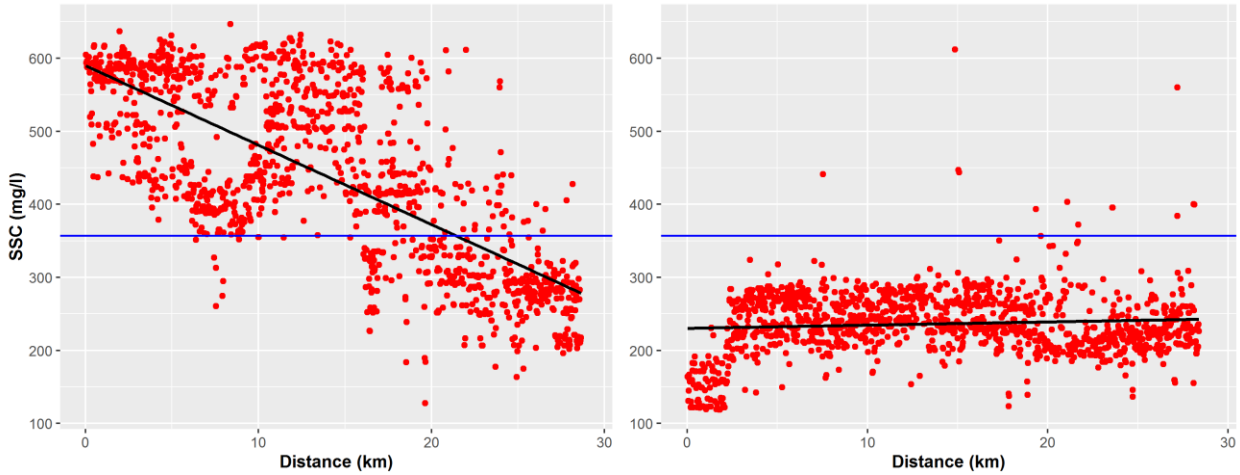

Figure 4.6: Longitudinal SSSC profile from the confluence to the location of complete mixing – 28 km downstream of the confluence. Each data point represents SSSC value in individual cell within the path drawn on each side of the river. The left figure represents longitudinal profile downstream of the confluence on the Missouri Side while the right one is for the Mississippi side.

4.5.2.2 Apparent mixing and increases in sediment concentration

In contrast to sediment decrease, surficial mixing can also be complicated by sediment addition in the water column by erosion of banks or from previously deposited sediments on the river bed. On April 24, 1991, discharge on both rivers was high. Mississippi River had more than double discharge than that in the Missouri River resulting in low QR and MR (Table 4.8). The temperature difference again is less than 1^{o}C, with mean temperature of 13.28^{o}C. Despite higher discharge, Mississippi River has less than three times SSSC (300 mg/l) than that of Missouri River (1,010 mg/l). Expected fully mixed SSSC value can be calculated using equation 4.7 which yields a value of 423 mg/l. Higher discharge along with lower SSSC of Mississippi River at similar temperature to the Missouri River indicates that Mississippi River was sediment

deprived. Figure 4.7a shows a strong contrast in SSSC near the upstream junction corner. The mixing interface is nearly vertical with mean SSSC difference of over 700 mg/l.

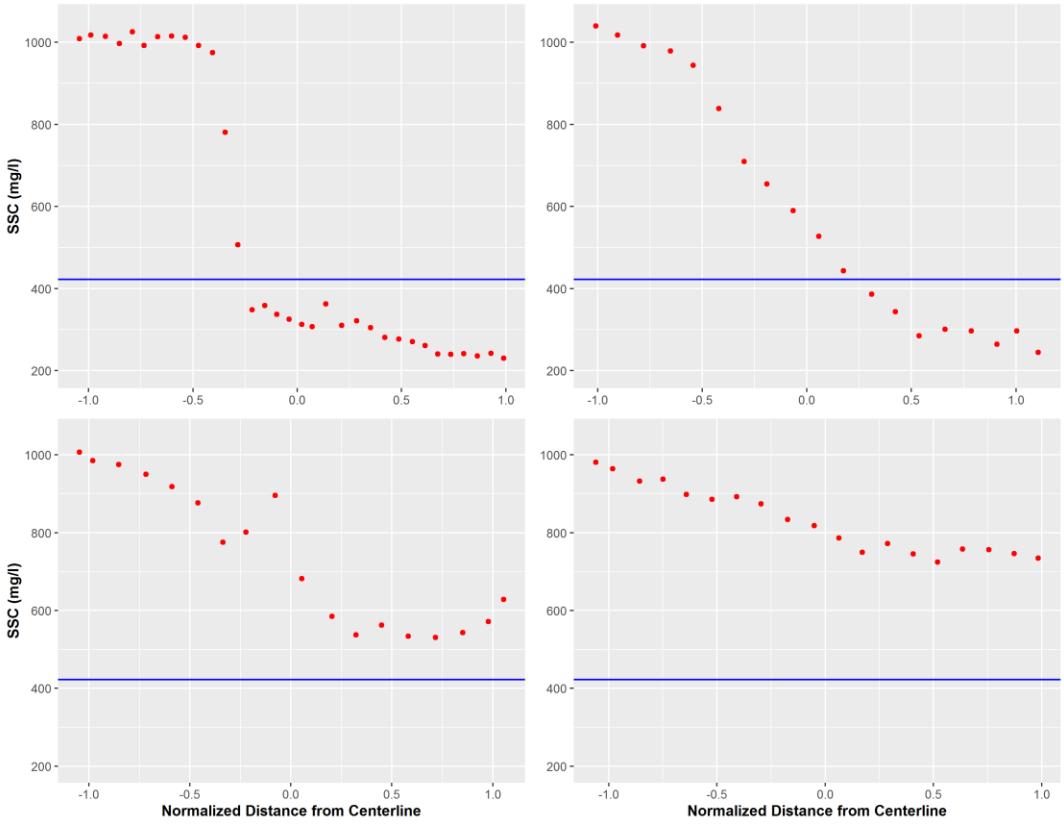

Figure 4.7: Cross section profile at 250m, 30 km, 60 km, and 100 km downstream of the upstream junction corner. Horizontal blue line indicates expected mixed value.

At about 30 km downstream of the confluence, the width of the mixing interface has widened to almost entire channel width, but the slope of the mixing interface is much more gradual than it was at the confluence. The extreme values of SSSC are still similar to the values at the first cross section, although only few pixels are left with these values (Figure 4.7b). Up until this point, it does not appear to have started to add sediment from the bed.

The cross-channel profile of SSSC at 60 km however, indicates that the SSSC values at the Mississippi River side are much higher than upstream value (Figure 4.7a and 4.7b) while concentration at the Missouri River is unchanged at about 1,000 mg/l. This increase in SSSC

indicates that suspended sediment has been added to the water column. As there are no significant tributaries joining the main channel over the entire study reach, the only source for sediment is the bed or the river banks. Figure 4.7c shows that the SSSC on the Mississippi side is now close to 600 mg/l, much higher than the expected value of 423 mg/l and almost double of its initial value 300 mg/l.

Further downstream, the trend of SSSC addition continues, bringing SSSC on the Mississippi Side closer to 800 mg/l, a value much greater than the expected mixed value of 423 mg/l, while the Missouri side has a SSSC of 1,000 mg/l. The sediment addition from the possible bed erosion has brought the Mississippi River's SSSC closer to that of Missouri River resulting in apparent mixing with a *Pmx* of 0.85 (Figure 4.7d). Figure 4.8 shows an upward trend of SSSC after a certain distance downstream of the confluence on the Mississippi side of the river, from confluence to the downstream end of the study reach.

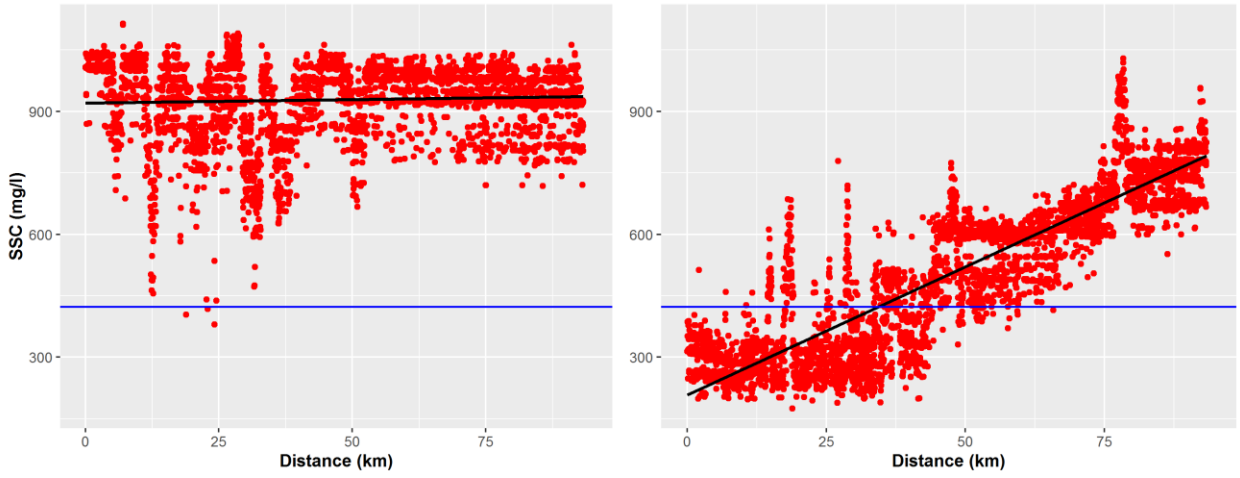

Figure 4.8: Longitudinal SSSC profile from the confluence to the location of complete mixing – 100 km downstream of the confluence. Each data point represents SSSC value in individual cell within the path drawn on each side of the river. The left figure represents longitudinal profile downstream of the confluence on the Missouri Side while the right one is for the Mississippi side

4.6 Discussion

This chapter examines surficial lateral mixing within the Mississippi and Missouri River confluences. It reports variations in surficial mixing patterns in response to the ratio of momentum flux of incoming flows, flow depth variations with different discharges, differences in SSSC, and the temperature of the incoming flows. Overall, the observed mixing patterns are found to be inconsistent with the results of past studies at small and large confluences (Constantinescu et al., 2016, 2011; Gaudet and Roy, 1995; Lane et al., 2008; Rhoads, Bruce, 1996; Rhoads and Kenworthy, 1995; Rhoads and Sukhodolov, 2001). Mixing rates and length scales are largely found to be independent of the ratios of momentum flux and discharge of incoming flows with poor r- squared and *P-values* except for the cases of mean depth at the confluence and width-depth ratio where P values indicate statistical significance of the relationship between the two variables and the mixing lengths. However, as mentioned earlier, for most of the cases observed here; mean depth and width-depth ratios did not vary significantly so the relationship may be biased. More research is needed with wide range of depth and width-depth ratio fluctuations to establish a definite relationship.

Although this study did not incorporate in detail the role of bathymetric morphology, USACE bathymetric data collected in 2001 and 2010 shows that both tributaries meet without any substantial bed discordance and hence, the effects on mixing due to bed discordance likely are not important at this confluence (Figures 4.9, 4.10). Cross-channel bed profiles on both tributaries just upstream of the confluence in 2001 and 2010 indicate that the two rivers have minimum bed elevations of about 115 to 117 m.

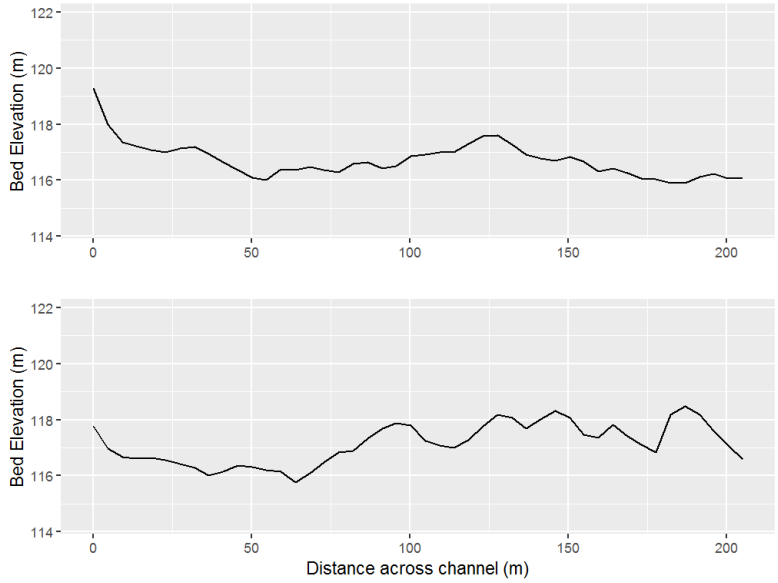

Figure 4.9: Cross sectional bathymetric profile at the Mississippi River just upstream of the confluence in 2001 (top) and 2010 (bottom).

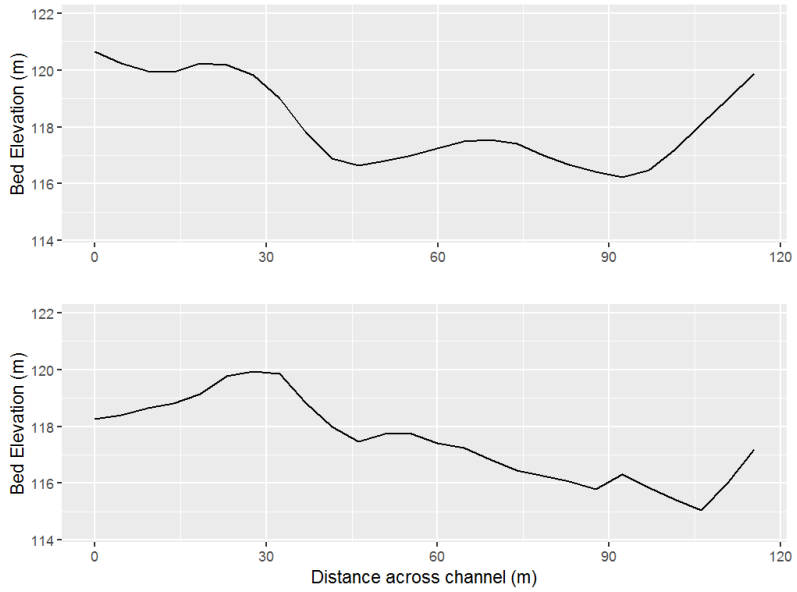

Figure 4.10: Cross sectional bathymetric profile at the Missouri River just upstream of the confluence in 2001 (top) and 2010 (bottom).

Flow from Missouri River often penetrates into the confluence with much higher momentum than the Mississippi River due to the higher slope of the Missouri compared to the Mississippi. Although no measurements of 3-D flows obtained at the confluence, the planform geometry of the confluence suggests the possibility of development of the secondary current on

the Missouri side because of curvature of flow from the Missouri River as it enters the Mississippi River. The presence of a secondary current on Mississippi side of the confluence is not very likely because the Mississippi River is relatively straight upstream of the confluence. The helical motion on Missouri side, if present, should enhance mixing at the CHZ. However, the plots of mixing rates (Figures 4.3, 4.4) show that hydrodynamics within the CHZ may not be as important at large river confluences as at small confluences. In the absence of channel-scale helical cells, mixing is controlled primarily by turbulent fluxes associated with shear between the incoming flows, the effects of which are insignificant compared to the advective fluxes due to channel-scale helical motion (Rhoads and Sukhodolov, 2008), especially in wide confluences (Rhoads, 2006). Furthermore, the shear between the flows decays rapidly in the downstream direction, resulting in sharp decline of mixing rates. The limited influence of CHZ hydrodynamic processes in controlling mixing rates downstream is also evident from the plots of different PCFs against rate of change of mixing within first 6 channel widths (Figure 4.11). These plots confirm that mixing rates for the distance of 30 channel widths are largely unaffected by flow conditions at the confluence (Figure 4.12).

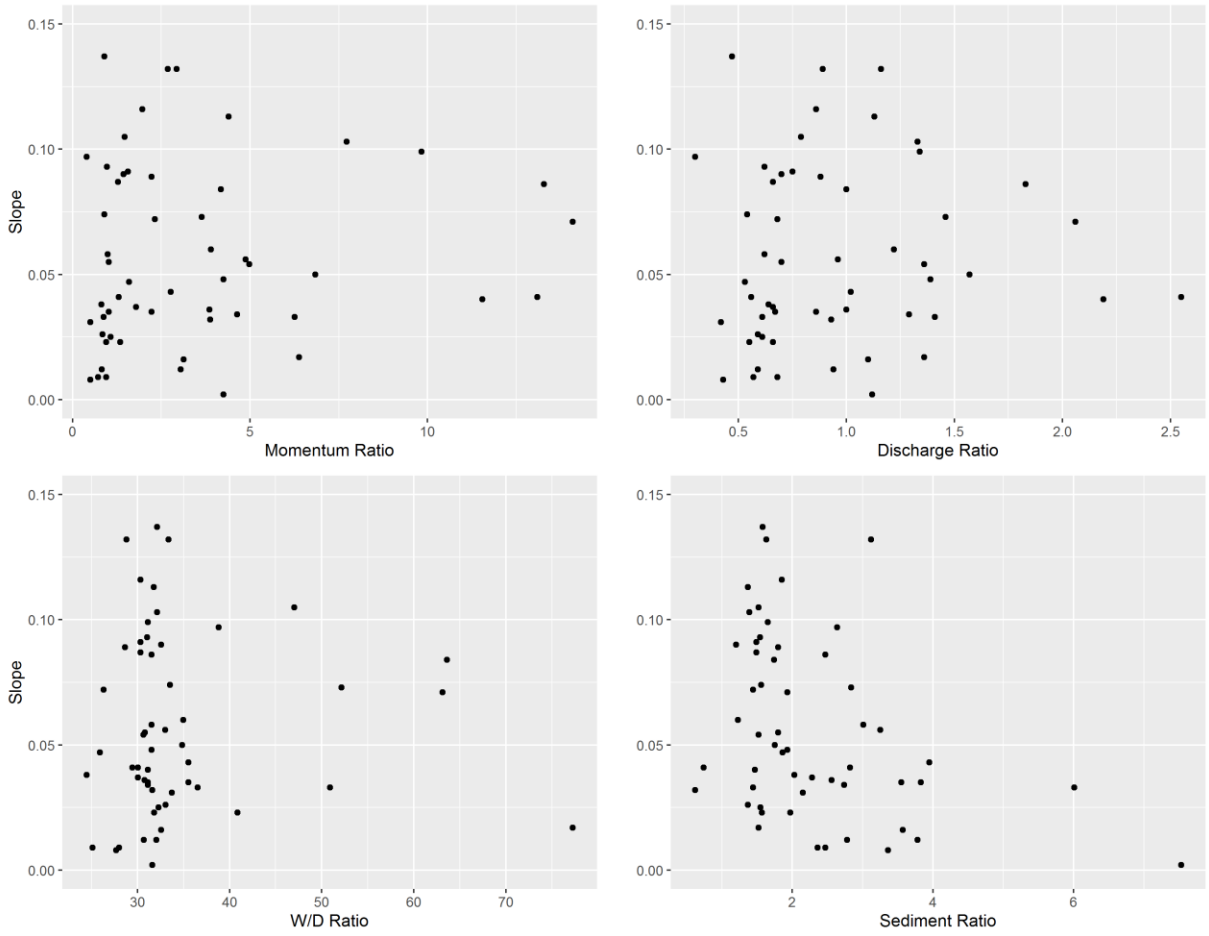

Figure 4.11: Variations in the mixing rates within initial six channel widths as functions of different PCFs. Higher slopes mean faster mixing.

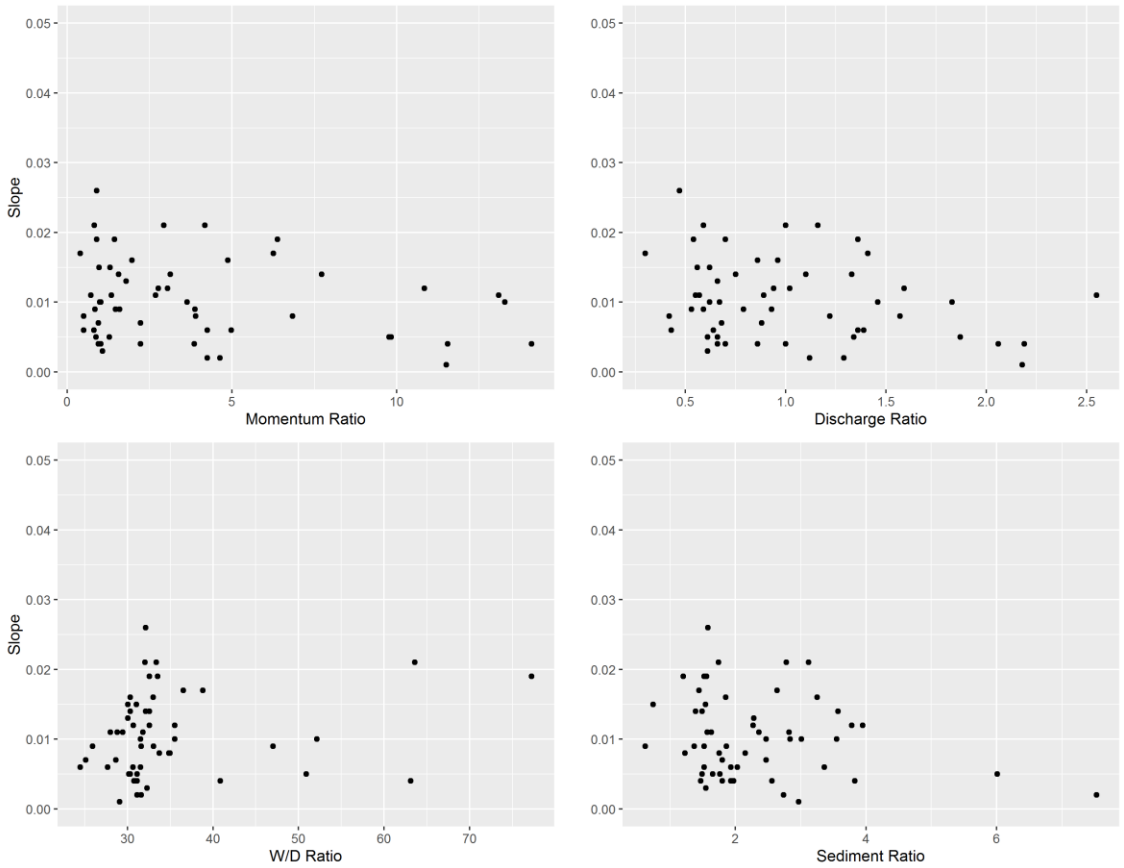

Figure 4.12: Variations in the mixing rates within initial 30 channel widths as functions of different PCFs.

The comparison of mean SSSC at every cross section downstream of the confluence to the mean upstream SSSC of both tributaries reveals that the surficial SSSC in water column is not a conservative property, but depends on flow conditions within the river. Surficial mixing can be complicated by the addition or loss of suspended sediment in the water column in the downstream direction. In the case of the reduction in SSSC on the March 30, 1988, slightly lower discharge in the Mississippi River compared to the discharge of Missouri River (Table 4.8), coupled with the slow mixing process, might have promoted a condition where flow expansion at wide sections of the river resulted in favorable conditions for sediment deposition. Widening of the river channel from 0.6km about 5km downstream of the confluence to 1.17km at 7.35 km downstream of the confluence may promoted deposition of sediment from the

Missouri River as flow on the west side of the Mississippi diverged and decelerated. Most of the deep side of the river channel at this location (Figure 4.5c) contains Mississippi water, whereas Missouri River water is presented on the shallow, outer side of the channel bend where a mid-channel bar is clearly visible at low flows. Most sediment probably fell out the water column before the river channel returned to the initial post-confluence width of about 0.6 km about 12 km downstream of the confluence. The effect of channel widening can be seen in Figure 4.6a where SSSC drops significantly on the Missouri side of the river from initial 600 mg/l to about 400 mg/l between a distance of 5 to 10 km downstream of the confluence. SSSC increases further downstream before decreasing again as the flow is constricted back to the channel with 0.6 km width.

Widening of the channel also affects *Pmx*. With higher width-depth ratio at wider portions of the river, the flow can spread over vast, shallower areas such that more satellite pixels will be covered with one type of flow while the flow at deeper part of the river may cover fewer number of pixels. The effect of this widening is depicted in Figure 4.13. Higher width-depth ratio will lead to some bias in the *Pmx* calculations as if the flows are unmixing, i.e. the decrease in *Pmx* values has nothing to do with mixing or unmixing.

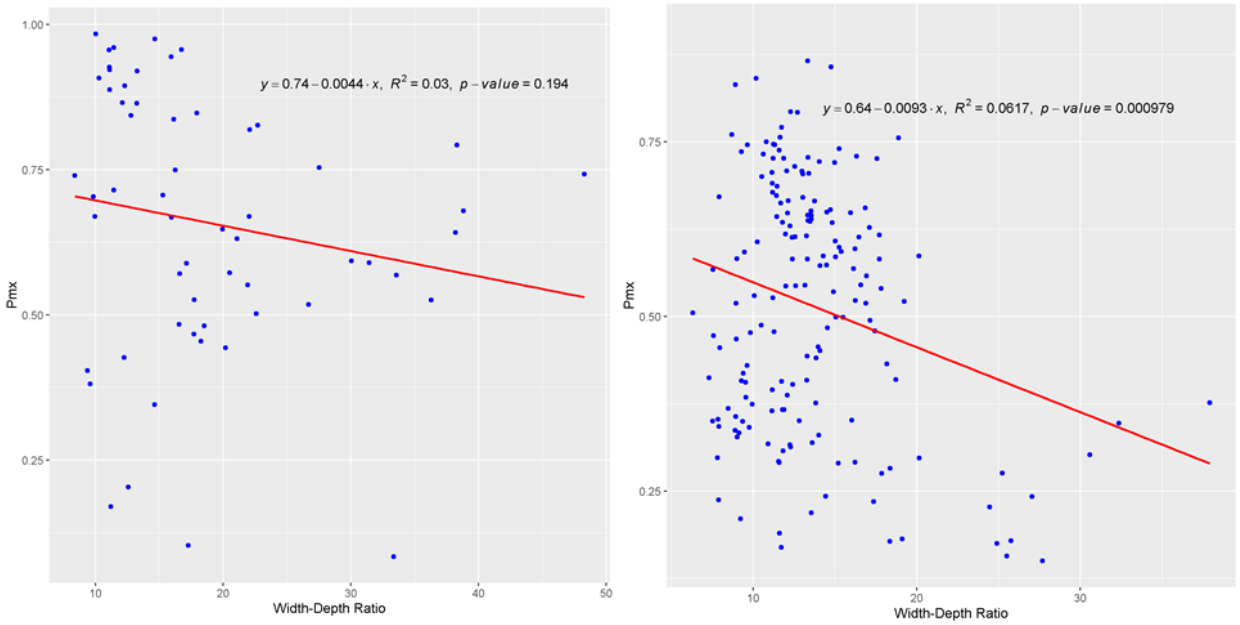

Figure 4.13: Variations in the mixing with longitudinal variations in width-depth ratio; for sediment reduction case (left), and for sediment addition case (right).

In the second case, on Apr 24, 1991, despite the Mississippi River having a discharge more than twice that of the Missouri River, the SSSC of Mississippi River is one-third that of the Missouri River (Table 4.8). Results indicate a slow mixing process where minor mixing has occurred within first 30 km, but the extremes of SSSC on each side of the channel remain similar to the initial concentrations. The slow rate of mixing at high discharge is consistent with the idea that the mixing rate is sensitive to the flow depth variations (Gaudet and Roy, 1995; Parsons et al., 2007).

The increase in SSSC between 30-60 km reach coincides with the straight but narrowest part of the river where the width of the channel decreases to only 0.45 km about 37 km downstream of the confluence and varies between 0.45 – 0.55 km within next 13 km before expanding back to the 0.6 km width. The flow convergence along with higher total discharge might have promoted erosion of the bed and banks of the river. However, the pattern of increasing SSSC does not cease even when the channel recovers to its average width.

Density differences could also control mixing processes by distorting mixing interface when relatively dense flow moves underneath the less dense flow. Laraque et al., (2009) found such example at Solimnões-Negro confluence where wedging of Solimnões under Negro distorted vertical orientation of the mixing interface into horizontal one. At the confluence of Segre and Ebro rivers in Spain, Ramõn et al., (2013) observed vertical stratification during summers with relatively larger density differences which inhibits mixing. For this research, the density differences of the incoming flows largely depended on the SSC rather than the temperature in all of the 57 cases observed due to the minimal difference between the temperatures of the incoming flows (Table 4.2). Thermal variations contribute an order of magnitude more to the density variations as compared to the variations in SSC. Therefore, density effects are not expected to be the major factor in controlling mixing at this confluence. In order to test the potential of a wedge formation from any of the tributary, densimetric Froude number was calculated for all cases using the equation;

$$F_r = \frac{U}{\sqrt{g'H}} \tag{4.8}$$

Where U is the cross sectional average flow velocity, H is the mean flow depth, $g' = g(\rho - \rho 0)/\rho 0$ is the reduced gravity, g is the gravitational acceleration, and ρ and $\rho 0$ are the densities of Missouri River and Mississippi River respectively. Figure 4.14 shows that all the values are well over critical value of unity. Ramon et al., (2014) found that density effects can be important for Fr <3. The minimum value among all observed cases is 3.42, indicating that the development of density wedges at the confluence is unlikely.

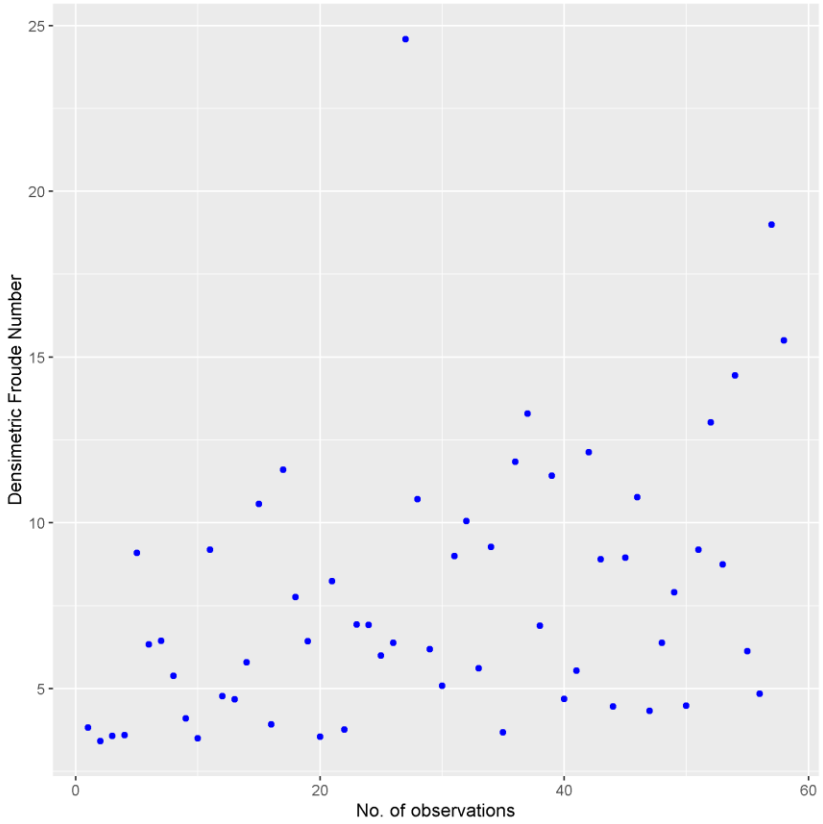

Figure 4.14: Densimetric Froude number distribution among all the observed cases.

4.7 Conclusion

This study used Landsat 5 TM data for the period of 1985-2011 and corresponding USGS gaging stations' data to model and predict suspended sediment concentrations within the study reach. Data on discharge, flow velocities and temperature were used to calculate density differences, momentum flux ratios and discharge ratios to examine the factors that influence mixing processes downstream of large river confluences. The results indicate the complexity of mixing at large rivers where mixing length scales vary significantly within same confluence under similar hydrological conditions. No clear statistical relationships could be established between PCFs and mixing lengths based on surficial patterns of mixing; therefore, comparison with past work on mixing at confluences is difficult. Major findings of this study include the following:

1. Momentum and discharge ratio at the confluence of the Missouri and Mississippi Rivers do not have any relationship with mixing lengths. Large discharge and momentum ratios shifts the mixing interface towards the outer bank, but the flow recovers quickly downstream without significant mixing. Cross sectional plots illustrate that the mixing interface moves back towards the channel centerline once the initial momentum effect subsides.
2. Mean flow depth at the confluence, and width-depth ratio show a statistically significant relationship with mixing; however, the relationship is extremely weak and the ranges of variation in depth and width-depth ratio are small.
3. The amount of mixing over first 6 and 30 channel widths also does not exhibit any strong relationships between PCFs and mixing lengths, suggesting that hydrodynamic conditions at the confluence do not have a substantial influence on mixing immediately downstream of the confluence.
4. Density differences between the two flows are insignificant; therefore, development of density wedges at the confluence is unlikely.
5. "Apparent" mixing can occur when SSSC increases or decreases on only one side of the river downstream of the confluence. The changes in SSSC on one side can make the channel appear mixed in *Pmx* calculations without any mixing processes involved. Thus, SSSC is not a conservative property of the flow for evaluating mixing over long distances downstream of the confluence.

The extent of applicability of these results on other large confluences is not clear. Additional research at other large confluences with different planform symmetry, geometry, and hydrological and climatic conditions is needed to compare the findings of this study. Further

work can combine satellite data with *in-situ* data to better understand localized processes, not related to the near field processes.

CHAPTER 5: COMPARISON OF OBSERVED MIXING LENGTHS VERSUS MIXING LENGTHS USING THE STREAMTUBE METHOD

5.1 Introduction

Natural channels are complex with meanders and non-uniform cross-sections. A depth-averaged mixing equation in rectangular Cartesian coordinates is not suitable for meandering rivers because cartesian x and z coordinates are not aligned with the downstream and cross stream directions. However, it is possible to transform from cartesian to curvilinear coordinates such that the major axis is always aligned with the downstream direction and the minor axis is aligned with the transverse direction. Yotsukura and Sayre, (1976)provided a detailed derivation of the depth-averaged mixing equation in cartesian coordinates. If the tracer source is steady, the time varying term of the mass conservation equation becomes zero, and the longitudinal dispersion term, being negligibly small, can be ignored (Yotsukura and Sayre, 1976). Furthermore, if the factor of diffusion is treated as constant across the channel, the result is the simplified stream-tube method (see section 2.3.2).

A simplified stream-tube method is applied in this study to estimate mixing lengths downstream of the Mississippi-Missouri confluence. A program written in R automates the process of calculating necessary parameters, defining streamtubes, and calculating mixing lengths. Mixing lengths from the streamtube method are compared with the mixing lengths computed from the methodology described in Chapter 4. Surface suspended sediment concentrations are used as tracer that is steadily being released into the water at the midpoint.

5.2 Methodology

5.2.1 Flow characteristics

A bathymetric survey conducted by USACE in 2001 for the Mississippi River from the Mississippi-Missouri river confluence to 87 km downstream of the confluence provided a basis

for mixing lengths analysis using the stream-tube method. Bathymetric point data were interpolated using the nearest neighbor interpolation technique to obtain continuous bathymetry of the river. Mean water surface slope (s) was determined using measured water surface elevations for U.S. Geological Survey gaging stations for the Mississippi River at St. Louis, MO, and the Mississippi River at Chester, IL. The two stations use NAVD88 as vertical datum. The datum height at St. Louis station is 115.7 m while the datum height at Chester, IL is 103.85 m. Water surface elevations (WSEs) at both stations were determined by adding gage heights to the corresponding datum elevations and uniform slopes were determined for each image by dividing the difference between the two WSEs by the streamwise distance between the two stations. A mean value of the water surface slopes for all image dates was determined to be 0.000099 (Figure 5.1). Using the slope and streamwise distance s from the upstream junction corner of the confluence to each pixel, WSEs are estimated for the entire study reach. Finally, the flow depths were determined by subtracting the bathymetric raster from the WSE raster for each image. The resultant raster represents flow depths at each pixel location.

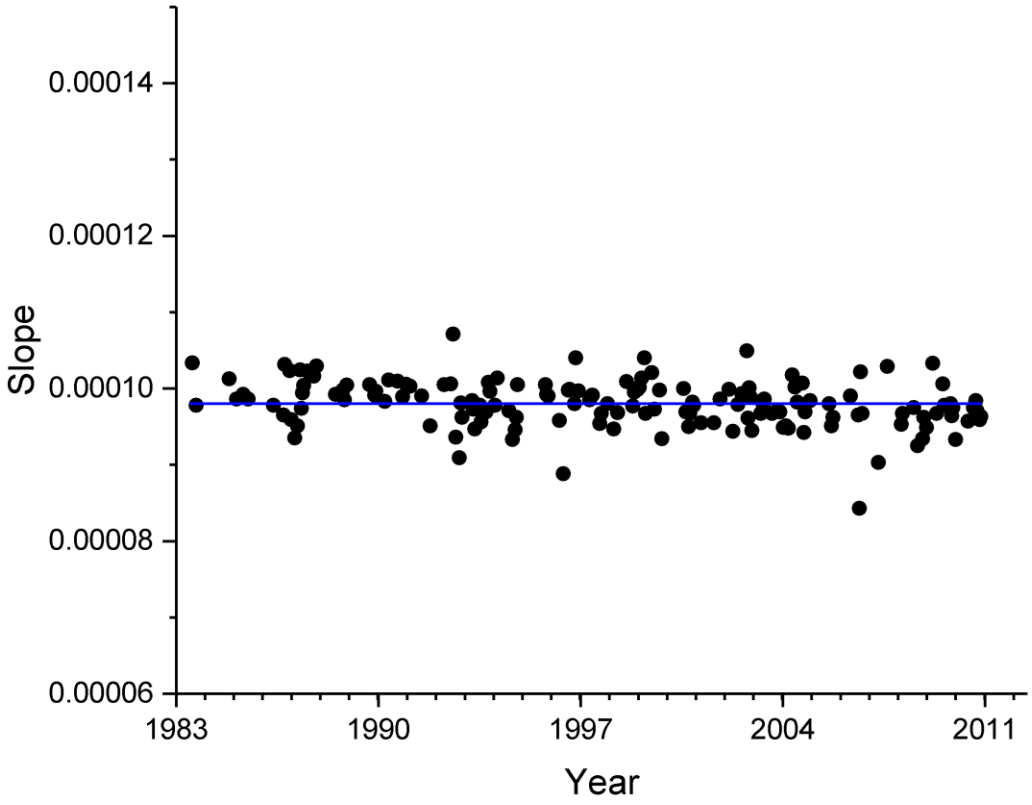

Figure 5.1: Water Surface slopes between St. Louis, MO and Chester, IL corresponding to Landsat image acquisition dates between 1984 and 2011.

5.2.2 Channel width

River widths (*b*) along the channel were determined by calculating lengths of the transects spaced at 500 m intervals along the river. The length of each transect along the river is based on the digitized water boundary as described in chapter 3. The locations of the transects were also used to obtain flow depths from the depth raster. All the raster pixels that intersected the transect lines were extracted and converted to point vector data for further processing. The converted point shapefile contains information about geographic locations and flow depths at each point location.

Because discharge varies over time, the width of the flow changes, and therefore an image's surface width may differ from the 2001 surveyed width. If the discharge for the

bathymetric survey date is less than the discharge for an image, the surface width of the 2001 survey date will be shorter than for the image. As flow depths can only be calculated where bathymetric information is available, the water-surface widths for some images may exceed the width of the channel for which flow depths are available (Figure 5.2). The effect is most pronounced on the shallow side of the channel in a meandering river.

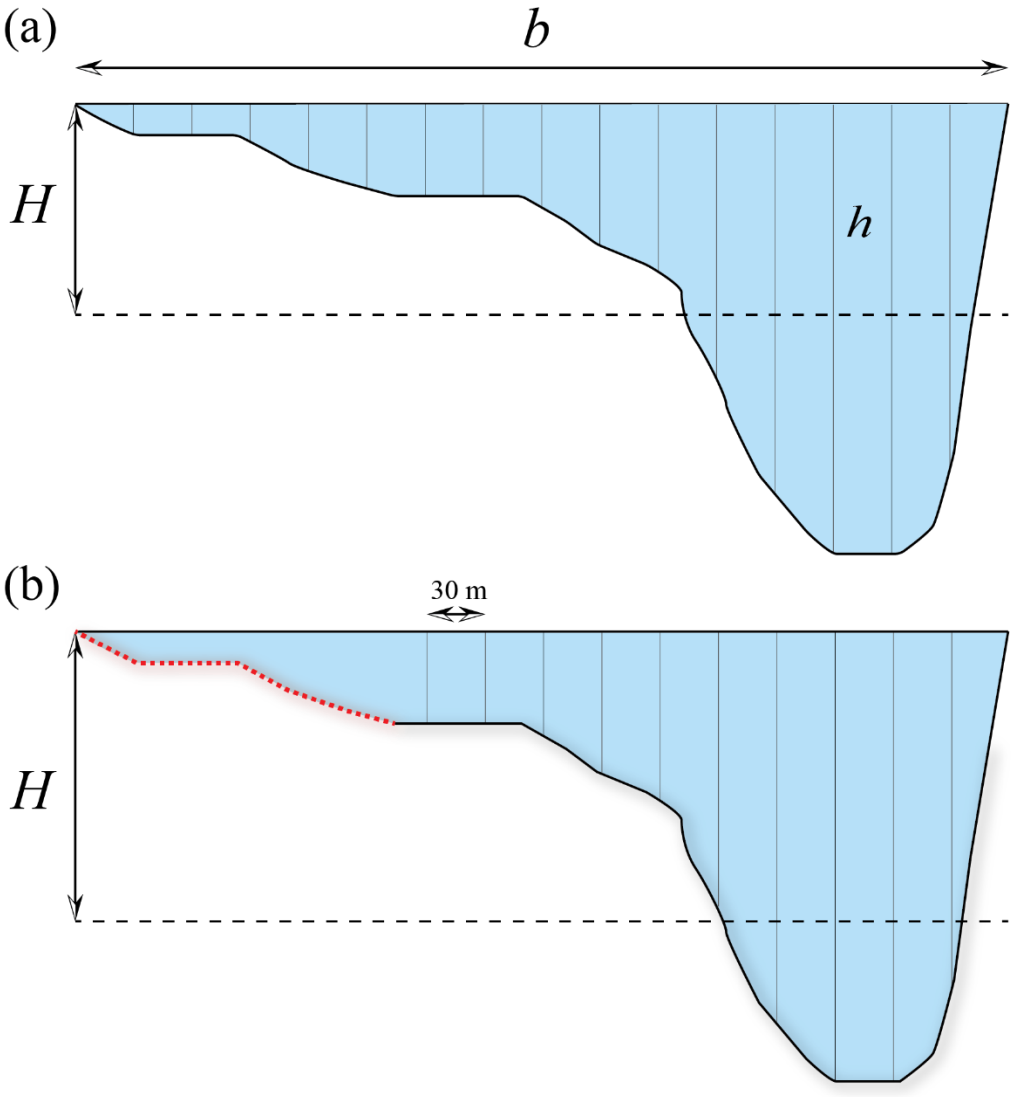

Figure 5.2: A hypothetical cross-sectional profile with complete bathymetric data (a) and with missing data (b). b is the surface width of the channel from the digitized river boundaries using Landsat Images, vertical lines in the channel represent local flow depths h measured at every pixel location from flow depth raster that intersected with the cross-section line, and H is the mean depth at the cross section. Red dotted line shows the areas where bathymetric data are not available.

The lack of bathymetric data, and hence flow depth data, for some portions of cross sections for discharges exceeding the 2001 discharge poses a challenge to compute cross-sectional velocity distributions. To deal with the missing data, the R program tests each cross section for width mismatch by comparing flow width calculated from the extracted flow depth pixels that are limited to the extent of 2001 surveyed width to the width of the cross section at the current location. If the widths are different, the program extends the last pixel on the shallowest side of the cross section from its current location to the edge of the cross section such that the distance between the first and the last pixels of the flow depth raster along a transect line roughly equals (±10 m) the length of the cross section (Figure 5.3). The approach can potentially increase or decrease the flow depths towards the shallow side of the channel. However, only the widest sections of the river, where in-channel bars are present, are susceptible to substantial changes in width. Because only two in-channel bars are present within the study reach, the net effect is localized and does not influence strongly the overall mixing length.

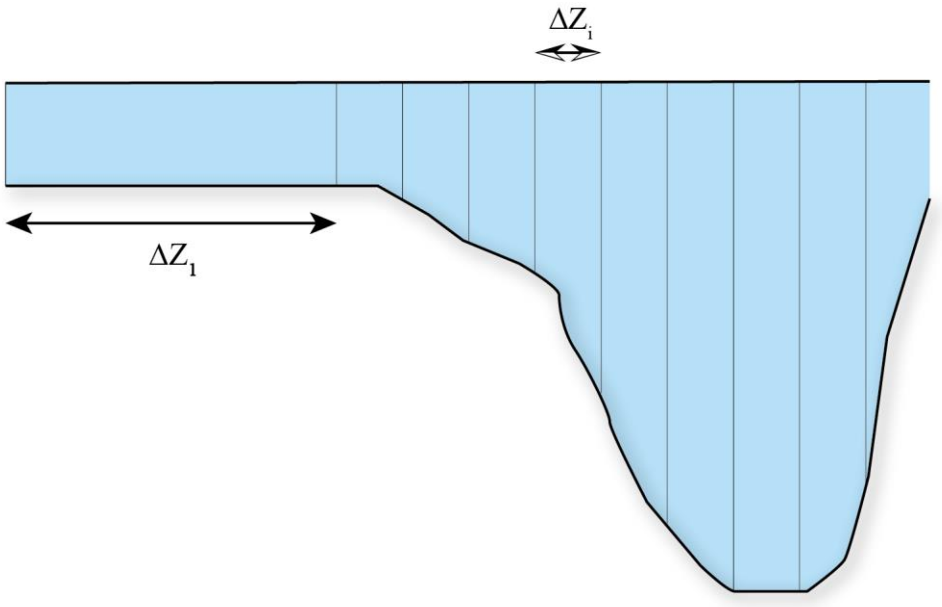

Figure 5.3: Shallower (left) side pixel from figure (2b) has been extended to the edge of the channel width resulting in an area of constant flow depth. Δz is the distance between two consecutive pixels. Notice a larger interval on the left side due to pixel's relocation to the channel boundary.

5.2.3 Local depth-averaged velocities

Using daily discharge (Q) values from the USGS gaging station at St. Louis, mean flow depth (H), water-surface width (b), and width-averaged flow velocities (V_x) were calculated at each cross section using the following relationship.

$$V_x = \frac{Q}{b\,H} \tag{5.1}$$

As cumulative flow distribution data are not available for the entire reach, a semi-empirical method (Yotsukura and Sayre, 1976) was used to estimate depth-averaged velocity distributions across the channel using the flow depths along the transect and mean width-averaged velocity.

$$v_x = V_x \left(\frac{h}{H}\right)^{2/3} \tag{5.2}$$

where v_x = local depth-averaged velocity, V_x = width-averaged velocity; h = local depth; and H = width-averaged depth.

5.2.4 Defining streamtubes

Streamtubes are defined on the basis of equal discharge intervals across the channel. Rutherford, (1994) has pointed out that a minimum of 10 or more streamtubes are desirable for the streamtube method. In this study, a total of 20 streamtubes were defined for all the cases. A multi-step procedure was used to define streamtubes at each cross section (Figure 5.4).

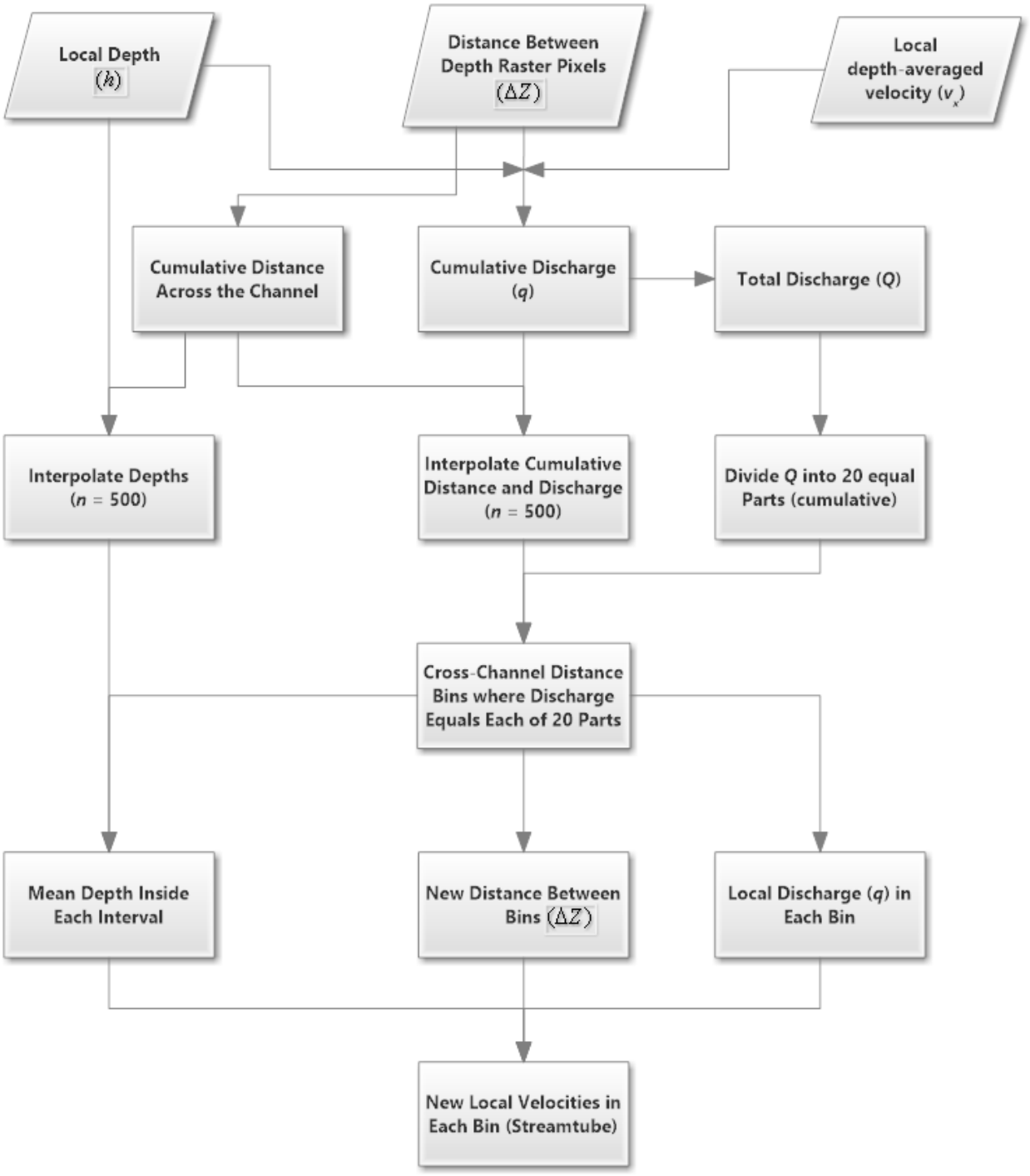

Figure 5.4: Flowchart of the procedure for defining 20 streamtubes. The procedure is performed at each cross section one by one along the entire study reach.

Equation 5.2 is used to compute v_x at each pixel location, which can be used to compute the cumulative discharge.

$$q_k = \sum_{i=1}^{k} v_{xi} h_i \Delta z_i \quad (5.3)$$

where q_k = cumulative discharge at a cross-section, v_{xi} and h_i= local depth-averaged velocity and depth at the location *i* respectively along the transect, Δz_i is the lateral distance across the channel between the centers of adjacent pixels and *k* is the total number of pixels along a cross section (Figure 5.3). The flow depths and cumulative discharge are available only at pixel locations at this point. To divide a cross section into equal discharge intervals, a more detailed distribution of flow depths across the channel, along with associated values of cumulative discharge, is required. Thus, the flow depth and cumulative discharge values are linearly interpolated into 500 points across the channel based on values calculated for pixels (Δz_i) (Figure 5.5).

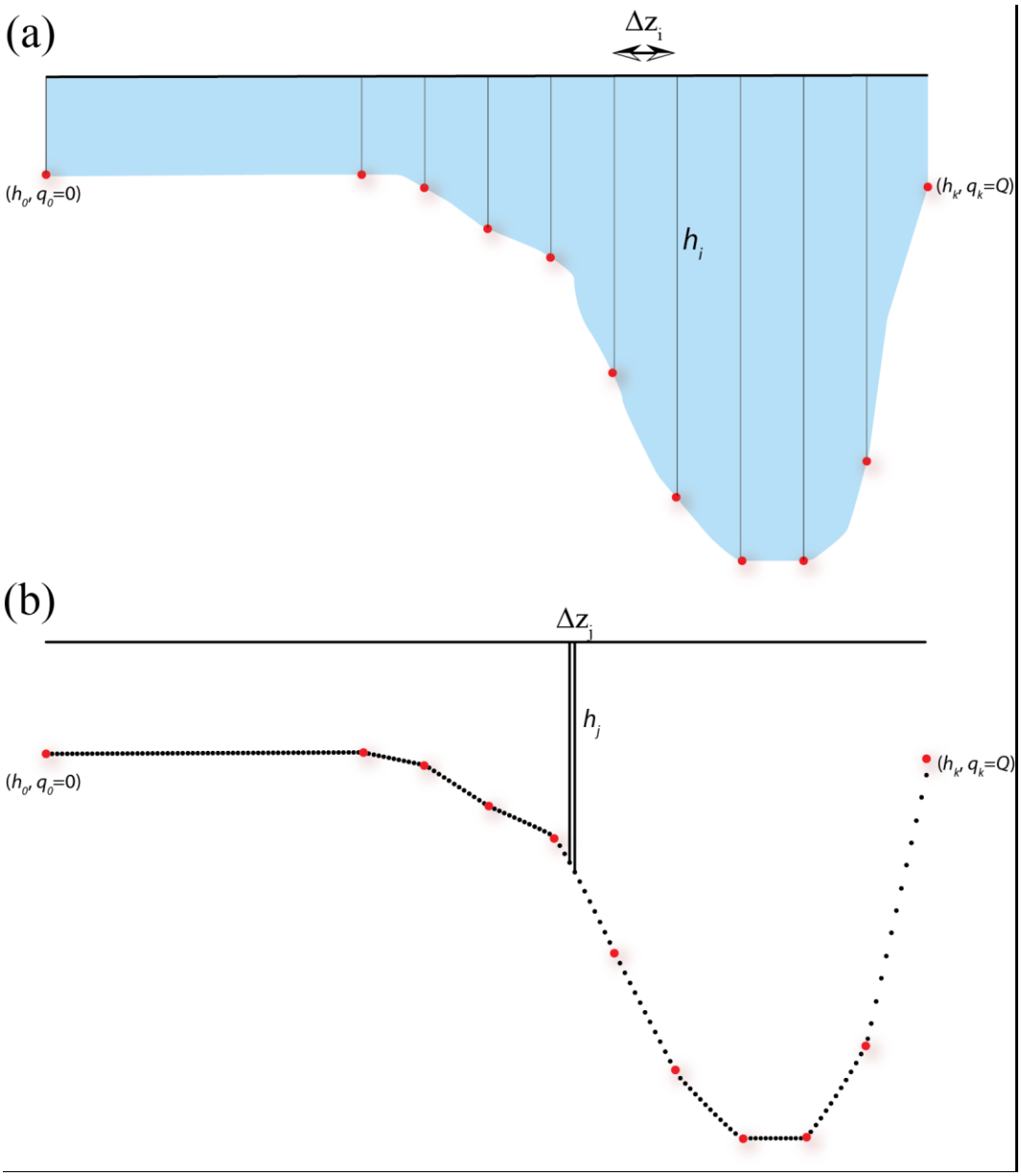

Figure 5.5: Transformation of original cross-section profile (a) into a more detailed profile (b) by linear interpolation between consecutive points. Each new point has a value for location, local depth and cumulative discharge. Red dots are the locations where flow depths and velocities and discharge values were initially available.

To facilitate division of the channel into equal discharge intervals (i.e. stream-tubes), the total discharge value for the entire cross section is divided into 20 equal parts to produce a set of cumulative discharge values that will be used to define width of each streamtube. For example, for a total discharge value of 2,000 m^3/s, each streamtube will have a discharge of 100 m^3/s and

therefore the set of cumulative discharge limits will be 100, 200, 300, and so on. The program then cumulates discharges across the channel for the 500 intervals centered on interpolated points (Δz_j) and identifies sets of lateral distance intervals where cumulative discharge values are equal to the cumulative discharge limit of each streamtube. These sets of lateral distance intervals are then binned together to create the streamtubes. The program starts from the right bank where cumulative discharge is 0. At each interpolated point (Figure 5.5b), the program will compute a new cumulative discharge value by adding the local discharge value to the cumulative discharge for the previous location until the new cumulative discharge value reaches 100 m^3/s. At this location, the program records the transverse distance from the right bank and assigns all intervening intervals to the first streamtube. The program continues laterally until it reaches a cumulative discharge of 200 m^3/s and assigns all intervals between 100 m^3/s and 200 m^3/s to the second streamtube. The process continues laterally, until all twenty streamtubes are identified, and longitudinally, until the end of the study reach. For each streamtube in each cross section, average local depths are calculated and mean local flow velocities are determined using the equation;

$$v_{xi} = \frac{q_{si}}{h_{si}\Delta z_{si}} \tag{5.4}$$

Where subscript *i* denotes the stream-tube *i*, q_s is the total discharge in streamtube *i*, h_s is the mean local depth in a streamtube *i*, and Δz_s is the width of the stream-tube.

5.2.5 Dimensionless shape factor

The dimensionless shape factor accounts for variations in channel planform geometry. The right and left bank lengths for each 500m sub reach are used to compute side lengths for each streamtube (Figure 5.6). The program estimates these lengths at each streamtube interval (Δz_s) computed in the previous step, by linearly interpolating between both banks (Figure 5.6).

As the length of the left bank is shorter than the left of the right bank in figure 5.6, at a certain distance ΔZ_1 from the left bank, where cumulative discharge is equal to the first cumulative discharge limit, the program has estimated side length to be 465 m. The process continues until side lengths are estimated for each streamtube.

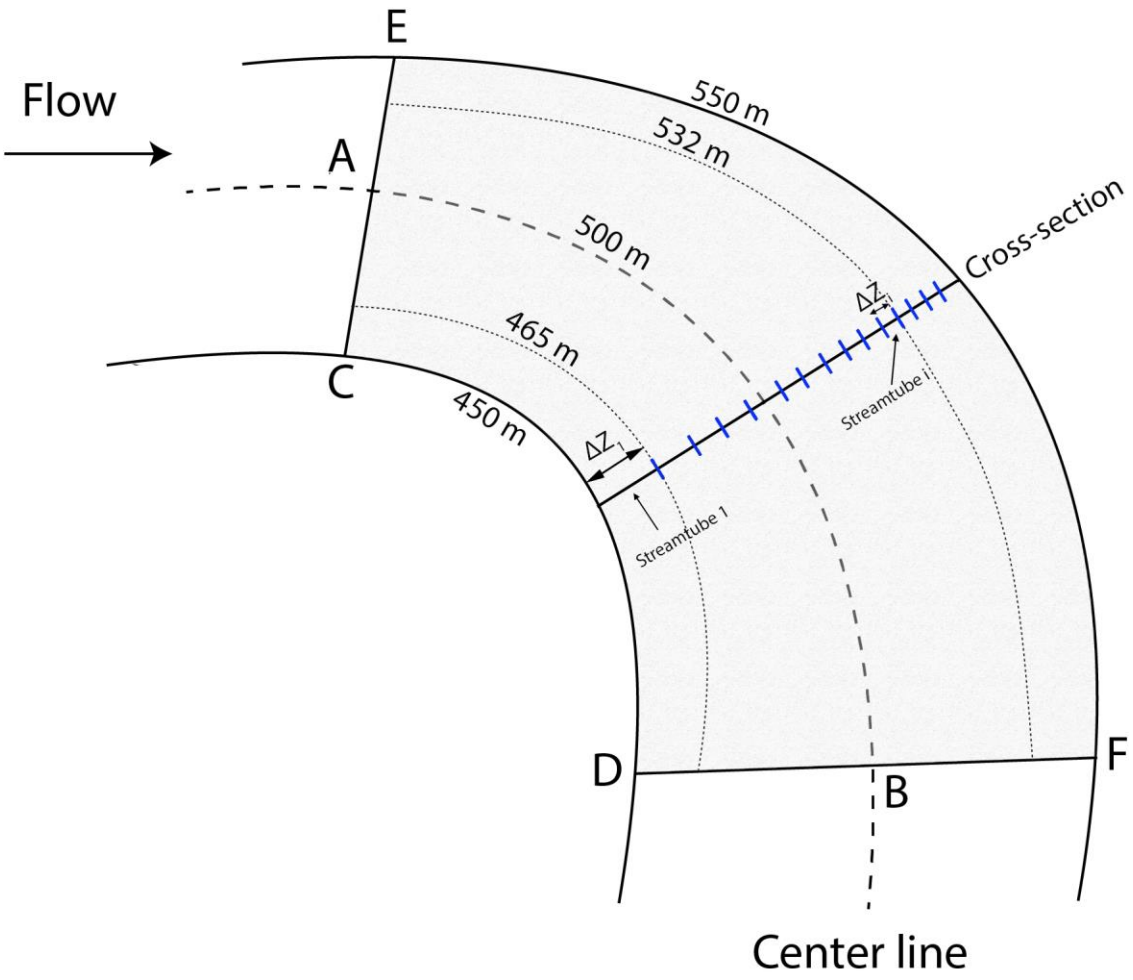

Figure 5.6: A hypothetical 500 m sub reach (shaded region) with 15 streamtubes. The dashed line is the channel centerline where longitudinal distance is measured to define sub reaches (AB). The central cross section is where width of the channel is determined and pixel values from flow depth raster are extracted. Streamtube intervals are shown in blue colors where discharge values are equal. Right bank (CD) is shorter than the left bank (EF). Linear interpolation between CD and EF will result in side lengths with values between 450 m and 550 m as shown in dotted lines for streamtube 1 and streamtube i.

The program uses the longer side length of each streamtube and divides it by the longitudinal length of a reach (500 m) to get the metric coefficient m_α for that streamtube. The

dimensionless shape factor is then computed for individual cross sections using the following equation;

$$\psi = \frac{1}{b}\sum_{i=1}^{N} m_{\alpha i}\frac{v_{xi}}{V_x}\left(\frac{h_i}{H}\right)^2 \Delta z_i \qquad (5.5)$$

where b = channel width; $m_{\alpha i}$ metric coefficient for stream-tube i; and N = total number of stream-tubes (N = 20). The value of the dimensionless shape factor ranges between 1 and 3.6 (Rutherford, 1994).

5.2.6 Transverse dispersion coefficient

The transverse dispersion coefficient k_z scales with the product of mean flow depth and the shear velocity (Rutherford, 1994). Yotsukura and Sayre, (1976) estimated the value of k_z around a bend in Missouri River using the bulk channel parameters, like channel width, mean flow depth, width-averaged velocity, radius of curvature, shear velocity etc.

$$\frac{k_z}{HU^*} = 0.4\left(\frac{V_x b}{U^* r_c}\right)^2 \qquad (5.6)$$

Where r_c = radius of curvature determined by fitting circles at each bend and determining their radius, and U^* = average shear velocity

$$U^* = \sqrt{gHs}$$

where g = acceleration due to gravity and s = water surface slope. However, Rutherford (1994) cautioned against using equation 5.6 because it did not fit well to the laboratory flume data of Yotsukura and Sayre, (1976) and Sayre, (1979). Sayre, (1979) found that for the Missouri River, the value of the constant 0.4 in equation 5.6 varied between 0.9-0.3 as the discharge increased from 565 to 1700 m^3/s. Because all discharge values in the present study exceed 1700 m^3/s (Table 4.2) and no other studies have examined the value of the constant for discharges this large, equation 5.6 has been used with the default value of 0.4. A lower value of the constant,

e.g. 0.3, will decrease the values of the dispersion coefficient, resulting in longer mixing lengths, but it will not have any impact on general trend between observed and computed mixing lengths.

Equations 5.5 and 5.6 can be used with cross-sectional mean values of flow depth and flow velocities to estimate factor of diffusion *D* at each transect.

$$D = \psi k_z V_x H^2 \tag{5.7}$$

A reach averaged value of *D* can then be calculated.

$$D = \frac{1}{L}\sum_{j=1}^{n} D_j \Delta x_j \tag{5.8}$$

where *L* = total reach length where bathymetric data is available (87 km); *ΔX*; = sub-reach length (constant 500 m for this study); *D*; = value of the factor of diffusion in sub-reach j from equation 5.7; and n = number of sub-reaches (n = 173). Finally, mixing length for a tracer source at mid-flow can be calculated using the following equation

$$L_z = 0.134\frac{Q^2}{D} \tag{5.9}$$

5.3 Results and discussion

The simplified stream-tube method has been used to compute mixing lengths in 11 cases where mixing was achieved within 110 km study reach. Bathymetric data obtained for the study reach by the U.S. Army Corps of Engineers in 2001 was used for all cases. The width of the channel changes significantly over the study reach with a mean standard deviation of 114.8 m for all cases. As flow depths are controlled by width variations, substantial variations are observed in cross-sectional mean flow depths and depth averaged velocities. The calculated streamtube parameters together with mixing lengths are listed in Table 5.1.

Table 5.1: Table of important variables. Range of values are provided for the variables that vary in the downstream direction

Image	Q (m^3/s)	Width (m)	Mean Depth (m)	Shear Velocity (m/s)	Dispersion Coefficient k_z (m^2/s)	Shape Factor	Factor of Diffusion (D)	Mean D	Mixing Length (Lz)
LT50240332011281	3,455	331-1053	4.4-11.8	0.06-0.1	0.02-3.0	0.8-3.2	1.6-155	21.0	76,297
LT50240332009339	6,484	310-1074	6.0-12.8	0.07-0.1	0.06-8.9	0.9-3	7.5-776	115.3	48,851
LT50240332009307	15,715	338-1075	9.6-14.0	0.09-0.1	0.2-26.6	0.8-1.5	91-6686	1256	26,350
LT50240332005232	2,692	226-1058	2.6-12.25	0.05-0.1	0.02-2.5	0.85-2.2	1.0-146	12.8	75,690
LT50240331998325	7,220	257-1055	7-13	0.07-0.1	0.7-9.2	0.9-1.8	10.4-1080	153.7	45,457
LT50240331997290	4,672	284-1019	5-12.5	0.06-0.1	0.03-4.8	0.8-2.2	3.6-399	51.6	56,683
LT50240331997082	9,033	251-1020	6.5-13.4	0.07-0.1	0.1-15	0.9-1.9	19.6-2428	304.5	35,910
LT50240331994090	6,456	300-1053	5.6-12.7	0.07-0.1	0.05-8.3	0.9-1.8	8-849	120	46,541
LT50240331992021	2,764	216-988	2.7-12.5	0.04-0.1	0.02-2	0.85-3.5	1-171	14	72,950
LT50240331988058	5,720	266-1019	5.5-12.8	0.07-0.1	0.04-6.8	0.85-1.9	5.6-572	85.3	51,415
LT50240331987343	4,276	176-991	4-13.2	0.05-0.1	0.03-3.7	0.9-2.25	2.8-395	42.2	57,956

5.3.1 Transverse dispersion coefficient

Transverse dispersion coefficient is important to determine the rate of mixing within a river channel. The dimensionless transverse dispersion coefficient, k_z/HU^*, has been estimated at each cross section and regressed against dimensionless hydraulic and geometric parameters of river channel to analyze the relationships between dispersion coefficient and different potential variables. Among these are channel aspect ratio (b/H), friction term (U/U^*), and channel curvature (b/Rc). The dispersion coefficient does not show any relationship with width-depth ratio and the velocity ratios. However, a strong positive relationship exists between dimensionless dispersion coefficient and width to radius-of-curvature ratio (Figure 5.7). This relationship can be explained by the presence of secondary currents in the meandering channels. The value of dispersion coefficient increases as the meander bends get tighter and the radius of

curvature becomes smaller, a condition that promotes development of secondary currents in the channel. Secondary currents are known to enhance transverse dispersion coefficient, and hence mixing in the rivers (Rutherford, 1994).

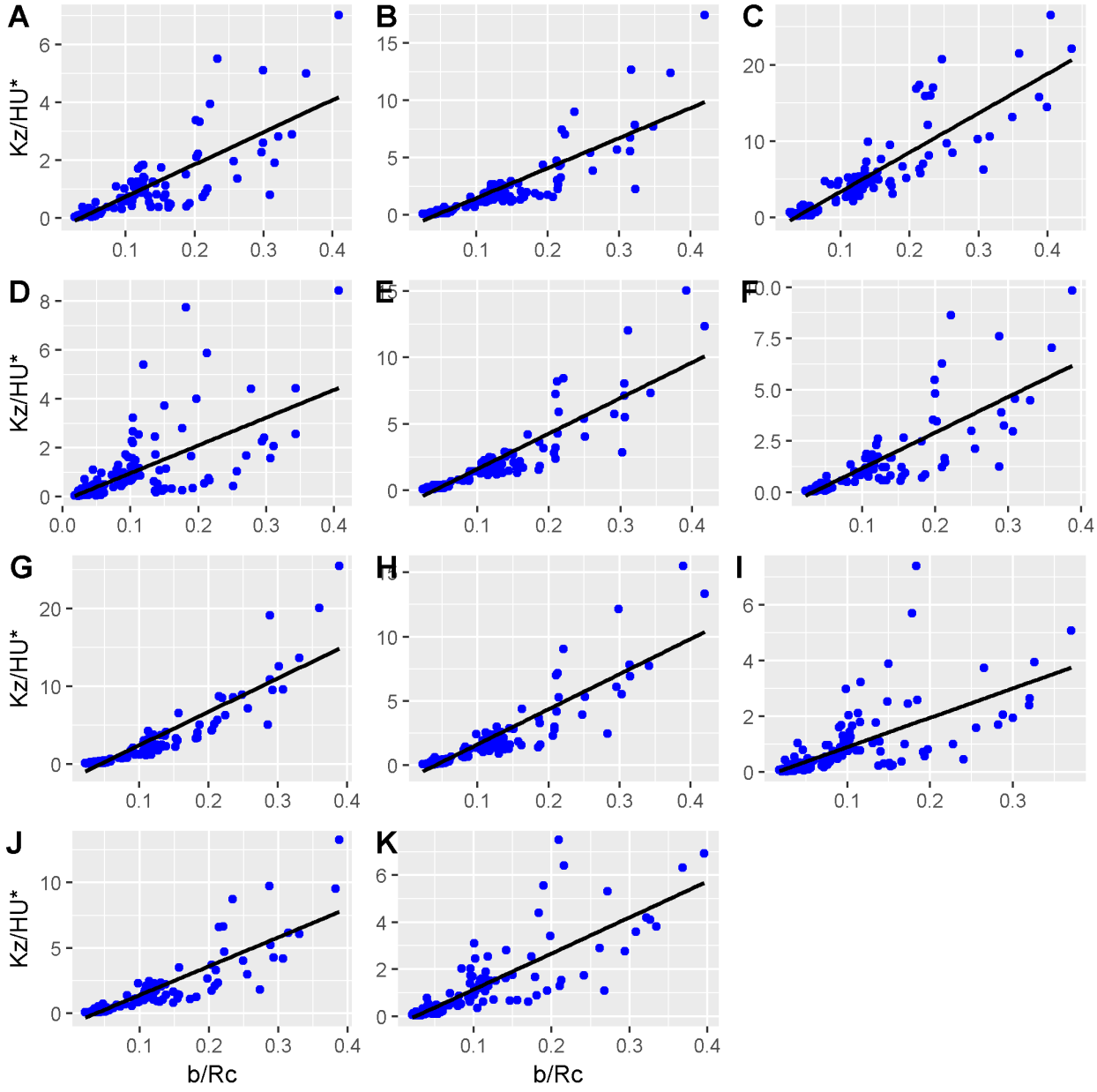

Figure 5.7: Relationship between dimensionless dispersion coefficient and b/Rc for the eleven cases.

To analyze the relationship between transverse dispersion coefficient, k_z and the value of the factor of diffusion, D, the values of D have been plotted against the estimated dispersion

coefficient (Figure 5.8). The factor of diffusion is directly related to the transverse dispersion coefficient, as suggested by the equation 5.7. Thus, for known dispersion coefficient values, the value of *D* can be estimated for a given discharge.

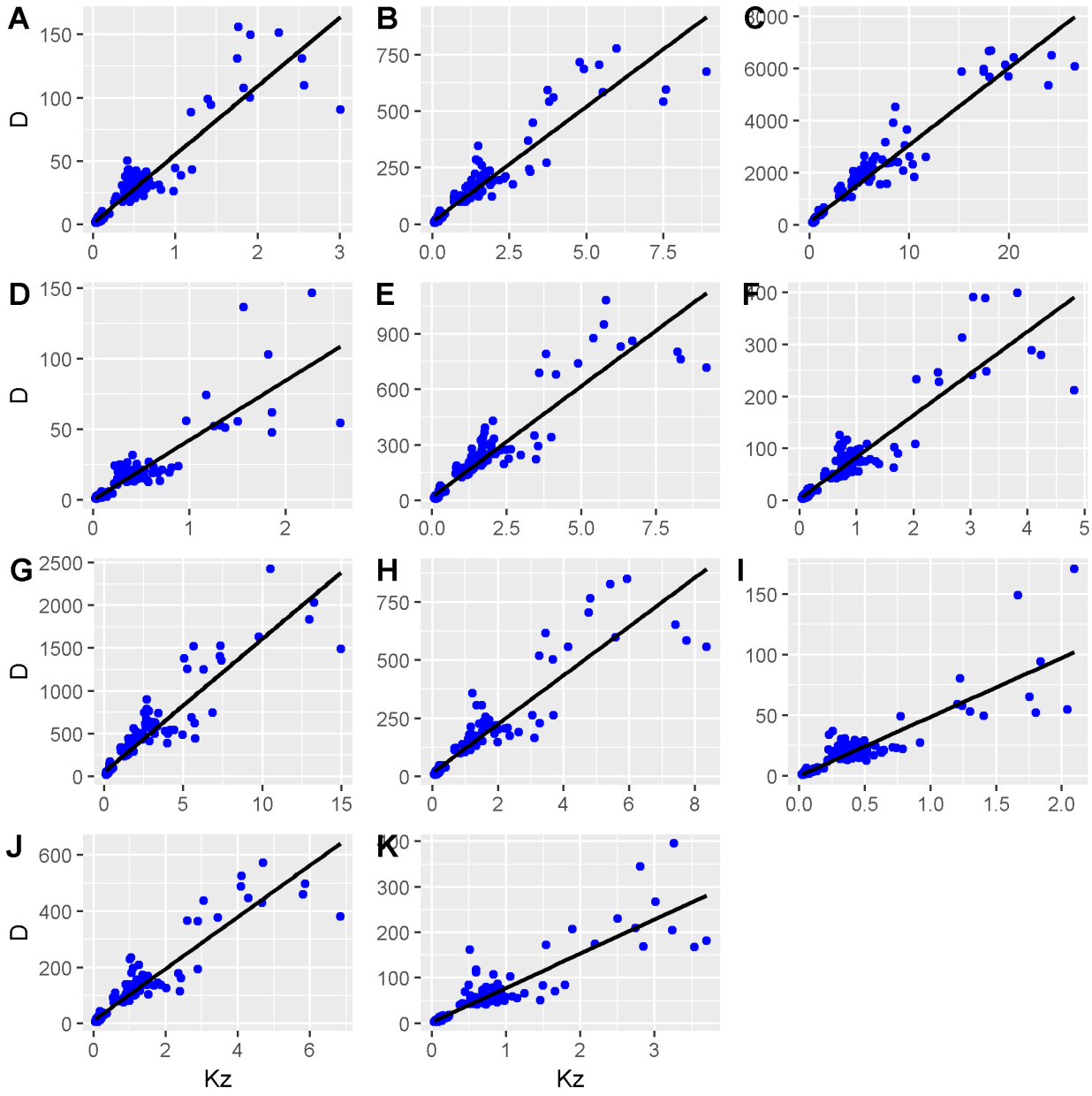

Figure 5.8: Relationship between transverse dispersion coefficient and the factor of diffusion for all the cases.

5.3.2 Factor of diffusion

For all the cases, a reach averaged value of diffusion factor is calculated using the equation 5.8. The reach-averaged values are important to get an initial estimate of the mixing lengths along a channel downstream of the source. It is clear from equation 5.7 that the factor of diffusion is a function of discharge. An increase in discharge results in a higher value for the factor of diffusion, enhancing the rate of mixing. As a result, the reach-averaged factor of diffusion is directly related to discharge (Figure 5.9), which results in a strong inverse relation between mixing length and discharge (Figure 5.10). Therefore, according to the streamtube method, discharge is the most important variable controlling the mixing process.

Despite the clear dependence of the mixing lengths on flow discharge in the streamtube method, mixing lengths have been found to vary significantly even with similar discharge values. Chapter 4 has documented multiple cases where strong variations in mixing lengths were observed for relatively similar discharges. Table 5.4 presents six such cases from chapter 4 where similar discharges (6,230-6995 m^3/s) yielded contrasting mixing lengths. For example, the minimum observed mixing length is 20km, whereas mixing did not occur in two of the cases over the entire length of the 110km study reach. In general, the pattern of mixing lengths seems to be opposite of what is expected from streamtube method, i.e. smaller discharges have shorter mixing length and higher discharges produce longer mixing length, although this relation does hold for all cases, as pointed out in the last chapter. The inverse relation between computed and observed mixing lengths for the 11 cases examined here indicates that processes that influence mixing downstream of the confluence of the Mississippi and Missouri rivers are more complex than the simple theoretical assumptions embodied in the streamtube model (Figure 5.11).

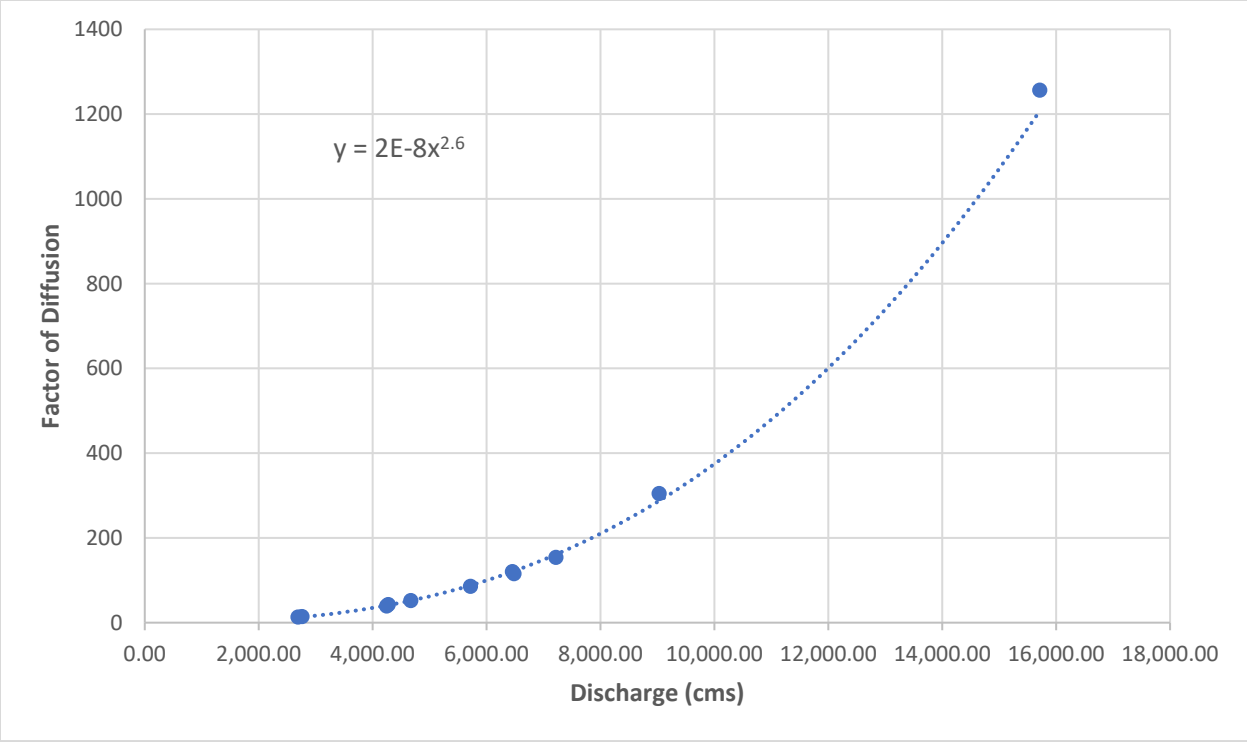

Figure 5.9: Relationship between flow discharge and reach-averaged factor of diffusion. The value of D increases as power function with discharge/

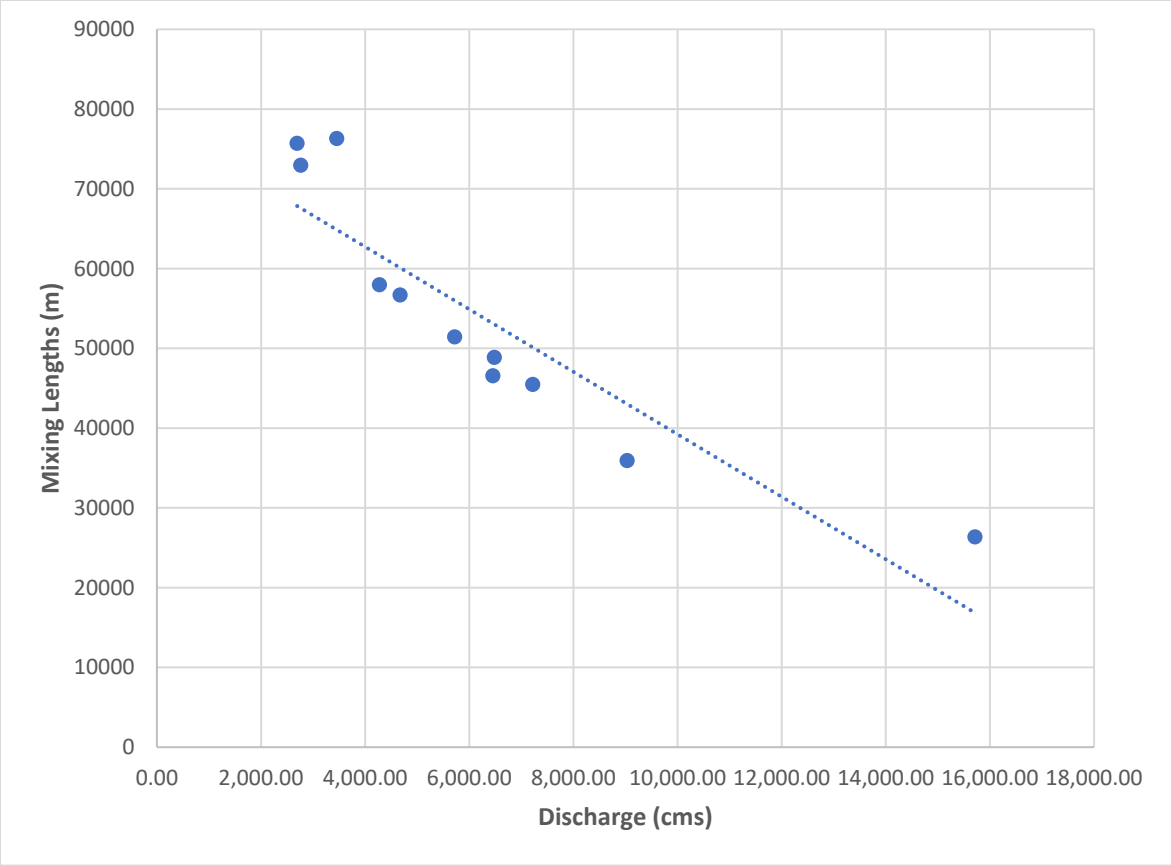

Figure 5.10: Relationship between flow discharge and mixing lengths computed through streamtube method.

Table 5.2: Mixing lengths observed at similar discharges. NAs represent the cases where streamtube method has not been applied.

	Image	Q (m^3/s)	Observed Length (km)	Streamtube Length (km)
1	LT50240331993311	6,230	20	NA
2	LT50240332004310	6,371	63	NA
3	LT50240331994090	6,456	60	46.5
4	LT50240332009339	6,484	90	49
5	LT50240332005056	6,824	No mixing	NA
6	LT50240332011249	6,994	No mixing	NA

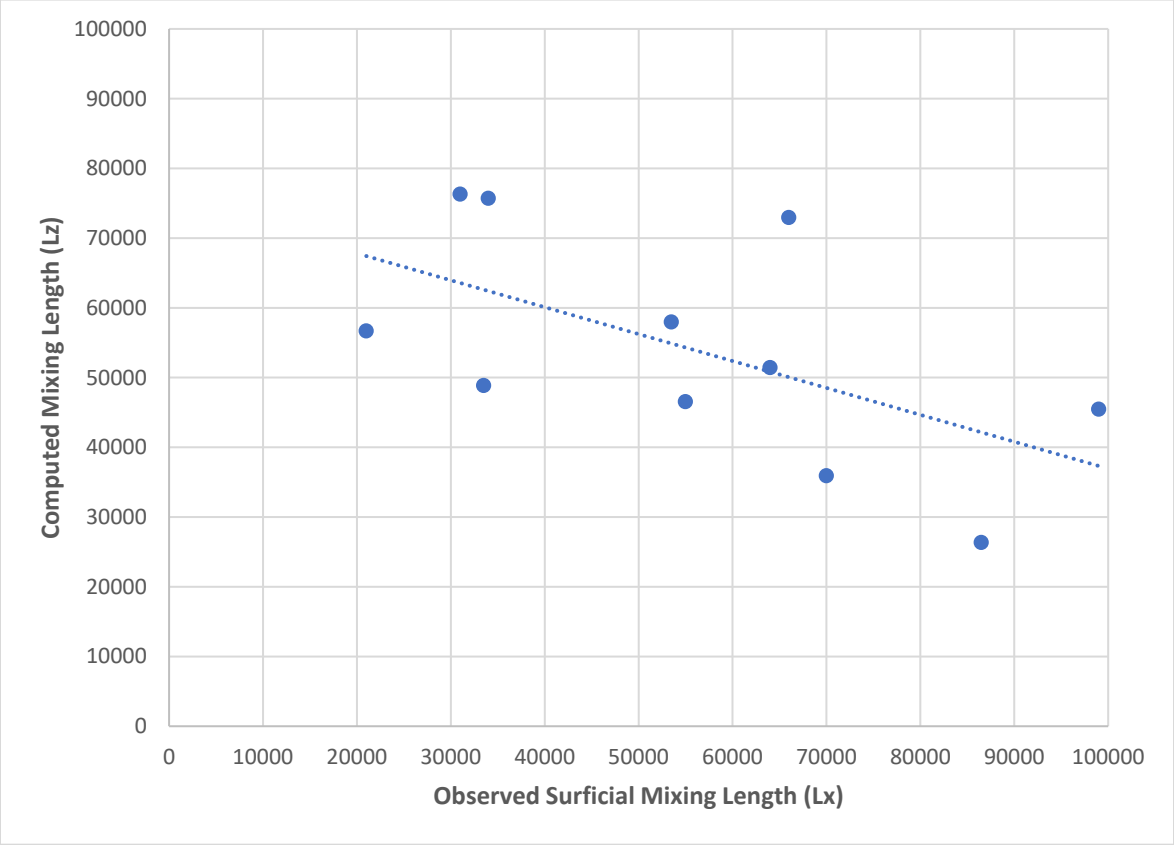

Figure 5.11: Comparison of mixing lengths obtained from the method reported in chapter 4 (Lx) and mixing lengths computed using the streamtube method (Lz).

5.4 Conclusion

A simplified streamtube method was applied to eleven cases in an 86 km reach where bathymetric data was available downstream of the Mississippi-Missouri River confluence in the Midwest USA. A method was developed for estimating mixing lengths downstream of a large river confluence using the geometric and hydraulic data in streamtube model. Twenty streamtubes were established and a program was written to compute necessary parameters for the implementation of the model. Transverse dispersion coefficients and diffusion factors were determined at regular intervals along the channel and the values were related to bulk parameters to explore relationships between different variables. Transverse dispersion coefficient and the

factor of diffusion are directly related to each other, while the diffusion factor is strongly inversely proportional to the mixing lengths.

Among all the cases, the streamtube method underpredicted mixing lengths for five of the cases, whereas mixing lengths were overestimated for the other six cases. The factor of diffusion is largely controlled by the flow discharge in the streamtube method, suggesting that higher discharges should result in shorter mixing lengths. However, this generalization does not hold for conditions downstream of the confluence of the Mississippi and Missouri Rivers. In many observed cases, similar discharges lead to very different mixing lengths. Similarly, cases with low discharges but rapid mixing or high discharges and slow mixing also deviate from model estimates. The discrepancy between observed and predicted mixing lengths is evident in the inverse relation between observed and predicted values. It can therefore be concluded that generalizing the pattern of mixing is difficult and streamtube method alone is not suitable for predicting mixing lengths. Mixing downstream of confluences in the streamtube model developed herein is treated as a tracer released at the center of the channel. For small tributaries it could also be treated as a tracer released near either bank. Under these conditions the constant in equation 5.9 has a value of 0.536 rather than 0.13. Such a treatment will increase mixing lengths, but the basic relationships in the model will remain the same.

The discrepancy between observed and predicted mixing lengths may originate from many factors. The streamtube model assumes that the factor of diffusion is constant across the channel. In natural rivers, channel depths vary across the channel and the factor of diffusion is expected to be less in the shallower areas than in the deeper areas. Not accounting for this spatial variation in diffusion introduces some error into predictions of mixing lengths. Additionally, Rutherford (1994) has stressed that caution must be taken while using transverse dispersion

coefficients computed using equation (5.6), given the uncertainty of estimates of dispersion calculated by this equation. The value of the constant in the equation 5.6 is found to vary between 0.3-0.9 depending on discharge values. Furthermore, as pointed out in the chapter 4, inherent problems with determining surficial mixing lengths from remote sensing data likely contribute to discrepancies between estimated and observed mixing lengths. Nevertheless, the large difference between predicted and observed mixing lengths strongly suggests that the streamtube method fails to adequately capture mixing processes. In particular, the strong dependence of mixing on discharge is not evident in the observed values of mixing. Further research is needed with detailed three-dimensional velocity measurements and bed characteristics using new technologies like acoustic doppler current profiler (ADCP) to accurately assess transverse dispersion coefficients and the factor of diffusions to be able to establish how different parameters control transverse mixing in rivers.

CHAPTER 6: CONCLUSION

6.1 Summary of findings

The primary goals of the research were: 1) to develop a methodology to detect suspended sediment concentrations distribution downstream of a large river confluence using flow and suspended sediment data from USGS gaging stations and satellite data from Landsat 5 and 2) to use the method on a large set of satellite images with wide range of hydrological conditions to examine the effects of varying potential controlling factors on the mixing rates and length scales. Successful application of the methodology on large number of cases contributes to the understanding of mixing processes downstream of large river confluences by providing insights into the relationships between the PCFs and observed mixing lengths over wide temporal and spatial scales. The research methodology developed in this dissertation provides basis for further mixing studies at and downstream of large river confluences around the world.

The dissertation research consisted of three main components. In the first part, 143 cloud free Landsat images, acquired for a large confluence in the US – Mississippi-Missouri River confluence, over a period of 1985-2011, were used with SSC data from USGS gaging stations within satellite image's footprint to relate the satellite spectral bands and spectral band indices for the stations' locations to the observed SSC. A model was developed to predict SSSC over the entire study reach and a new mixing metric was proposed to compute mixing quantitatively along the study reach. The methodology that was developed was applied to three images to demonstrate model's applicability and performance of the proposed mixing metric. In the second part, the method was applied to selected 57 images from initial 143 images based on visible contrast in the SSSC of incoming flows and the effects of discharge ratios, momentum ratios, flow depths, width-depth ratio, SSSC ratio and temperature ratios on the observed mixing rates

and length scales were documented. It is concluded that the potential factors that are important for small confluences may have minimal effect in large confluences. In the third part, a new methodology was introduced to implement streamtube method using river planform data from the satellite images, hydrologic data from USGS, and bathymetric data from USACE. The method was applied to eleven cases selected from second part of the dissertation research where complete mixing occurred within the study reach. The results from the model were compared with the results achieved in the second part to understand how well the model predicts mixing downstream of the Mississippi-Missouri confluence. The conclusions of this research suggest that mixing at large river confluences is more complex than in small confluences and simplified semi-theoretical models do not accurately predict transverse mixing.

The research was guided by the research objectives described in Chapter 1. Each of the objectives is restated again as a recap and summary of the processes and main findings are presented below.

1) Develop a satellite remote-sensing-based methodology to determine spatial patterns of suspended sediment downstream of a large river confluence

Investigations of mixing processes downstream of a large rivers confluence require measurements of tracer gradients across the channel as the tracer cloud moves downstream. The mixing however may not happen for tens and hundreds of kilometers downstream of the confluence. Therefore, field measurements are not often feasible for large rivers. Satellite remote sensing data, if used in combination with ground data, has the potential for aiding and enabling river mixing studies at large confluences. A model was developed using 143 cloud free Landsat 5 TM scenes over a period of 26 years and flow and SSC data from USGS gaging stations (see Chapter 3). Landsat spectral bands were used to calculate spectral indices that are known to

perform well for the detection of SSC in water bodies. Cross sectional averaged values of spectral bands and spectral indices information at the locations of USGS stations were combined with the observed cross sectional average SSSC values at these locations that resulted in a total of 271 data records from which half of the data was randomly selected to generate model and the rest of the data was used for model's performance testing. RF model produced an r-squared value of 0.7. The model was applied to Landsat images that produced rasters where each pixel indicating SSSC value at that location. Spatial patterns of SSSC downstream of the confluence can be analyzed by extracting cross sectional values at any desired location. However, because of the turbulence in rivers, reflectance varies locally over space and time that can cause strong pixel to pixel variations even within a fully mixed channel. To mitigate this effect, data are spatially averaged before computing the proposed mixing metric. A spatial averaging technique averages SSSC values at certain longitudinal distances, 500 m in this study, and produces a representative cross section with averaged SSSC values. The method acknowledges the fact that width of the channel changes over the distance in natural rivers. Geographic coordinates of each pixel locations are transformed to local *s* and *n* coordinate system before all the pixel values are averaged so that their *n* values can be normalized based on width of the central cross section. This way the pixels near the banks fall near the bank of the representative cross section and so on. The proposed mixing metric was then used to compute mixing at each spatially averaged cross section, 500 m apart. The new metric offers some advantages over previous metrics because it accounts for initial SSSC differences and unlike previous metrics, does not produce high mixing values for the cases where initial contrast in sediment concentrations within incoming flows is low. Additionally, a new term has been introduced in the mixing metric to account for variance in SSCs within the incoming flows. The metric produces values between 0

and 1 where 0 represents no mixing and 1 represents complete lateral mixing. The metric can be used to map spatial variation in mixing downstream of the confluence. The whole procedure can be automated that enables application of the model on large set of datasets.

2) Apply the methodology to a large river confluence to evaluate rates and length scales of transverse surficial mixing of suspended sediment for a wide range of hydrological conditions

The method developed for first objective was applied to large number of satellite images with wide range of hydrological conditions. From a pool of 143 images of a large confluence in the US – Mississippi-Missouri River confluence, acquired for a period of 1985-2011, 57 were selected for further analysis based on visible SSSC contrast between the incoming flows. For each image, values of SSSC were predicted at and downstream of the confluence, SSSC values were averaged spatially over a longitudinal distance of 500 m, and amount of mixing was determined using the confluence mixing metric. Mixing lengths were documented for the cases where mixing metric reached the threshold value of $Pmx > 0.97$ within the study reach. Out of 57 observed cases, complete lateral mixing was achieved in 44 cases within 110 km study reach while mixing could not be achieved in rest of the 13 cases.

3) Evaluate the effects of potential controlling factors (PCFs), such as momentum ratio, total flow discharge, width-depth ratio, sediment-concentration ratios, and density differences on rates and length scales of mixing downstream of a large river confluence.

Examination of mixing lengths in response to the PCFs elucidates how patterns of mixing are influenced by the variations in each of the controlling factors. Stage and discharge data from USGS gaging stations, bathymetric data from USACE, and SSSC and temperature data derived

from remote sensing data were used to calculate flow depths and flow densities which in turn were used to calculate PCFs such as momentum ratio, discharge ratio, width-depth ratio, SSSC ratio, and temperature ratios (see Chapter 4). The results illustrate the complexity of mixing processes at this confluence. For the most part, mixing lengths exhibit either very weak relationships or none at all with the different PCFs. Momentum flux ratio, discharge ratio, SSSC ratio, and temperature ratio were all found to have no substantial influence on mixing processes and hence mixing lengths. Relations derived from linear regressions of mean flow depths and width-depth ratios at the confluence against observed mixing lengths are statistically significant, but values of R^2 are low (< 0.2) and these relationships are based on data that is limited in range.

Analysis of the cases with high momentum flux ratios reveals a strong influence of momentum within initial three channel widths downstream where Missouri River impinges Mississippi River to the outer bank. This initial effect however, does not have significant effect on lateral mixing. The plot of mixing rates in first six channel widths did not show any positive relationship of momentum flux ratio with the mixing rates. The flow quickly recovers downstream of the CHZ and often stays unmixed for large distances downstream. The lack of mixing at the confluence can be explained by analysis of bed topography, which shows the lack of significant "step" that could distort the mixing interface and hence increase mixing. Additionally, the Mississippi River is relatively straight upstream of the confluence and therefore existence of a secondary flow on of the Mississippi side of the confluence is unlikely. The Missouri River curves to join the Mississippi River and may develop secondary circulation as flow curves to align with the receiving channel. If secondary circulation does develop from this effect, it does not appear to have a strong influence on mixing. Furthermore, the density

differences between the flows are not great enough to form a density wedge, which could have increased mixing rates.

4) Determine whether changes in the "apparent" amount of mixing, as determined from a mixing metric, might reflect factors other than mixing, such as additions or losses of sediment from the water column over distance.

In addition to mixing metric reporting a complete lateral mixing ($Pmx > 0.97$) due to mixing processes, detailed analysis of mean SSSC profile downstream of the confluence relative to the upstream mean SSSC reveals another possibility for a flow to appear completely mixed without actual mixing processes, i.e. by changes in surficial SSC values on one side of the river, either by addition or reduction of SSSC. Two of such cases were presented where complete mixing were reported within the study reach, however, the mean SSSC at the mixed location did not merge at the expected SSSC (see Chapter 4). Investigation of SSSC reduction case revealed that SSSC reduction corresponded to the longitudinal changes in channel dimensions. Most of the sediment was lost at the location where channel is wider, and the Missouri River water was spread over shallower area and probably decelerated. For the sediment addition case, the Mississippi River was at a high flow stage, but had had a low sediment concentration upstream of the confluence. Downstream of the confluence, the SSSC on the Mississippi side of the river started increasing about 30 km downstream of the confluence. The mixing metric reported complete mixing when SSSC of Mississippi increased to a similar value to that of the Missouri River, which maintained its original SSSC value over the distance of 100 km. The mixed SSSC value in this case was much higher than the expected value. These finding illustrate that the non-conservative properties of suspended sediment need to be considered when evaluating mixing downstream of confluences in large river systems.

5) Develop a stream-tube model of mixing lengths and compare predicted lengths scales of mixing with observed length scales of surface mixing derived from remote sensing analysis

A semi-theoretical model based on the streamtube method has been developed to predict transverse mixing in the Mississippi River downstream of the confluence with the Missouri River. River stages and discharge data were obtained from USGS and water surface slopes were determined between St. Louis, MO and Chester, IL. The slopes were used in combination with the 2001 bathymetric data from USACE to determine complete flow depths profile along the entire study reach. Flow discharge was used in the model to estimate cross-channel velocity distribution at each cross-section. Twenty streamtubes were defined and a program in R was written to compute discharge and width of each streamtube. The program also determined streamtube model parameters including the transverse dispersion coefficient and the factor of dispersion averaged for the entire reach. The calibrated model was used to estimate transverse mixing lengths for each of the eleven days corresponding to dates when transverse mixing occurred within the study reach according to information derived from Landsat images. The streamtube model relies heavily on the discharge and predicted mixing lengths are inversely related to the magnitude of discharge. This finding is inconsistent with the empirical findings in the earlier section where a weak direct relationship was found between mixing lengths and discharge. Overall the streamtube model performed poorly in predicting mixing lengths, indicating that the process of mixing downstream of the confluence of the Mississippi and Missouri rivers is more complex than characterized by this relatively simple mixing model.

6.2 Future work

This research has investigated the relationships between PCFs and mixing rates and length scales in a large river confluence over long spatial and temporal scales by developing a new model capable of detecting SSSC quantitatively, applying that model to large number of satellite images, developing a spatial averaging technique, and calculating mixing using the mixing metric. Although, the methodology provided in this dissertation worked well for large number of cases, the results show the complexity of the mixing processes at large river confluences. Additional work at different large river confluences is needed to clarify whether these findings are site specific or ubiquitous. This site has been subjected to wide range of ongoing anthropogenic modifications which may have affected the flow and sediment dynamics at the confluence.

The model developed in this dissertation should theoretically be applicable to anywhere around the world given the SSSC is less than the SSSC for which the model was trained for, i.e. SSSC <= 1700 mg/l. However, the performance of the model should be tested before applications at a different site. If found practical, the methodology can be used in future on a large number of cases to explore the influence of potential controlling factors including planform symmetry on the downstream rates of lateral mixing. However, future work should integrate surface processes with subsurface processes by combining remote sensing data with field data in order to better understand mixing downstream of large river confluences. Statistical analysis failed to reveal any strong relations between potential controlling factors and mixing lengths. Thus, analyses based on data derived from remote sensing and from other secondary sources (gaging data, bathymetric data) was not sufficient to determine factors controlling mixing lengths. An approach that combines remote sensing and field campaigns appears necessary.

Such an approach can provide the basis for linking process-based field measurements of hydrodynamics and mixing at specific locations downstream of a confluence with spatially extended patterns of mixing detected by remote sensing. A potential concern for future work however, is that Landsat 5 has developed problem with its solar arrays (Furby and Wu, 2009) and it has already exceeded its life expectancy with little fuel left for operational purposes (Marx and Loboda, 2013; Wulder et al., 2009). Also, Landsat 7's image quality has deteriorated due to SLC failure, resulting in black stripes in the images. Nevertheless, the same technique can be used in future with the newly available Landsat 8 that was launched in January 2013. Landsat 8 has potential to be an ideal sensor for inland water quality applications with an additional deep blue band that has been specifically added for research on water bodies, along with refined heritage bands in visible and near IR range. Additionally, with its better residence time and higher radiometric resolution (12-bit data as compared to 8-bit data of Landsat 5 and 7), Landsat 8 will be able to detect subtle gradations in reflected light intensity and hence it will allow more detailed mixing dynamics studies at confluences.

Future work using remote sensing may also be undertaken at the sites where detailed field data were collected (e.g. Lane et al., 2008) to test how well remote sensing data can reproduce observations on the ground. Such work would require a minimum discharge and bathymetric information in both tributaries. With SSSC and temperature derived from satellite data, remote sensing data should be able to detect density wedges associated with density differences. However, remote sensing has limited capability when it comes to disruption of mixing interfaces associated with bed discordance.

REFERENCES

Ashmore, P., Parker, G., 1983. Confluence scour in coarse braided streams. Water Resour. Res. 19, 392–402. doi:10.1029/WR019i002p00392

Ashmore, P.E., Ferguson, R.I., Prestegaard, K.L., Ashworth, P.J., Paola, C., 1992. Secondary flow in anabranch confluences of a braided, gravel-bed stream. Earth Surf. Process. Landforms 17, 299–311. doi:10.1002/esp.3290170308

Beltaos, S., 1980. Longitudinal dispersion in rivers. J. Hydraul. Div. ASCE HY1, 151–172.

Benda, L., Andras, K., Miller, D., Bigelow, P., 2004. Confluence effects in rivers: Interactions of basin scale, network geometry, and disturbance regimes. Water Resour. Res. 40, n/a-n/a. doi:10.1029/2003WR002583

Beschta, R.L., Bilby, R.E., Brown, G.W., Holtby, L.B., Hofstra, T.D., 1987. Stream temperature and aquatic habitat: fisheries and forestry interactions, in: Salo, E.O., Cundy, T.W. (Eds.), Streamside Management: Forestry and Fishery Interactions. Institute of Forest Resources, University of Washington, Seattle, Washington, pp. 191–232.

Best, J.L., 1988. Sediment transport and bed morphology at river channel confluences. Sedimentology 35, 481–498. doi:10.1111/j.1365-3091.1988.tb00999.x

Best, J.L., 1987. Flow dynamics at river channel confluences: implications for sediment transport and bed morphology, in: Recent Developments in Fluvial Sedimentology. SEPM (Society for Sedimentary Geology), pp. 27–35. doi:10.2110/pec.87.39.0027

Best, J.L., Reid, I., 1984. Separation Zone at Open-Channel Junctions. J. Hydraul. Eng. 110, 1588–1594. doi:10.1061/(ASCE)0733-9429(1984)110:11(1588)

Best, J.L., Rhoads, B.L., 2008. Sediment Transport, Bed Morphology and the Sedimentology of River Channel Confluences, in: River Confluences, Tributaries and the Fluvial Network.

John Wiley & Sons, Ltd, Chichester, UK, pp. 45–72. doi:10.1002/9780470760383.ch4

Best, J.L., Roy, A.G., 1991. Mixing-layer distortion at the confluence of channels of different depth. Nature 350, 411–413. doi:10.1038/350411a0

Biron, P., Best, J.L., Roy, A.G., 1996. Effects of Bed Discordance on Flow Dynamics at Open Channel Confluences. J. Hydraul. Eng. 122, 676–682. doi:10.1061/(ASCE)0733-9429(1996)122:12(676)

Biron, P., Roy, A., Best, J.L., Boyer, C.J., 1993. Bed morphology and sedimentology at the confluence of unequal depth channels. Geomorphology 8, 115–129. doi:10.1016/0169-555X(93)90032-W

Biron, P., Roy, A.G., Best, J.L., 1996. Turbulent flow structure at concordant and discordant open-channel confluences. Exp. Fluids 21. doi:10.1007/BF00189046

Biron, P.M., Ramamurthy, A.S., Han, S., 2004. Three-Dimensional Numerical Modeling of Mixing at River Confluences. J. Hydraul. Eng. 130, 243–253. doi:10.1061/(ASCE)0733-9429(2004)130:3(243)

Bouchez, J., Lajeunesse, E., Gaillardet, J., 2011. Reply to the Comment made by C. Gualtieri on "Turbulent mixing in the Amazon River: The isotopic memory of confluences", by J. Bouchez, E. Lajeunesse, J. Gaillardet, C. France-Lanord, P. Dutra-Maia and L. Maurice. Earth Planet. Sci. Lett. 311, 451–452. doi:10.1016/j.epsl.2011.09.026

Bouchez, J., Lajeunesse, E., Gaillardet, J., France-Lanord, C., Dutra-Maia, P., Maurice, L., 2010. Turbulent mixing in the Amazon River: The isotopic memory of confluences. Earth Planet. Sci. Lett. 290, 37–43. doi:10.1016/j.epsl.2009.11.054

Boxall, J.B., Guymer, I., 2003. Analysis and Prediction of Transverse Mixing Coefficients in Natural Channels. J. Hydraul. Eng. 129, 129–139. doi:10.1061/(ASCE)0733-

9429(2003)129:2(129)

Boyer, C., Roy, A.G., Best, J.L., 2006. Dynamics of a river channel confluence with discordant beds: Flow turbulence, bed load sediment transport, and bed morphology. J. Geophys. Res. 111, F04007. doi:10.1029/2005JF000458

Bradbrook, K.F., Biron, P.M., Lane, S.N., Richards, K.S., Roy, A.G., 1998. Investigation of controls on secondary circulation in a simple confluence geometry using a three-dimensional numerical model. Hydrol. Process. 12, 1371–1396. doi:10.1002/(SICI)1099-1085(19980630)12:8<1371::AID-HYP620>3.0.CO;2-C

Bradbrook, K.F., Lane, S.N., Richards, K.S., 2000. Numerical simulation of three-dimensional, time-averaged flow structure at river channel confluences. Water Resour. Res. 36, 2731–2746. doi:10.1029/2000WR900011

Bradbrook, K.F., Lane, S.N., Richards, K.S., Biron, P.M., Roy, A.G., 2001. Role of Bed Discordance at Asymmetrical River Confluences. J. Hydraul. Eng. 127, 351–368. doi:10.1061/(ASCE)0733-9429(2001)127:5(351)

Breiman, L., 2001. Random Forests. Mach. Learn. 45, 5–32. doi:10.1023/A:1010933404324

Brezonik, P., Menken, K.D., Bauer, M., 2005. Landsat-based remote sensing of lake water quality characteristics, including chlorophyll and colored dissolved organic matter (CDOM). Lake Reserv. Manag. 21, 373–382. doi:10.1080/07438140509354442

Brönmark, C., Hansson, L.-A., 2002. Environmental issues in lakes and ponds: current state and perspectives. Environ. Conserv. 29. doi:10.1017/S0376892902000218

Carlston, C.W., 1969. Longitudinal Slope Characteristics Of Rivers of The Midcontinent And The Atlantic East Gulf Slopes. Int. Assoc. Sci. Hydrol. Bull. 14, 21–31. doi:10.1080/02626666909493751

Chang, K.-W., Shen, Y., Chen, P.-C., 2004. Predicting algal bloom in the Techi reservoir using Landsat TM data. Int. J. Remote Sens. 25, 3411–3422. doi:10.1080/01431160310001620786

Constantinescu, G., Miyawaki, S., Rhoads, B., Sukhodolov, A., 2016. Influence of planform geometry and momentum ratio on thermal mixing at a stream confluence with a concordant bed. Environ. Fluid Mech. 16, 845–873. doi:10.1007/s10652-016-9457-0

Constantinescu, G., Miyawaki, S., Rhoads, B., Sukhodolov, A., 2012. Numerical analysis of the effect of momentum ratio on the dynamics and sediment-entrainment capacity of coherent flow structures at a stream confluence. J. Geophys. Res. Earth Surf. 117, n/a-n/a. doi:10.1029/2012JF002452

Constantinescu, G., Miyawaki, S., Rhoads, B., Sukhodolov, A., Kirkil, G., 2011. Structure of turbulent flow at a river confluence with momentum and velocity ratios close to 1: Insight provided by an eddy-resolving numerical simulation. Water Resour. Res. 47, W05507. doi:10.1029/2010WR010018

Cox, R.M., Forsythe, R.D., Vaughan, G.E., Olmsted, L.L., 1998. Assessing Water Quality in Catawba River Reservoirs Using Landsat Thematic Mapper Satellite Data. Lake Reserv. Manag. 14, 405–416. doi:10.1080/07438149809354347

Cutler, D.R., Edwards, T.C., Beard, K.H., Cutler, A., Hess, K.T., Gibson, J., Lawler, J.J., 2007. Random Forests for Classification in Ecology. Ecology 88, 2783–2792. doi:10.1890/07-0539.1

De Serres, B., Roy, A.G., Biron, P.M., Best, J.L., 1999. Three-dimensional structure of flow at a confluence of river channels with discordant beds. Geomorphology 26, 313–335. doi:10.1016/S0169-555X(98)00064-6

Dekker, A.G., Vos, R.J., Peters, S.W.M., 2002. Analytical algorithms for lake water TSM estimation for retrospective analyses of TM and SPOT sensor data. Int. J. Remote Sens. 23, 15–35. doi:10.1080/01431160010006917

Dekker, A.G., Vos, R.J., Peters, S.W.M., 2001. Comparison of remote sensing data, model results and in situ data for total suspended matter (TSM) in the southern Frisian lakes. Sci. Total Environ. 268, 197–214. doi:10.1016/S0048-9697(00)00679-3

Diplas, P., Dancey, C.L., Celik, A.O., Valyrakis, M., Greer, K., Akar, T., 2008. The Role of Impulse on the Initiation of Particle Movement Under Turbulent Flow Conditions. Science (80-.). 322, 717–720. doi:10.1126/science.1158954

Doxaran, D., Castaing, P., Lavender, S.J., 2006. Monitoring the maximum turbidity zone and detecting fine-scale turbidity features in the Gironde estuary using high spatial resolution satellite sensor (SPOT HRV, Landsat ETM+) data. Int. J. Remote Sens. 27, 2303–2321. doi:10.1080/01431160500396865

Doxaran, D., Froidefond, J.-M., Castaing, P., 2003. Remote-sensing reflectance of turbid sediment-dominated waters Reduction of sediment type variations and changing illumination conditions effects by use of reflectance ratios. Appl. Opt. 42, 2623. doi:10.1364/AO.42.002623

Doxaran, D., Froidefond, J.-M., Castaing, P., 2002a. A reflectance band ratio used to estimate suspended matter concentrations in sediment-dominated coastal waters. Int. J. Remote Sens. 23, 5079–5085. doi:10.1080/0143116021000009912

Doxaran, D., Froidefond, J.-M., Castaing, P., Babin, M., 2009. Dynamics of the turbidity maximum zone in a macrotidal estuary (the Gironde, France): Observations from field and MODIS satellite data. Estuar. Coast. Shelf Sci. 81, 321–332. doi:10.1016/j.ecss.2008.11.013

Doxaran, D., Froidefond, J.-M., Lavender, S., Castaing, P., 2002b. Spectral signature of highly turbid waters. Remote Sens. Environ. 81, 149–161. doi:10.1016/S0034-4257(01)00341-8

Duan, H., Ma, R., Zhang, Y., Zhang, B., 2009. Remote-sensing assessment of regional inland lake water clarity in northeast China. Limnology 10, 135–141. doi:10.1007/s10201-009-0263-y

Duker, L., Borre, L., 2001. Biodiversity conservation of the world's lakes: A preliminary framework for identifying priorities. Annapolis, Maryland USA.

Edwards, T.K., Glysson, G.D., 1999. Field methods for measurement of fluvial sediment: U.S. Geological Survey Techniques of Water-Resources Investigations, in: Book 3, Applications of Hydraulics. p. 89.

Edwards, T.K., Glysson, G.D., 1988. Field methods for measurement of fluvial sediment: U.S. Geological Survey Open-File Report 86-531.

Elhadi, N., Harrington, a., Hill, I., Lau, Y.L., Krishnappan, B.G., 1984. River mixing—A state-of-the-art report. Can. J. Civ. Eng. 11, 585–609. doi:10.1139/l84-076

Fick, A., 1855. On liquid diffusion. Poggendorffs Ann. 94.

Fischer, H.B., List, E.J., Koh, R.C.Y., Imberger, J., Brooks, N.H., 1979. Mixing in Inland and Coastal Waters. Academic, San Diego, Calif.

Furby, S.L., Wu, X., 2009. Evaluation of Alternative Sensors for a Landsat-Based Monitoring Program, in: Jones, S., Reinke, K. (Eds.), Innovations in Remote Sensing and Photogrammetry, Lecture Notes in Geoinformation and Cartography. Springer-Verlag, Berlin Heidleberg, pp. 75–90. doi:10.1007/978-3-540-93962-7_7

Gaudet, J.M., Roy, A.G., 1995. Effect of bed morphology on flow mixing length at river confluences. Nature 373, 138–139. doi:10.1038/373138a0

Guerrero, M., Rüther, N., Szupiany, R., Haun, S., Baranya, S., Latosinski, F., 2016. The Acoustic Properties of Suspended Sediment in Large Rivers: Consequences on ADCP Methods Applicability. Water 8, 13. doi:10.3390/w8010013

Güneralp, İ., Rhoads, B.L., 2007. Continuous Characterization of the Planform Geometry and Curvature of Meandering Rivers. Geogr. Anal. 40, 1–25. doi:10.1111/j.0016-7363.2007.00711.x

Härmä, P., Vepsäläinen, J., Hannonen, T., Pyhälahti, T., Kämäri, J., Kallio, K., Eloheimo, K., Koponen, S., 2001. Detection of water quality using simulated satellite data and semi-empirical algorithms in Finland. Sci. Total Environ. 268, 107–121. doi:10.1016/S0048-9697(00)00688-4

Heimann, D.C., Sprague, L.A., Blevins, D.W., 2011. Trends in suspended-sediment loads and concentrations in the Mississippi River Basin. 1950–2009: U.S. Geological Survey Scientific Investigations Report 2011–5200.

Hellweger, F.L., Miller, W., Oshodi, K.S., 2007. Mapping Turbidity in the Charles River, Boston Using a High-resolution Satellite. Environ. Monit. Assess. 132, 311–320. doi:10.1007/s10661-006-9535-8

Hellweger, F.L., Schlosser, P., Lall, U., Weissel, J.K., 2004. Use of satellite imagery for water quality studies in New York Harbor. Estuar. Coast. Shelf Sci. 61, 437–448. doi:10.1016/j.ecss.2004.06.019

Hestir, E.L., Brando, V.E., Bresciani, M., Giardino, C., Matta, E., Villa, P., Dekker, A.G., 2015. Measuring freshwater aquatic ecosystems: The need for a hyperspectral global mapping satellite mission. Remote Sens. Environ. 167, 181–195. doi:10.1016/j.rse.2015.05.023

Holly, F.M., 1985. Dispersion in rivers and coastal waters. 1. Physical principles and dispersion

equations., in: Developments in Hydraulic Engineering. Elsevier Applied Science.

IOCCG, 2006. Remote Sensing of Inherent Optical Properties : Fundamentals , Tests of Algorithms , and Application, in: Lee, Z.-P. (Ed.), Reports of the International Ocean-Colour Coordinating Group, No. 5. IOCCG, Dartmouth, Canada.

Jonathan, A.G., 2014. spatial.tools: R functions for working with spatial data. R Packag. version 1.4.8.

Kabeya, N., Kubota, T., Shimizu, A., Nobuhiro, T., Tsuboyama, Y., Chann, S., Tith, N., 2008. Isotopic investigation of river water mixing around the confluence of the Tonle Sap and Mekong rivers. Hydrol. Process. 22, 1351–1358. doi:10.1002/hyp.6944

Kallio, K., Attila, J., Härmä, P., Koponen, S., Pulliainen, J., Hyytiäinen, U.-M., Pyhälahti, T., 2008. Landsat ETM+ Images in the Estimation of Seasonal Lake Water Quality in Boreal River Basins. Environ. Manage. 42, 511–522. doi:10.1007/s00267-008-9146-y

Kenworthy, S.T., Rhoads, B.L., 1995. Hydrologic control of spatial patterns of suspended sediment concentration at a stream confluence. J. Hydrol. 168, 251–263. doi:10.1016/0022-1694(94)02644-Q

Kloiber, S.M., Brezonik, P.L., Olmanson, L.G., Bauer, M.E., 2002. A procedure for regional lake water clarity assessment using Landsat multispectral data. Remote Sens. Environ. 82, 38–47. doi:10.1016/S0034-4257(02)00022-6

Konsoer, K.M., Rhoads, B.L., 2013. Spatial–temporal structure of mixing interface turbulence at two large river confluences. Environ. Fluid Mech. doi:10.1007/s10652-013-9304-5

Krouse, H.R., Mackay, J.R., 1971. Application of H 2 18 O/H 2 16 O Abundances to the Problem of Lateral Mixing in the Liard–Mackenzie River System. Can. J. Earth Sci. 8, 1107–1109. doi:10.1139/e71-096

Kutser, T., Pierson, D.C., Kallio, K.Y., Reinart, A., Sobek, S., 2005. Mapping lake CDOM by satellite remote sensing. Remote Sens. Environ. 94, 535–540. doi:10.1016/j.rse.2004.11.009

Lane, S.N., Parsons, D.R., Best, J.L., Orfeo, O., Kostaschuk, R. a., Hardy, R.J., 2008. Causes of rapid mixing at a junction of two large rivers: Río Paraná and Río Paraguay, Argentina. J. Geophys. Res. Earth Surf. 113, 1–16. doi:10.1029/2006JF000745

Laraque, A., Guyot, J.L., Filizola, N., 2009. Mixing processes in the Amazon River at the confluences of the Negro and Solimões Rivers, Encontro das Águas, Manaus, Brazil. Hydrol. Process. 23, 3131–3140. doi:10.1002/hyp.7388

Lathrop, R.G., 1992. Landsat Thematic Mapper monitoring of turbid inland water quality. Photogramm. Eng. Remote Sens. 58, 465–470.

Lathrop, R.G., Lillesand, T.M., 1989. Monitoring Water-Quality and River Plume Transport in Green Bay, Lake-Michigan with Spot-1 Imagery. Photogramm. Eng. Remote Sensing 55, 349–354.

Lathrop, R.G., Lillesand, T.M., 1986. Use of thematic mapper data to assess water quality in Green Bay and Central Lake Michigan. Photogramm. Eng. Remote Sensing 52, 671–680.

Lau, Y.L., Krishnappan, B.G., 1981. Modeling Transverse Mixing in Natural Streams. J. Hydraul. Div. 107, 209–226.

Laursen, E.M., 1958. The Total Sediment Load of Streams. J. Hydraul. Div. 84, 1–36.

Lavery, P., Pattiaratchi, C., Wyllie, A., Hick, P., 1993. Water quality monitoring in estuarine waters using the landsat thematic mapper. Remote Sens. Environ. 46, 268–280. doi:10.1016/0034-4257(93)90047-2

Legleiter, C.J., Kyriakidis, P.C., 2007. Forward and Inverse Transformations between Cartesian and Channel-fitted Coordinate Systems for Meandering Rivers. Math. Geol. 38, 927–958.

doi:10.1007/s11004-006-9056-6

Leopold, L.B., Maddock, T., 1953. The hydraulic geometry of stream channels and some physiographic implicationsThe hydraulic geometry of stream channels and some physiographic implications.

Lewis, Q.W., Rhoads, B.L., 2015a. Resolving two-dimensional flow structure in rivers using large-scale particle image velocimetry: An example from a stream confluence. Water Resour. Res. 51, 7977–7994. doi:10.1002/2015WR017783

Lewis, Q.W., Rhoads, B.L., 2015b. Rates and patterns of thermal mixing at a small stream confluence under variable incoming flow conditions. Hydrol. Process. 29, 4442–4456. doi:10.1002/hyp.10496

Liaw, A., Wiener, M., 2002. Classification and Regression by randomForest 2(3). R News 2, 18–22.

Lymburner, L., Botha, E., Hestir, E., Anstee, J., Sagar, S., Dekker, A., Malthus, T., 2016. Landsat 8: Providing continuity and increased precision for measuring multi-decadal time series of total suspended matter. Remote Sens. Environ. doi:10.1016/j.rse.2016.04.011

Mackay, J.R., 1970. Lateral mixing of the Liard and Mackenzie rivers downstream from their confluence. Can. J. Earth Sci. 7, 111–124. doi:10.1139/e70-008

Marx, A.J., Loboda, T.V., 2013. Landsat-based early warning system to detect the destruction of villages in Darfur, Sudan. Remote Sens. Environ. 136, 126–134. doi:10.1016/j.rse.2013.05.006

Masek, J.G., Vermote, E.F., Saleous, N., Wolfe, R., Hall, F.G., Huemmrich, F., Gao, F., Kutler, J., Lim, T.K., 2013. LEDAPS Calibration, Reflectance, Atmospheric Correction Preprocessing Code, Version 2. Model product. doi:10.3334/ORNLDAAC/1146

Matsui, E., Salati, F., Friedman, I., Brinkman, W.L.F., 1976. Isotopic hydrology in the Amazonia: 2. Relative discharges of the Negro and Solimões rivers through 18 O concentrations. Water Resour. Res. 12, 781–785. doi:10.1029/WR012i004p00781

Matthews, M.W., 2011. A current review of empirical procedures of remote sensing in inland and near-coastal transitional waters. Int. J. Remote Sens. 32, 6855–6899. doi:10.1080/01431161.2010.512947

Maurice-Bourgoin, L., Quemerais, B., Moreira-Turcq, P., Seyler, P., 2003. Transport, distribution and speciation of mercury in the Amazon River at the confluence of black and white waters of the Negro and Solimões Rivers. Hydrol. Process. 17, 1405–1417. doi:10.1002/hyp.1292

McLelland, S.J., Ashworth, P.J., Best, J.L., 1996. The origin and downstream development of coherent flow structures at channel junctions, in: Ashworth, P.J., Bennett, S.J., Best, J.L., McLelland, S.J. (Eds.), Coherent Flow Structures in Open Channels. John Wiley and Sons Ltd, pp. 459–490.

Miller, R.L., McKee, B.A., 2004. Using MODIS Terra 250 m imagery to map concentrations of total suspended matter in coastal waters. Remote Sens. Environ. 93, 259–266. doi:10.1016/j.rse.2004.07.012

Morel, A., Prieur, L., 1977. Analysis of variations in ocean color1. Limnol. Oceanogr. 22, 709–722. doi:10.4319/lo.1977.22.4.0709

Mosley, P.M., 1976. An experimental study of channel confluences. J. Geol. 84, 535–562.

Navalgund, R.R., Jayaraman, V., Roy, P.S., 2007. Remote sensing applications: an overview. Curr. Sci. 1747–1766.

Odermatt, D., Gitelson, A., Brando, V.E., Schaepman, M., 2012. Review of constituent retrieval

in optically deep and complex waters from satellite imagery. Remote Sens. Environ. 118, 116–126. doi:10.1016/j.rse.2011.11.013

Olmanson, L.G., Bauer, M.E., Brezonik, P.L., 2008. A 20-year Landsat water clarity census of Minnesota's 10,000 lakes. Remote Sens. Environ. 112, 4086–4097. doi:10.1016/j.rse.2007.12.013

Onderka, M., Pekárová, P., 2008. Retrieval of suspended particulate matter concentrations in the Danube River from Landsat ETM data. Sci. Total Environ. 397, 238–243. doi:10.1016/j.scitotenv.2008.02.044

Osawa, T., Mitsuhashi, H., Niwa, H., Ushimaru, A., 2011. The role of river confluences and meanderings in preserving local hot spots for threatened plant species in riparian ecosystems. Aquat. Conserv. Mar. Freshw. Ecosyst. 21, 358–363. doi:10.1002/aqc.1194

Östlund, C., Flink, P., Strömbeck, N., Pierson, D., Lindell, T., 2001. Mapping of the water quality of Lake Erken, Sweden, from Imaging Spectrometry and Landsat Thematic Mapper. Sci. Total Environ. 268, 139–154. doi:10.1016/S0048-9697(00)00683-5

Palmer, S.C.J., Kutser, T., Hunter, P.D., 2015. Remote sensing of inland waters: Challenges, progress and future directions. Remote Sens. Environ. 157, 1–8. doi:10.1016/j.rse.2014.09.021

Paola, C., 1997. When streams collide. Nature 387, 232–233. doi:10.1038/387232a0

Park, E., Latrubesse, E.M., 2014. Modeling suspended sediment distribution patterns of the Amazon River using MODIS data. Remote Sens. Environ. 147, 232–242. doi:10.1016/j.rse.2014.03.013

Parsons, D.R., Best, J.L., Lane, S.N., Kostaschuk, R.A., Hardy, R.J., Orfeo, O., Amsler, M.L., Szupiany, R.N., 2008. Large River Channel Confluences, in: River Confluences, Tributaries

and the Fluvial Network. John Wiley & Sons, Ltd, Chichester, UK, pp. 73–91. doi:10.1002/9780470760383.ch5

Parsons, D.R., Best, J.L., Lane, S.N., Orfeo, O., Hardy, R.J., Kostaschuk, R., 2007. Form roughness and the absence of secondary flow in a large confluence–diffluence, Rio Paraná, Argentina. Earth Surf. Process. Landforms 32, 155–162. doi:10.1002/esp.1457

Pattiaratchi, C., Lavery, P., Wyllie, A., HICK, P., WYLLLIE, A., HICK, P., Wyllie, A., HICK, P., 1994. Estimates of water quality in coastal waters using multi-date Landsat Thematic Mapper data. Int. J. Remote Sens. 15, 1571–1584. doi:10.1080/01431169408954192

Porterfield, G., 1977. Computation of fluvial-sediment discharge, in: Techniques of Water-Resources Investigations of the U.S. Geological Survey. U.S. Geological Survey, Washington, D.C., p. 66.

Ramón, C.L., Armengol, J., Dolz, J., Prats, J., Rueda, F.J., 2014. Mixing dynamics at the confluence of two large rivers undergoing weak density variations. J. Geophys. Res. Ocean. 119, 2386–2402. doi:10.1002/2013JC009488

Ramõn, C.L., Hoyer, A.B., Armengol, J., Dolz, J., Rueda, F.J., 2013. Mixing and circulation at the confluence of two rivers entering a meandering reservoir. Water Resour. Res. 49, 1429–1445. doi:10.1002/wrcr.20131

Rathbun, R.E., Rostad, C.E., 2004. Lateral mixing in the Mississippi River below the confluence with the Ohio River. Water Resour. Res. 40. doi:10.1029/2003WR002381

Rhoads, Bruce, L., 1996. Mean Structure of Transport-effective Flows at an Asymmetrical Confluence when the Main Stream is Dominant, in: Ashworth, P.J., Bennett, S.J., Best, J.L., McLelland, S. (Eds.), Coherent Flow Structures in Open Channels: Origins, Scales and Interactions with Sediment Transport and Bed Morphology. John Wiley and Sons Ltd,

Chichester, UK, pp. 491–517.

Rhoads, B., 2006. Scaling of confluence dynamics in river systems: some general considerations, in: Parker, G., García, M.H. (Eds.), River, Coastal and Estuarine Morphodynamics: Proceedings of the 4th IAHR Symposium on River, Coastal and Estuarine Morphodynamics. Taylor & Francis. doi:10.1201/9781439833896.ch42

Rhoads, B.L., Kenworthy, S.T., 1998. Time-averaged flow structure in the central region of a stream confluence. Earth Surf. Process. Landforms 23, 171–191. doi:10.1002/(SICI)1096-9837(199802)23:2<171::AID-ESP842>3.0.CO;2-T

Rhoads, B.L., Kenworthy, S.T., 1995. Flow structure at an asymmetrical stream confluence. Geomorphology 11, 273–293. doi:10.1016/0169-555X(94)00069-4

Rhoads, B.L., Riley, J.D., Mayer, D.R., 2009. Response of bed morphology and bed material texture to hydrological conditions at an asymmetrical stream confluence. Geomorphology 109, 161–173. doi:10.1016/j.geomorph.2009.02.029

Rhoads, B.L., Sukhodolov, A.N., 2008. Lateral momentum flux and the spatial evolution of flow within a confluence mixing interface. Water Resour. Res. 44, n/a-n/a. doi:10.1029/2007WR006634

Rhoads, B.L., Sukhodolov, A.N., 2004. Spatial and temporal structure of shear layer turbulence at a stream confluence. Water Resour. Res. 40, n/a-n/a. doi:10.1029/2003WR002811

Rhoads, B.L., Sukhodolov, A.N., 2001. Field investigation of three-dimensional flow structure at stream confluences: 1. Thermal mixing and time-averaged velocities. Water Resour. Res. 37, 2393–2410. doi:10.1029/2001WR000316

Robert, J.H., 2016. raster: Geographic Data Analysis and Modeling. R Packag.

Rodriguez-Galiano, V.F., Ghimire, B., Rogan, J., Chica-Olmo, M., Rigol-Sanchez, J.P., 2012.

An assessment of the effectiveness of a random forest classifier for land-cover classification. ISPRS J. Photogramm. Remote Sens. 67, 93–104. doi:10.1016/j.isprsjprs.2011.11.002

Roy, A.G., Biron, P.M., Buffin-Bélanger, T., Levasseur, M., 1999. Combined visual and quantitative techniques in the study of natural turbulent flows. Water Resour. Res. 35, 871–877. doi:10.1029/1998WR900079

Rutherford, J.C., 1994. River Mixing. Wiley, Chichester.

Sayre, W.W., 1979. Shore-attched thermal plumes in river, in: Shen, H.W. (Ed.), Modelling in Rivers. Wiley-Interscience, London.

Seo, I., Baek, K.O., Jeon, T.M., 2006. Analysis of transverse mixing in natural streams under slug tests. J. Hydraul. Res. 44, 350–362. doi:10.1080/00221686.2006.9521687

Shen, H.W., Hung, C.S., 1972. An engineering approach to total bed-material load by regression analysis, in: Proceedings of the Sedimentation Symposium. pp. 14–17.

Stallard, R.F., 1987. Cross-channel mixing and its effect on sedimentation in the Orinoco River. Water Resour. Res. 23, 1977. doi:10.1029/WR023i010p01977

Sukhodolov, A.N., Rhoads, B.L., 2001. Field investigation of three-dimensional flow. Water Resour. Res. 37, 2411–2424.

Sváb, E., Tyler, A.N., Preston, T., Présing, M., Balogh, K. V., 2005. Characterizing the spectral reflectance of algae in lake waters with high suspended sediment concentrations. Int. J. Remote Sens. 26, 919–928. doi:10.1080/0143116042000274087

Szupiany, R., Amsler, M., Parsons, D., Best, J., Haydel, R., 2007. Comparisons of morphology and flow structure at two braid-bar confluences in a large river, in: River, Coastal and Estuarine Morphodynamics: RCEM 2007, Two Volume Set. CRC Press, pp. 807–814.

doi:10.1201/NOE0415453639-c102

Szupiany, R.N., Amsler, M.L., Hernandez, J., Parsons, D.R., Best, J.L., Fornari, E., Trento, A., 2012. Flow fields, bed shear stresses, and suspended bed sediment dynamics in bifurcations of a large river. Water Resour. Res. 48, n/a-n/a. doi:10.1029/2011WR011677

Szupiany, R.N., Amsler, M.L., Parsons, D.R., Best, J.L., 2009. Morphology, flow structure, and suspended bed sediment transport at two large braid-bar confluences. Water Resour. Res. 45, n/a-n/a. doi:10.1029/2008WR007428

Thiemann, S., Kaufmann, H., 2000. Determination of Chlorophyll Content and Trophic State of Lakes Using Field Spectrometer and IRS-1C Satellite Data in the Mecklenburg Lake District, Germany. Remote Sens. Environ. 73, 227–235. doi:10.1016/S0034-4257(00)00097-3

Tyler, A.N., Svab, E., Preston, T., Présing, M., Kovács, W.A., 2006. Remote sensing of the water quality of shallow lakes: A mixture modelling approach to quantifying phytoplankton in water characterized by high-suspended sediment. Int. J. Remote Sens. 27, 1521–1537. doi:10.1080/01431160500419311

Vincent, R.K., Qin, X., McKay, R.M.L., Miner, J., Czajkowski, K., Savino, J., Bridgeman, T., 2004. Phycocyanin detection from LANDSAT TM data for mapping cyanobacterial blooms in Lake Erie. Remote Sens. Environ. 89, 381–392. doi:10.1016/j.rse.2003.10.014

Wang, F., Han, L., Kung, H. -T., Van Arsdale, R.B., 2006. Applications of Landsat-5 TM imagery in assessing and mapping water quality in Reelfoot Lake, Tennessee. Int. J. Remote Sens. 27, 5269–5283. doi:10.1080/01431160500191704

Wu, G., De Leeuw, J., Skidmore, A.K., Prins, H.H.T., Liu, Y., 2008. Comparison of MODIS and Landsat TM5 images for mapping tempo–spatial dynamics of Secchi disk depths in Poyang

Lake National Nature Reserve, China. Int. J. Remote Sens. 29, 2183–2198. doi:10.1080/01431160701422254

Wulder, M.A., White, J.C., Andrew, M.E., Seitz, N.E., Coops, N.C., 2009. Forest fragmentation, structure, and age characteristics as a legacy of forest management. For. Ecol. Manage. 258, 1938–1949. doi:10.1016/j.foreco.2009.07.041

Yang, C.T., 1979. Unit stream power equations for total load. J. Hydrol. 40, 123–138. doi:10.1016/0022-1694(79)90092-1

Yotsukura, N., Cobb, E.D., 1972. Transverse Diffusion of Solutes in Natural Streams. US Geol. Surv. Prof. Pap. 582-C.

Yotsukura, N., Sayre, W.W., 1976. Transverse Mixing in Natural Channels. Water Resour. Res. 12, 695–704.

Zhang, W., Zhu, D.Z., 2011. Transverse Mixing in an Unregulated Northern River. J. Hydraul. Eng. 137, 1426–1440. doi:10.1061/(ASCE)HY.1943-7900.0000453